Studies on Construction of the Capillary Chromatography Based on Specific Fluidic Behavior of Mixed Solvent Solution in Microspace and Consideration of the Fluidic Behavior

Satoshi Fujinaga

Doshisha University

Kyoto, Japan

November 2015

Contents

Chapter 1

Introduction

Microfluidic behaviors of solvents, confined in microspace, e. g., microchannels in a microchip or capillary tubes, have been investigated since the nineteenth century, and are known to generate interesting and useful physical or hydrodynamic phenomena, such as electroosmotic and laminar flows. Electroosmotic flow was first reported in 1809 by Reuss.[1] In the last century, capillary electrophoresis,[2] micellar electokinetic chromatography,[3] and capillary electrochromatography[4] were developed on the basis of electroosmotic flow. Such flow is instigated under high-applied voltages. Laminar flow was reported by Hagen in 1839[5] and Poiseuille in 1841.[6] Reynolds, who later studied turbulent and laminar flows, formulated a dimensionless parameter, known as the Reynolds number in fluid mechanics.[7] In the last century, the application of laminar flow led to the development of hydrodynamic chromatography,[8] wide-bore hydrodynamic chromatography,[9] and field flow fraction chromatography.[10]

Recently, the microfluidic behavior of solvents, based on electroosmotic and laminar flows, has been examined by using varying channel configuration, solvent flow rates, aqueous–organic solvent mixtures, and by introducing specific obstacles into the microchannel.[11-13] The fluidic behavior of solvents in the microchannel is related to the separation, diffusion, and reaction of the solutes. The development of novel microfluidic behaviors of solvents is important and useful to design microreactors or micro total analysis systems.[14,15] An interesting and unique microfluidic behavior based on a mixed solvent systems confined in a microspace have reported,[16-21] and it was named as the tube radial

distribution phenomenon (TRDP). A two-phase separation system changes from a homogeneous (single-phase) to a heterogeneous (two-phase) solution upon temperature and/or pressure changes. When the homogeneous solutions of two-phase separation systems are delivered to a microspace, the homogeneous solutions change to the heterogeneous solutions, generating a hydrodynamic liquid-liquid interface with inner and outer phases. For example, when the ternary water-hydrophilic/hydrophobic organic solvents mixed solution are fed into microspace, the phase with the larger volume ratio formed as the inner phase. Such process was termed as the TRDP. The TRDP is observed in mainly ternary water-hydrophilic/hydrophobic organic solvents mixed solutions.[16-20] The TRDP induces the formation of a kinetic liquid-liquid interface in microfluidic flow by the generation of inner and outer phases.

A capillary chromatography system, operating under the TRDP, where the outer phase functions as a pseudo-stationary phase under laminar flow conditions, has been developed. Such a system is referred to as tube radial distribution chromatography (TRDC).[22-24] The TRDP have been also applied for extraction,[25,26] chemical reaction,[27,28] and mixing processes.[29]

Since the TRDC is separation system based on the TRDP, it is important to investigate the condition to generate the TRDP in order to separate analytes in higher performance. In Chapter 2, fluorescence photographs of the dyes dissolved in water–hydrophilic/hydrophobic organic solvent mixture solution in the TRDC were examined under various

conditions concerning the inner diameters, tube temperatures, tube effective lengths, and flow rates (or average linear velocities). In addition, The model analyte solution of 1-naphthol, 1-naphthalenesulfonic acid, 2,6-naphthalenedisulfonic acid, and 1,3,6-naphthalenetrisulfonic acid was subjected to TRDC. They were separated and detected in this order with 50, 75, and 100 μm inner diameters of the open-tubular capillaries completely.

In Chapter 3, to examine the influence of the physical properties of the organic solvent gives the separation of TRDC, the author examined separation performance in the TRDC system using various water–hydrophilic/hydrophobic organic solvent mixture solution. Mixtures of a hydrophilic organic solvent (acetonitrile, ethanol, methanol, 1-propanol, or 1,4-dioxane) and a hydrophobic solvent (ethyl acetate, hexane, 1-butanol, or chloroform) were examined as the carrier solution, the TRDC was investigated using phase diagrams, chromatograms, and fluorescence photographs.

The TRDC system using water–hydrophilic/hydrophobic organic solvent mixture carrier solution separates analytes by its hydrophilicities. Therefore, samples not having hydrophilicity, such as metal ions, cannot be separated by the TRDC. Additionally, metal ions have little absorbance, it is difficult to absorption detection. In Chapter 4, Chrome Azurol S as an absorption reagent was introduced into the TRDC system for metal ion separation and online detection. By introduction of Chrome Azurol S, characteristic individual absorption characteristics and elution times were obtained as the result of complex formation between the metal ions and

Chrome Azurol S in the water–acetonitrile–ethyl acetate mixture solution.

Investigation of the TRDP has begun in 2009. Thereby, the history of study is not long and the principle of TRDP is not certain. Therefore, the author studied to elucidate the principle of TRDP. In Chapter 5, dimensionless number, Weber number, of the inner and outer phases in the TRDP process was estimated for the water–acetonitrile–ethyl acetate and water–acetonitrile–chloroform systems. And then, as an attempt, a relationship between the Weber number and TRDP formation was examined for the two model systems in this experiment. The TRDP was observed in both systems when the Weber numbers of the organic solvent-rich and water-rich phases were different. However, an either excessively large or small difference in the Weber numbers did not instigate TRDP. TRDP was discussed using Weber number that assesses the effect of the inertial force and the interfacial tension.

The TRDP is arisen by using a two-phase separation system. Therefore, the author examine the TRDP by a two-phase separation system other than water–hydrophilic/hydrophobic organic solvent mixture solution in Chapter 6. Specifically, TRDP by using water–surfactant, water–ionic liquid, and fluorous/organic solvents is observed. When the TRDP is observed by these mixed solutions, the phase with the larger viscosity formed an inner phase regardless of the volume ratios in some solution system and the phase with the larger volume formed an inner phase in other solution. When the TRDP is observed by these mixed solutions, in some solution system, the phase with the larger viscosity formed an inner

phase regardless of the volume ratios, and in the other solutions, the phase with the larger volume formed an inner phase. In this chapter, the factors influencing the formation of inner and outer phases in the TRDP using the above-mentioned mixed solvent solutions were investigated. The author examined phase diagrams, viscosities of the two phases (upper and lower phases in a batch vessel), volume ratios of the phases, and bright-light or fluorescence photographs of the TRDP.

For the phase formation in the TRDP, when the difference in viscosities between the two phases was large, the phase with the larger viscosity formed an inner phase regardless of the volume ratios, whereas when the difference was small, the phase with the larger volume formed an inner phase. In Chapter 7, the factors influencing the configuration of the inner and outer phases in TRDP using the various mixed solutions were considered from the viewpoint of viscous dissipation in fluidic flows.

References

1) F. F. Reuss, *Proceedings of the Imperial Society of Naturalists of Moscow*, **2**, 327 (1809).
2) J.W.Jorgenson and K. D. Lukacs, *Anal. Chem.*, **53**, 1298 (1981).
3) S. Terabe, K. Otsuka, K.Ichikawa, A. Tsuchiya, and T.Ando, *Anai. Chem.*, **56**, 111 (1984).
4) T. Tsuda, *Anal. Chem.*, **59**, 521 (1987).
5) G. Hagen, *Ann. Phys. Chem*., **46**, 423 (1839).

6) R. B. Bird, W. E. Stewart, and E. N. Lightfoot, *Transport Phenomena, 2nd edn*., Chap. 2, (2002).

7) O. Reynolds, *Phil. Trans. R. Soc.*., **174**, 935 (1883).

8) H. Small, *J. Colloid Interface Sci.*, **48**, 147 (1974).

9) M. Harada, T. Kido, T. Matsudo, and T. Okada, *Anal. Sci.*, **21**, 491 (2005).

10) J. C. Giddings, M. N. Myers, G.-C. Lin, and M. Martin, *J. Chromatogr., A*, **142**, 23 (1977).

11) Y. Kikutani, H. Hisamoto, M. Tokeshi, and T. Kitamori, *Lab Chip*, **4**, 328 (2004).

12) A. Hibara, M. Tokeshi, K. Uchiyama, H. Hisamoto, and T. Kitamori, *Anal. Sci.*, **17**, 89 (2001).

13) N. Kaji, Y. Okamoto, M. Tokeshi, and Y. Baba, *Chem. Soc. Rev.*, **39**, 948 (2010).

14) H. Nakamura, Y. Yamaguchi, M. Miyazaki, H. Maeda, and M. Uehara, *Chem. Commun.*, **23**, 2844 (2002).

15) H. Kawazumi, A. Tashiro, K. Ogino, and H. Maeda, *Lab. Chip*, **2**, 8, (2002).

16) N. Jinno, M. Hashimoto, and K. Tsukagoshi, *Anal. Sci.*, **25**, 145, (2009).

17) N. Jinno, M. Itano, M. Hashimoto, and K. Tsukagoshi, *Talanta*, **79**, 1348, (2009).

18) M. Murakami, N. Jinno, M. Hashimoto, and K. Tsukagoshi, *Chem. Lett.*, **39**, 272 (2010).

19) N. Jinno, M. Murakami, K. Mizohata, M. Hashimoto, and K. Tsukagoshi,

Analyst, **135**, 927 (2011).

20) M. Murakami, N. Jinno, M. Hashimoto, and K. Tsukagoshi, *Anal. Sci.*, **27**, 793 (2011).

21) K. Tsukagoshi, *Bunseki Kagaku*, **62**, 393 (2013).

22) N. Jinno, M. Murakami, M. Hashimoto, and K. Tsukagoshi, *Anal. Sci.*, **26**, 737 (2010)

23) S. Fujinaga, N. Jinno, M. Hashimoto, and K. Tsukagoshi, *J. Sep. Sci.*, **34**, 2833 (2011).

24) Y. Kudo, H. Kan, N. Jinno, M. Hashimoto, and K. Tsukagoshi, *Anal. Methods*, **4**, 906 (2012).

25) N. Jinno, M. Hashimoto, and K. Tsukagoshi, *Chem. Lett.*, **40**, 654 (2011).

26) N. Jinno, M. Hashimoto, and K. Tsukagoshi, *J. Anal. Sci. Methods Instrum.*, **2**, 49 (2012).

27) Y. Masuhara, N. Jinno, M. Hashimoto, and K. Tsukagoshi, *Chem. Lett.*, **40**, 804 (2011).

28) Y. Masuhara, N. Jinno, M. Hashimoto, and K. Tsukagoshi, *Anal. Sci*., **28**, 439 (2012).

29) K. Nishiyama, N. Jinno, M. Hashimoto, and K. Tsukagoshi, *Anal. Sci.*, **28**, 423 (2012).

The literatures reported by the author regarding the TRDP are as follows:

1) “Use of Tube Radial Distribution of Ternary Mixed Carrier Solvents for Introduction of Absorption Reagent for Metal Ion Separation and On-Line Detection into Capillary”, *J. Sep. Sci*, **34**, 2833 (2011).

2) “Specific Microfluidic Behavior of Ternary Mixed Carrier Solvents of Water–Acetonitrile–Ethyl Acetate in Open-Tubular Capillary Chromatography and the Chromatograms”, *Anal. Methods*, **4**, 3884 (2012).

3) “Elution Behavior of Lambda-DNA with Ternary Mixed Carrier Solvents in an Open-Tubular Capillary under Laminar Flow Conditions”, *Anal. Sci.*, **28**, 617 (2012).

4) “Investigations into Tie Lines and Solubility Curves on Phase Diagrams in Open-Tubular Capillary Chromatography Using Ternary Mixed-Carrier Solvents”, *Anal. Sci.*, **28**, 921 (2012).

5) “Fluidic Behavior of Polymer Compounds in an Open-Tubular Capillary with Ternary Mixed Carrier Solvents under Laminar Flow Conditions”, *J. Flow Inject. Anal.*, **29**, 21 (2012).

6) “Capillary Chromatography Based on Tube Radial Distribution of

Ternary Mixed Solvents: Construction of the Phase Diagram and the Separation performance", *Sci. Eng. Rev. Doshisha Univ.*, **53**, 167 (2013).

7) "Capillary Chromatography Using an Annular and Sluggish Flow in the Ternary Water–Acetonitrile–Ethyl Acetate System as Carrier Solution", *Chem. Lett.*, **43**, 1318 (2014).

8) "Investigation of Inner and Outer Phase Formation in Tube Radial Distribution Phenomenon Using Various Types of Mixed Solvent Solutions", *Anal. Sci.*, **30**, 1005 (2014).

9) "Investigation of the Composition for a Ternary Solvent System in Tube Radial Distribution Chromatography", *J. Liq. Chromatogr. Relat. Technol.*, **38**, 600 (2015).

10) "Separation of Metal Complexes with Tube Radial Distribution Chromatography Using a Ternary Solvent Containing 8-Quinolinol", *Anal. Sci.*, in press.

11) "Consideration of Tube Radial Distribution Phenomenon under Laminar Flow Conditions Based on the Weber Number", *J. Chem. Eng. Jpn.*, in press.

12) “Microfluidic Inverted Flow of Aqueous and Organic Solvent Mixed Solution in a Microchannel under Laminar Flow Conditions”, *Haris Sci. Rev. Doshisha Univ.*, **56**, 155 (2015).

13) “Consideration of Inner and Outer Phase Configuration in Tube Radial Distribution Phenomenon Based on Viscous Dissipation in a Microfluidic Flow Using Various Types of Mixed Solvent Solutions”, *Anal. Sci*., submitted.

Chapter 2

Influences of Inner Diameters, Tube Temperatures, Tube Effective Lengths, and Flow Rates on Tube Radial Distribution Phenomenon

2.1. Introduction

Recently, the tube radial distribution phenomenon of ternary mixed carrier solvents in a microspace was reported,[1-4] which the author call the “tube radial distribution phenomenon (TRDP)”. When the ternary mixed carrier solvents of water–hydrophilic/hydrophobic organic solvent mixtures are delivered into a microspace, such as a microchannel or a capillary tube, the carrier solvent molecules are radially distributed in the microspace, generating inner and outer phases. For example, when a carrier solution of water–acetonitrile–ethyl acetate (3:8:4 volume ratio) (the organic solvent-rich carrier solution) was fed into a fused-silica capillary tube, an organic solvent-rich major phase was generated around the middle of the tube as an inner phase far from the inner wall, while a water-rich minor phase formed near the inner wall as an outer phase, or capillary wall phase. A capillary chromatography system where the outer phase functions as a pseudo-stationary phase under laminar flow conditions has been developed based on the TRDP. This chromatography system is call this “tube radial distribution chromatography (TRDC)”.[5-8]

The TRDP, i.e., the creation of kinetic liquid-liquid interface in a microfluidic flow, is interested but also involved by its nature. The TRDP have left several subjects to have to be investigated to clear the microfluidic behavior. In this chapter, the tube radial distribution of the carrier solvents were examined under various conditions through the fluorescence microscope-CCD camera system. Also, separation

performance was examined for the model mixture analytes in the capillary chromatography, i.e., TRDC.

2.2. Experimental

2.2.1. Reagents and capillary tubes

Water was purified with an Elix 3 UV (Millipore Co., Billerica, MA). All reagents used were commercially available and of analytical grade. 1-Naphthol, 1-naphthalenesulfonic acid, 2,6-naphthalenedisulfonic acid, 1,3,6-naphthalenetrisulfonic acid, Eosin Y, perylene, acetonitrile, and ethyl acetate were purchased from Wako Pure Chemical Industries, Ltd. (Osaka, Japan). Fused-silica capillary tubes were purchased from GL Science (Tokyo, Japan).

2.2.2. Fluorescence photographs

A capillary tube was set up for the fluorescence microscope-CCD camera system (Fig. 2-1) to confirm the tube radial distribution of the carrier solvents, i.e., TRDP. The water–acetonitrile–ethyl acetate mixture (3:8:4 volume ratio) including 1 mM Eosin Y and 0.1 mM perylene solutions was delivered into the capillary tube. The fluorescence in the capillary tube was monitored using a fluorescence microscope (BX51; Olympus, Tokyo, Japan) equipped with a Hg lamp, a filter (U-MWU2, ex 330-385 nm, em >

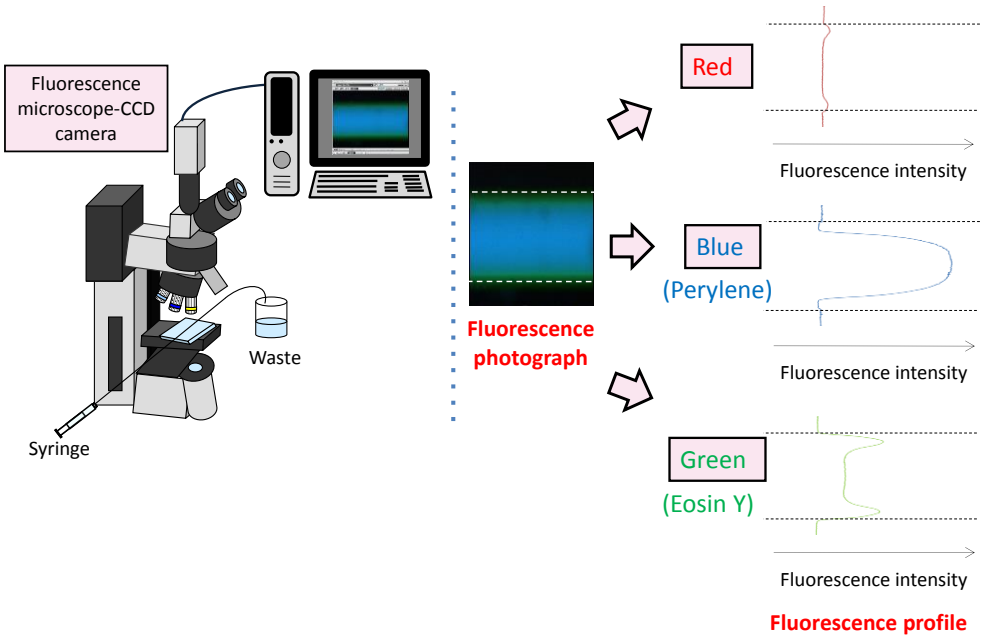

Fig. 2-1 Schematic diagram of fluorescence microscope-CCD camera and the transformation of fluorescence photograph to fluorescence profile through the computer.

420 nm), and a CCD camera (JK-TU53H). Fluorescence photographs, which mainly consisted of blue and green, because perylene and Eosin Y emit light at 470 and 550 nm, respectively, were transformed into line drawings to assess the color (red, green, and blue (RGB)) depth. These were expressed as digital data on a computer, and the numbers were standardized to the line drawing data to give the fluorescence profiles.

2.2.3. Open-tubular capillary chromatography

A schematic diagram of the present capillary chromatographysystem comprised of an open fused-silica capillary tube, microsyringe pump (MF-9090; Bioanalytical Systems, Inc., West Lafayette, IN), and fluorescence detector (modified FR-535 fluorescence detector; Shimadzu Co., Kyoto, Japan) is shown in Fig. 2-2. The tube temperature was controlled by dipping the capillary tube in water maintained at a definite temperature in a beaker with stirring. Water–acetonitrile–ethyl acetate mixtures with volume ratios of 3:8:4 were used as carrier solutions. Analyte solutions were prepared with the carrier solutions. The analyte solution was introduced directly into the capillary inlet side by the gravity method. After analyte injection, the capillary inlet was connected through a joint to a microsyringe. The syringe was set on the microsyringe pump. The carrier solution was fed into the capillary tube at a definite flow rate under laminar flow conditions. On-capillary fluorescence detection (ex. 495 nm and em. 520 nm) was performed with the detector.

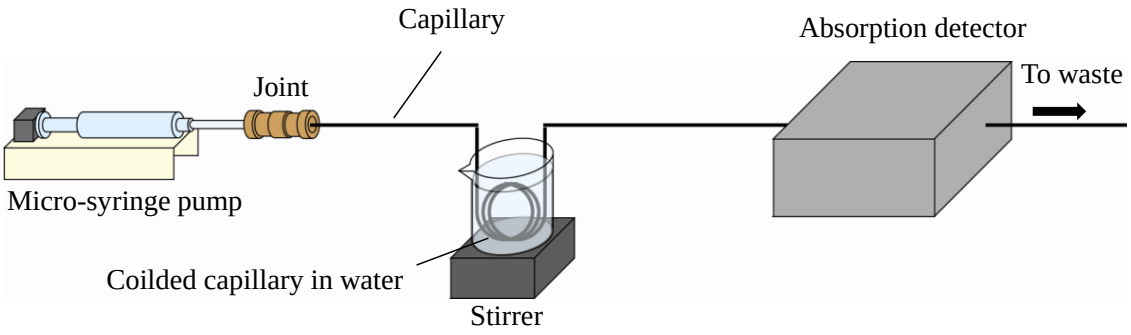

Fig. 2-2 Schematic diagram of the open tubular capillary chromatography (TRDC system).

2.3. Results and Discussion

2.3.1. Phase diagram for water–acetonitrile–ethyl acetate mixture

A phase diagram for the ternary mixture solvents of water–acetonitrile (hydrophilic organic solvent)–ethyl acetate (hydrophobic organic solvent) was examined in a vessel at 0 and 20 °C under a constant pressure or atmospheric pressure (Fig. 2-3a)) as well as at atmospheric pressure (1 atm) and 1.3 atm at a constant temperature of 20 °C (Fig. 2-3 b)). The obtained phase diagrams are shown in Fig. 2-3. The dotted curves in the diagrams indicate the boundary between homogeneous and heterogeneous phases. The phase diagram showed that each component ratio of the solvents made a homogeneous (one homogeneous phase) or a heterogeneous (two homogeneous phases) solution. As shown in Fig. 2-3, lower temperature and higher pressure expanded the boundary curves outside in the phase diagrams.

The author proposed a view of the inner and outer phase formation in the TRDP, based on the above experimental data. A specific homogeneous solution, whose component ratio was near the boundary between homogeneous and heterogeneous in the phase diagram, was cooled lower than 20 °C (room temperature) or pressurized greater than atmospheric pressure in a batch vessel where it was under the control of gravity. In an organic solvent-rich solution (e.g., water–acetonitrile–ethyl acetate mixture; 3:8:4 volume ratio), the homogeneous solution first became an

a)

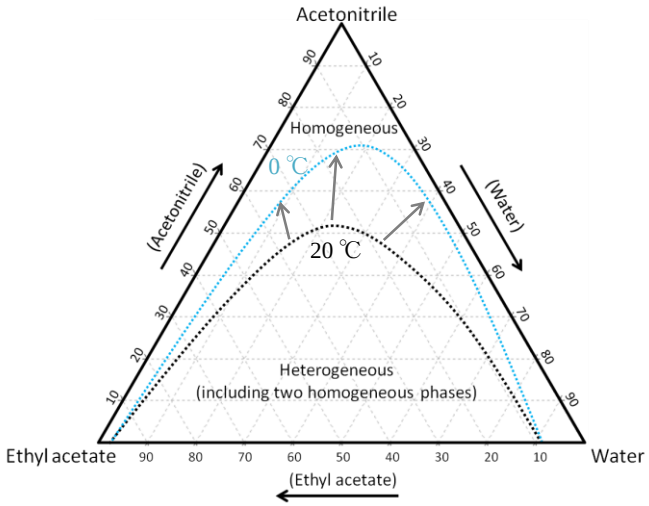

b)

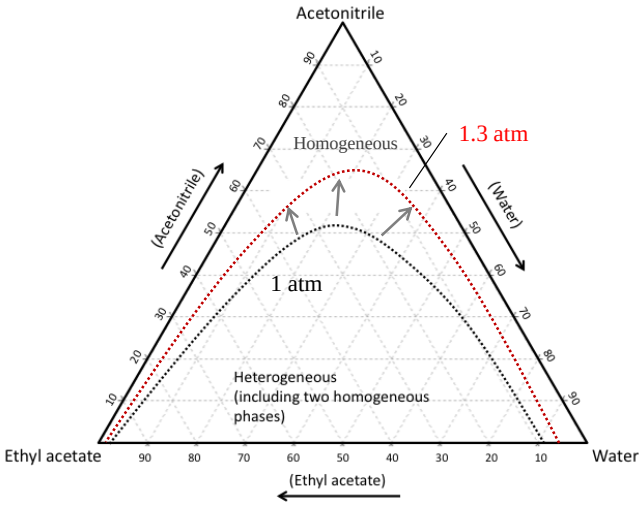

Fig. 2-3 Phase diagram for the ternary water–acetonitrile–ethyl acetate mixture solution.

a) Pressure constant (atomospheric pressure) and b) temperature constant (20 °C).

emulsion or nontransparent solution that included minor solvent or water-rich tiny droplets and then changes to a heterogeneous solution that included an upper major organic solvent-rich solution and a lower minor water-rich solution under the control of gravity.

The phase formation of the ternary mixed solvents in a capillary tube under the change of temperature and pressure is estimated as follows, where it is not under the control of gravity. A specific homogeneous solution with a component ratio near the boundary between homogeneous and heterogeneous in the phase diagram is delivered under laminar flow conditions that produce a constant pressure to the radial face and/or under the lower temperature. In an organic solvent-rich solution, the homogeneous solution first becomes an emulsion solution that includes minor solvent or water-rich tiny droplets. The water-rich tiny droplets start to aggregate near the inner wall where the linear velocity is lowest under laminar flow conditions. Consequently, the ternary mixed solvent solution in a tube changes to a heterogeneous solution that includes a major inner organic solvent-rich solution and a minor outer water-rich solution, where it is not under the control of gravity. The consideration of the TRDP process is illustrated in Fig. 2-4.

In a similar way, in a water-rich solution, the homogeneous solution first became an emulsion solution that included minor solvent or organic solvent-rich tiny droplets, and then changed to a heterogeneous solution that included an upper minor organic solvent-rich solution and a lower major water-rich solution in a batch vessel. The phase formation of the

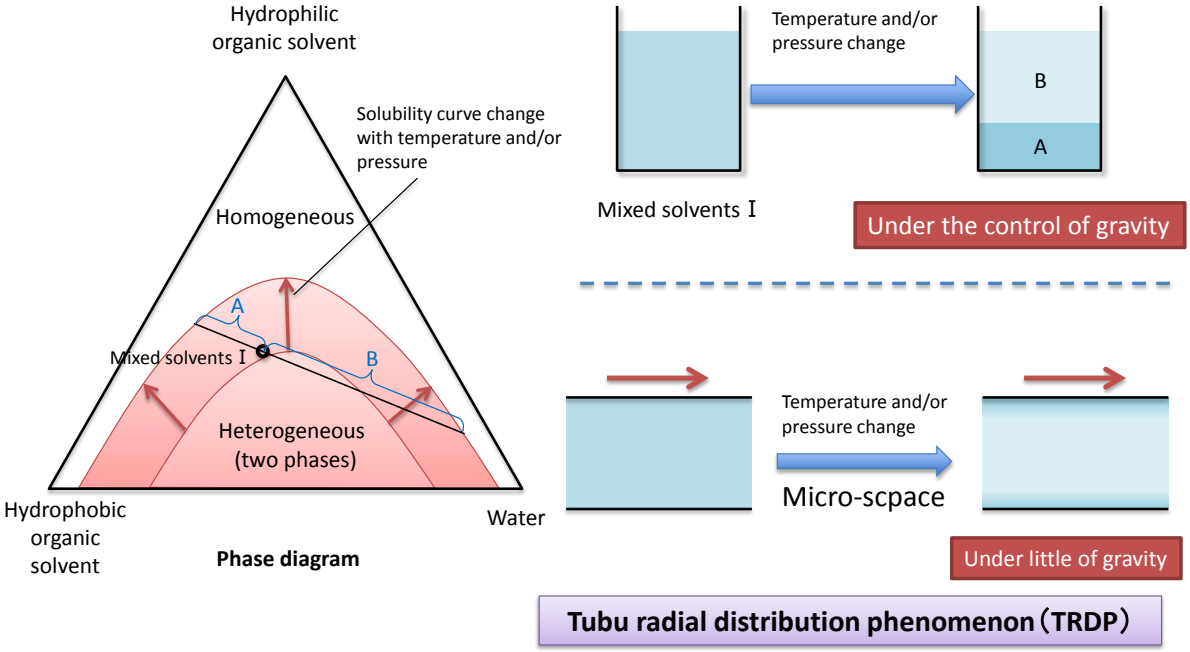

Fig. 2-4 Illustration of creation in a micro-space of tube radial distribution phenomenon appearance.

ternary mixed solvents in a capillary tube under pressure due to laminar flow is estimated as follows, where it is not under the control of gravity. In a water-rich solution, the homogeneous solution becomes an emulsion solution that includes minor solvent or organic solvent-rich tiny droplets. The organic solvent-rich tiny droplets start to aggregate near the inner wall where the velocity is lowest under laminar flow conditions. The ternary mixed solvent solution in a tube changes to a heterogeneous solution that includes a major inner water-rich solution and a minor outer organic solvent-rich solution where it is not under the control of gravity.

2.3.2. Effects of flow rates in the capillary tube

Fluorescence photographs were observed for a capillary tube in which the organic solvent-rich carrier solution (volume ratio 3:8:4) containing perylene (0.1 mM) and Eosin Y (1.0 mM) was delivered at flow rates of 0.1–4.0 μL min^{-1} with the inner diameter of 50, 75, and 100 μm. The hydrophobic perylene molecules (blue) were distributed around the middle of the tube, while the relatively hydrophilic Eosin Y molecules (green) were distributed near the tube's inner wall at flow rates of 0.5–2.5 μL min^{-1} with 50 μm, 0.5–2.0 μL min^{-1} with 75 μm, and 0.5–1.0 μL min^{-1} with 100 μm, respectively; the inflections were observed on the fluorescence profiles of Eosin Y. Comparatively, at lower flow rates, the author did not observe the tube radial distributions; the dissolved dyes were distributed in the axial direction, while, at higher flow rates, the tube

radial distributions of the dyes were not observed and the fluorescence profiles showed that the dyes were homogeneously distributed in the ternary mixed solvent. That is, the fluidic behavior at high flow rates leads to homogeneous solutions, where the molecular aggregates are dispersed homogeneously in the solvent.

The data obtained using an organic solvent-rich carrier solution (3:8:4, volume ratio) containing perylene (0.1 mM) and Eosin Y (1 mM) in a capillary tube are used to investigate the relationships between the flow rates, pressures, and phase formation. The pressure in the capillary tube under laminar flow conditions was calculated at each flow rate (0.1–4.0 μL min^{-1}) using the following Hagen–Poiseuille equation:

$$Q = \frac{\pi a^4}{8\mu}\frac{\Delta p}{L}$$

where Q is the flow rate, a the inner radius, Δp the pressure (or pressure loss), L the viscosity, and L the effective capillary length (the length from the observation point to the capillary outlet). The pressures in the capillary tube were calculated using Q, a, μ, and L values of 0.1–4.0 μL min^{-1}, 37.5 mm, 6.89 × 10^{-4} $kgm^{-1}s^{-1}$, and 2.0 × 10^{-1} m, respectively.

The formation/non-formation of the inner and outer phases indicating TRDP creation/non-creation, respectively, are plotted in the pressure vs flow rate graph in Fig. 2-5. The formation/non-formation of the inner and outer phases are presented with symbol of ○ and ×, and partially TRDP observation is presented with symbol of △. From the data, it can be seen that the flow rate and pressure in a capillary tube, as well as the

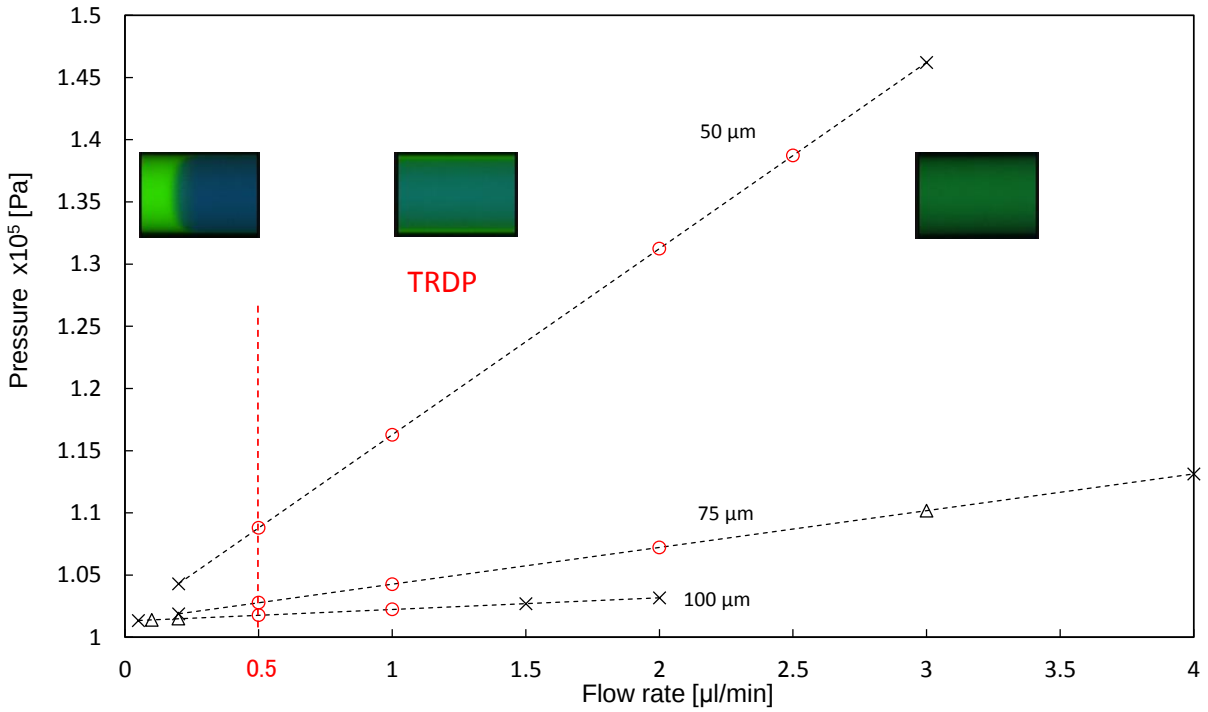

Fig. 2-5 Relationships between flow rates and pressures in tube radial distribution phenomenon of the ternary mixed solvents at tube temperature of 20 °C.

Conditions: Capillary tube, 110 cm (effective length: 90 cm) of 50, 75, and 100 µm i.d. fused-silica; carrier, water–acetonitrile–ethyl acetate (3:8:4 volume ratio) containing perylene (0.1 mM) and Eosin Y (1.0 mM).

component ratios of the mixed solvents play important roles in determining TRDP in the solvents.

2.3.3. Effects of temperature and pressure on TRDP formation

Fluorescence photographs were observed similary to the above section, but at tube temperature of 0 °C instead of 20 °C. Interesting, the TRDP could be observed up to 50 μL min^{-1}, with all capillary inner diameters, 50, 75, and 100 μm and 20, 50 and 80 cm effective lengths, where the limitation flow rates, 50 μL min^{-1}, were determined in the present microsyringe pump's capacity. Thinking of the phase diagrams shown in Fig. 2-3, the effects of both temperature and pressure must lead to stable TRDP formation in a large range of flow rates up to 50 μL min^{-1} (the data not shown).

Relationships between the flow rates and pressure as well as those between the average linear velocities and pressure are shown in Fig. 2-6. The formation and non-formation are presented with the symbols of ○ and ×, respectively. It was found out from the data that border average linear velocity in the TRDP between formation and non-formation was the same for all conditions of inner diameters and effective lengths. The energy generated by the average linear velocity, 1.13 cm min^{-1}, might be required for the break of the axial distribution of the solvents.

2.3.4. Effects of tube inner diameter on fluorescence photographs

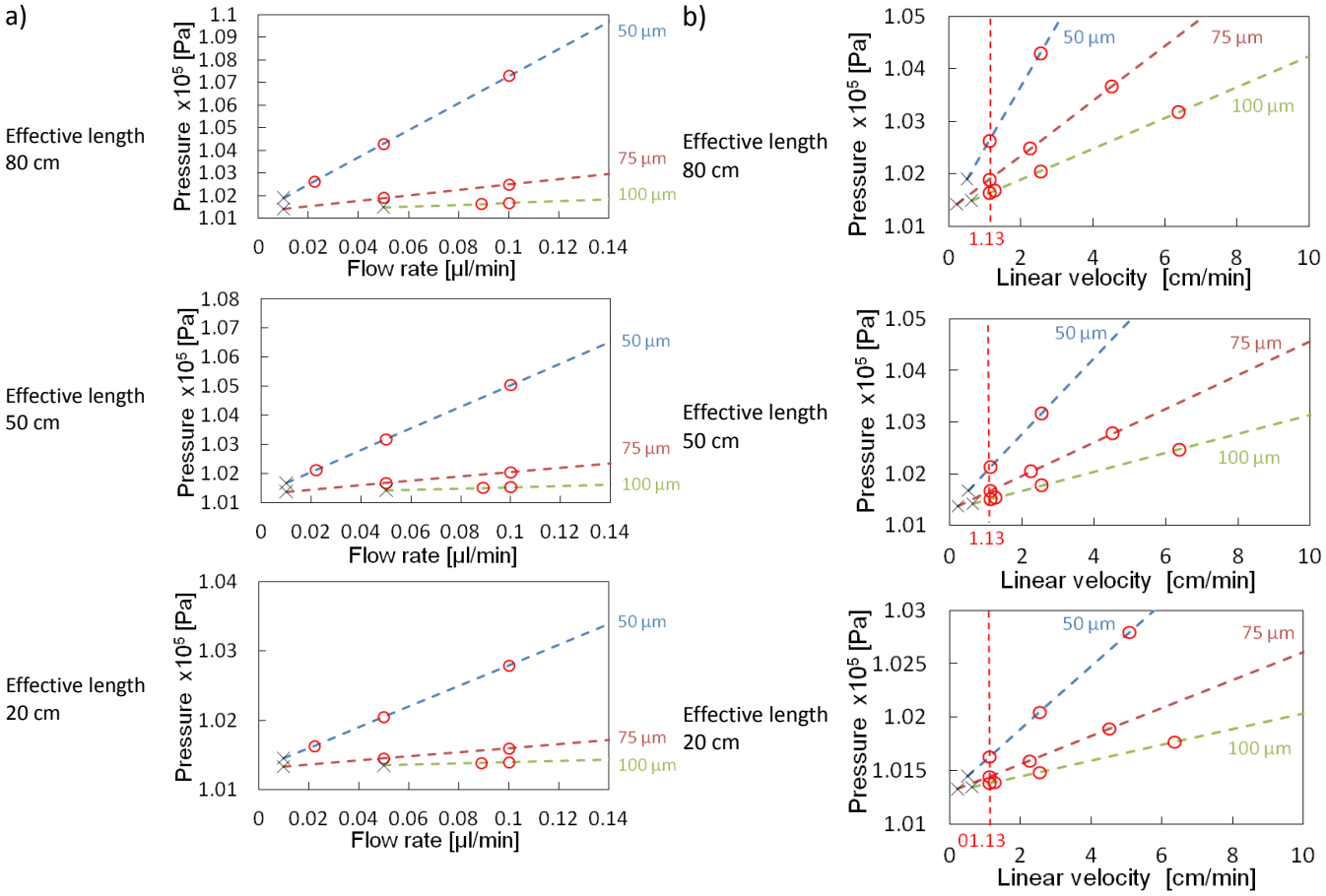

Fig. 2-6 Relationships between a) flow rates and pressure as well as b) average linear velocities and pressures in tube radial distribution phenomenon of the ternary mixed solvents at tube temperature of 0 °C.

Conditions: Capillary tube, 110 cm (effective length: 20, 50, and 80 cm cm) of 50, 75, and 100 μm i.d. fused-silica; carrier, water–acetonitrile–ethyl acetate (3:8:4 volume ratio) containing perylene (0.1 mM) and Eosin Y (1.0 mM).

The author examined the effects of the tube inner diameter on fluorescence photograph in the TRDC system. The author attempted to use commercially available fused-silica capillary tubes with various inner diameters; the capillary tubes with i.d. 50–700 μm were used here. The obtained fluorescence photographs are shown in Fig. 2-7 together with the analytical conditions. The flow rates for all the capillary tubes were adjusted to provide almost the same average linear velocity of ca. 22 cm min^{-1}. The inner and outer formation was observed in the fluorescence photographs.

2.3.5. Separation of mixture solution including four analytes

The author examined a mixture analyte solution of 1-naphthol, 1-naphthalenesulfonic acid, 2,6-naphthalenedisulfonic acid, and 1,3,6-naphthalenetrisulfonic acid using the present TRDC system with organic solvent-rich carrier solution. The obtained chromatograms are shown in Fig. 2-8 together with the analytical conditions. 1-Naphthol, 1-naphthalenesulfonic acid, 2,6-naphthalenedisulfonic acid, and 1,3,6-naphthalenetrisulfonic acid were eluted in this order, leading to good separation with the organic solvent-rich carrier solution in the inner diameters of 50, 75 and 100 μm (Fig. 2-8). The elution order seemed to be consistent with the hydrophilic character. With 200, 250, and 300 μm inner diameter, 2,6-naphthalenedisulfonic acid and 1,3,6-naphthalenetrisulfonic acid were not separated. With 530 μm inner diameter, 1-Naphthol and

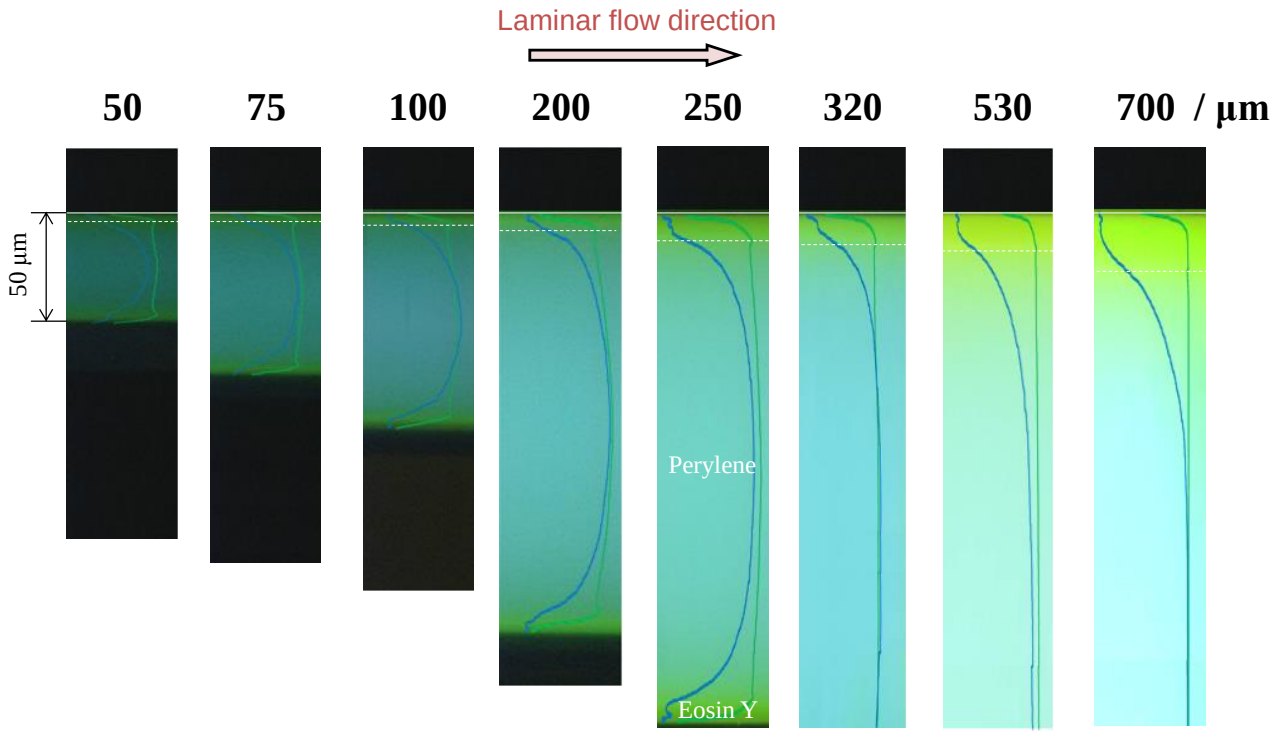

Fig. 2-7 Fluorescence photographs in the capillary tubes having various inner diameters. Capillary inner diameter, 50, 75, 100, 200, 250, 320, 530, and 700 µm.

Conditions: Capillary tube, 110 cm (effective length: 80 cm) of fused-silica; carrier, water–acetonitrile–ethyl acetate (3:8:4 volume ratio) containing perylene (0.1 mM) and Eosin Y (1.0 mM), and average linear velocity of 11 cm min^{-1} for all tubes.

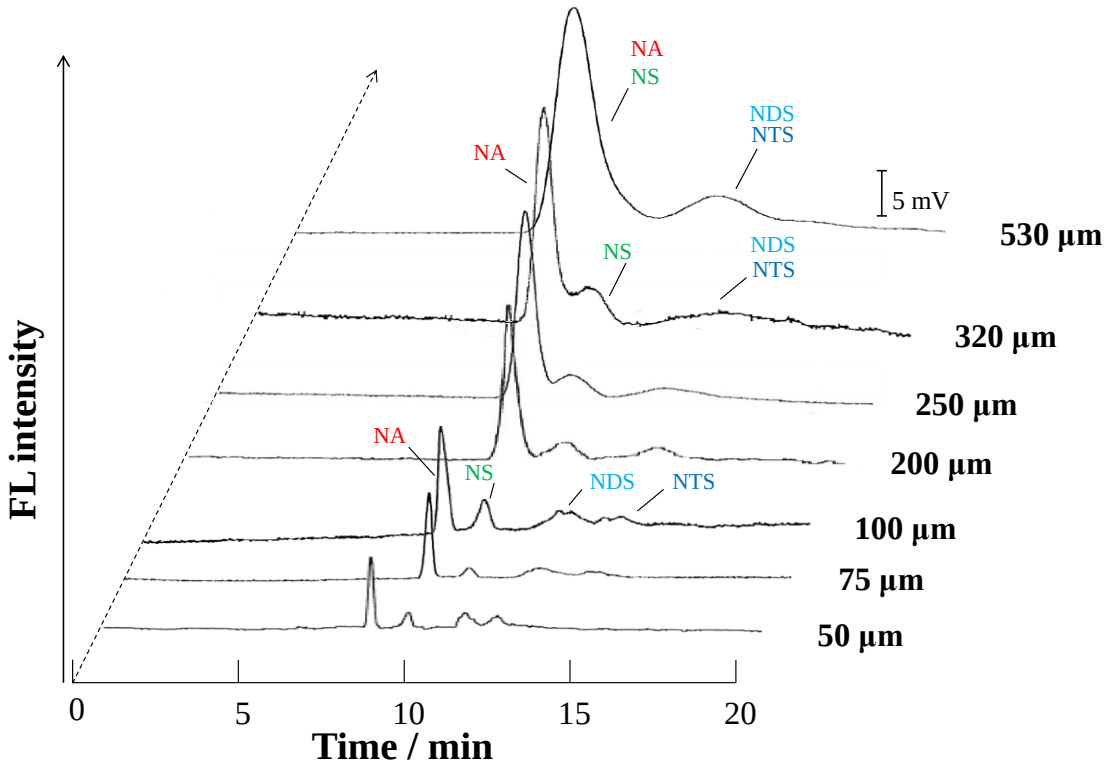

Fig. 2-8 Chromatograms of a mixture analyte solution of 1-naphthol (NA), 1-naphthalenesulfonic acid (NS), 2,6-naphthalenedisulfonic acid (NDS), and 1,3,6-naphthalenetrisulfonoc acid (NTS) obtained by the present TRDC system.

Conditions: Capillary tube, 120 cm (effective length: 100 cm) of 75 µm i.d. fused-silica; carrier, water–acetonitrile–ethyl acetate (3:8:4 v/v/v) mixture solution; sample injection, gravity method from 20 cm height (5.4 mm sample length); average linear velocity, 11 cm min^{-1}; temperature, 20 °C; and 1-naphthol, 1-naphthalenesulfonic acid; detection, fluorescence, ex. 290 nm and em. 355 nm; and 2,6-naphthalenedisulfonic acid, 1 mM, 1,3,6-naphthalenetrisulfonic acid, 2.0 mM.

1-naphthalenesulfonic acid as well as 2,6-naphthalenedisulfonic acid and 1,3,6-naphthalenetrisulfonic acid were not separated on the chromatogram.

2.4. Conclusion

The tube radial distribution of the carrier solvents was examined at various conditions through the fluorescence microscope-CCD camera system to get new information concerning TRDP. Also, separation performance was examined for the model mixture analytes in the capillary chromatography, i.e., TRDC. As a result, the linear velocity to generate TRDP is turned out and separation performance of TRDC in various diameter capillary is confirmed.

References

1) N. Jinno, M. Itano, M. Hashimoto, and K. Tsukagoshi, *Talanta*, **79**, 1348 (2009).
2) M. Murakami, N. Jinno, M. Hashimoto, and K. Tsukagoshi, *Anal. Sci.*, **27**, 793 (2011).
3) N. Jinno, M. Hashimoto, and K. Tsukagoshi, *Anal. Sci.*, **27**, 259 (2011).
4) N. Jinno, M. Murakami, K. Mizohata, M. Hashimoto, and K. Tsukagoshi, *Analyst*, **136**, 927 (2011).
5) N. Jinno, M. Murakami, M. Hashimoto, and K. Tsukagoshi, *Anal. Sci.*, **26**, 737 (2010).

6) S. Fujinaga, N. Jinno, M. Hashimoto, and K. Tsukagoshi, *J. Sep. Sci.*, **34**, 2833 (2011).

7) Y. Kudo, H. Kan, N. Jinno, M. Hashimoto, and K. Tsukagoshi, *Anal. Methods*, **4**, 906 (2012).

8) N. Jinno, M. Murakami, K. Mizohata, M. Hashimoto, and K. Tsukagoshi, *J. Liq. Chromatogr. Relat. Technol.*, **35**, 1750 (2012).

Chapter 3

Influence of Composition of Ternary Mixture Solvent System for Tube Radial Distribution Chromatography

3.1. Introduction

In this chapter, the types of solvents and their volume ratios in a ternary solvent mixture of water–hydrophilic organic solvent–hydrophobic organic solvent were investigated for TRDC. The optimum solvent mixture was determined using phase diagrams, chromatograms, and fluorescence photographs. A hydrophilic organic solvent (acetonitrile, ethanol, methanol, 1-propanol, or 1,4-dioxane) and hydrophobic organic solvent (ethyl acetate, hexane, 1-butanol, or chloroform) were mixed with water to produce a ternary water–hydrophilic organic solvent–hydrophobic organic solvent system. The water–acetonitrile–chloroform solvent system was examined in detail and compared with a water–acetonitrile–ethyl acetate solvent system, which is commonly used in the TRDC.

3.2. Experimental

3.2.1. Reagents and capillary tubes

Water was purified with an Elix 3 UV system (Millipore Co., Billerica, MA, USA). All reagents used were commercially available and of analytical grade. 1-Naphthol, 1-naphthalenesulfonic acid, 2,6-naphthalenedisulfonic acid, 1,3,6-naphthalenetrisulfonic acid, acetonitrile, methanol, ethanol, 1-propanol, 1,4-dioxane, ethyl acetate, 1-butanol, chloroform, hexane, Eosin Y, and perylene were purchased from Wako Pure Chemical Industries,

Ltd. (Osaka, Japan). Fused-silica capillary tubes (inner diameter: 50 μm) were purchased from GL Science Co. (Tokyo, Japan).

3.2.2. Open-tubular capillary chromatography

The TRDC system included an open fused-silica capillary tube (total length 120 cm and effective length 100 cm), microsyringe pump (MF-9090; Bioanalytical Systems, Inc., West Lafayette, IN, USA), and absorption detector (modified SPD-10AV spectrophotometric detector; Shimadzu Co., Kyoto, Japan) (Fig. 3-1 a)). The tube temperature was controlled by dipping the capillary tube in water maintained at a set temperature in a beaker with stirring. Various water–hydrophilic organic solvent–hydrophobic organic solvent systems were used as the carrier solution. Analyte solutions were prepared with the carrier solutions.

The analyte solution was introduced directly into the capillary inlet by the gravity method (from a height of 20 cm and for 30 s). After analyte injection, the capillary inlet was connected to a microsyringe attached to a pump. The carrier solution was fed into the capillary tube at a set flow rate under laminar flow conditions. On-capillary absorption detection (254 nm) was performed.

3.2.3. Fluorescence microscope-charge coupled device (CCD) camera system

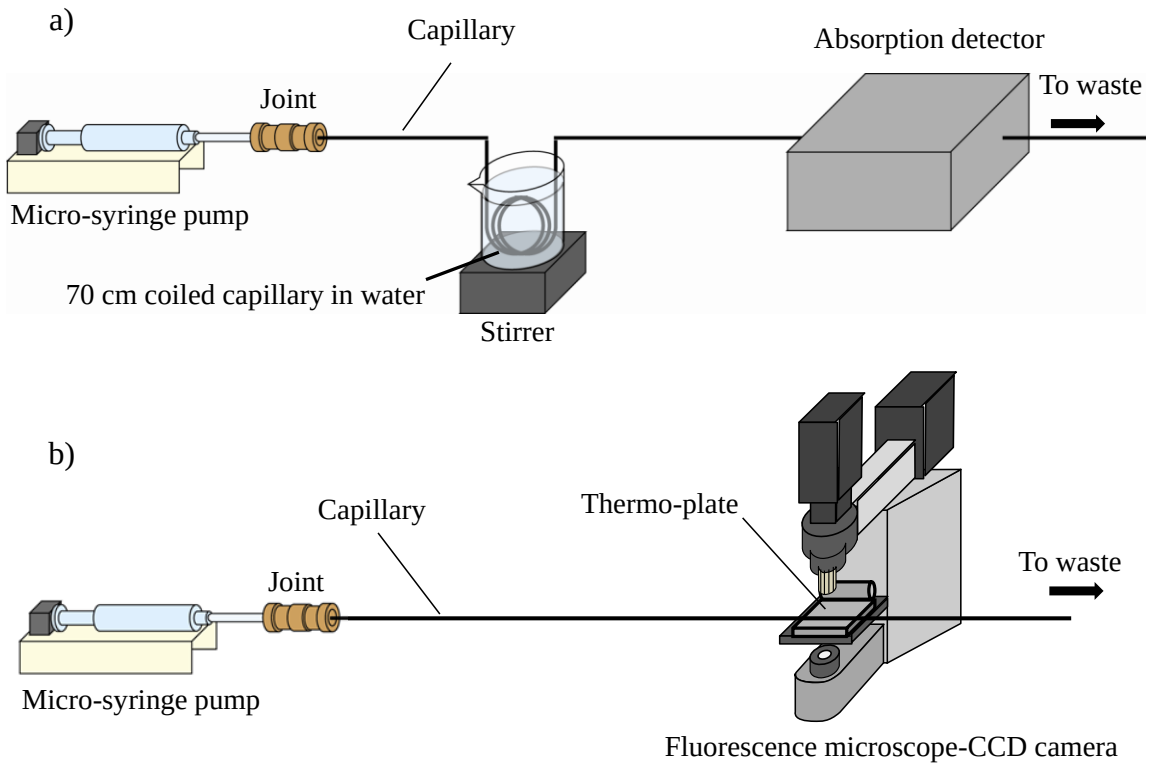

Fig. 3-1 Schematic diagrams of a) the present TRDC and b) the fluorescence microscope-CCD camera.

To monitor TRDP with the solvent system, the capillary tube was set up with a fluorescence microscope-CCD camera system (Fig. 3-1 b). Ternary water–hydrophilic organic solvent–hydrophobic organic solvent systems, with various volume ratios and containing perylene and Eosin Y, were used. The fluorescence in the capillary tube was monitored using a fluorescence microscope (BX51; Olympus, Tokyo, Japan) equipped with an Hg lamp, a filter (U-MWU2, excitation 330–385 nm, emission >420 nm), and a CCD camera (JK-TU53H). Perylene and Eosin Y emit light at 470 and 550 nm, respectively, and because of this the resulting fluorescence was mainly blue and green. The fluorescence photographs were transformed into line drawings to assess the color (red, green, and blue) depth. These were expressed as digital data on a computer, and the numbers were standardized to the line drawing data to give the fluorescence profiles.

3.3. Results and Discussion

3.3.1. Preliminary experiment

The hydrophilic organic solvent was acetonitrile, methanol, ethanol, 1-propanol, or 1,4-dioxane. Phase diagrams of water–hydrophilic organic solvent–ethyl acetate ternary solutions were examined at 0 and 20 °C (Fig. 3-2). The curves in the phase diagram show the boundary or solubility curves between homogeneous (single phase) and heterogeneous (two phases) solutions. The separation performance for a model analyte mixture

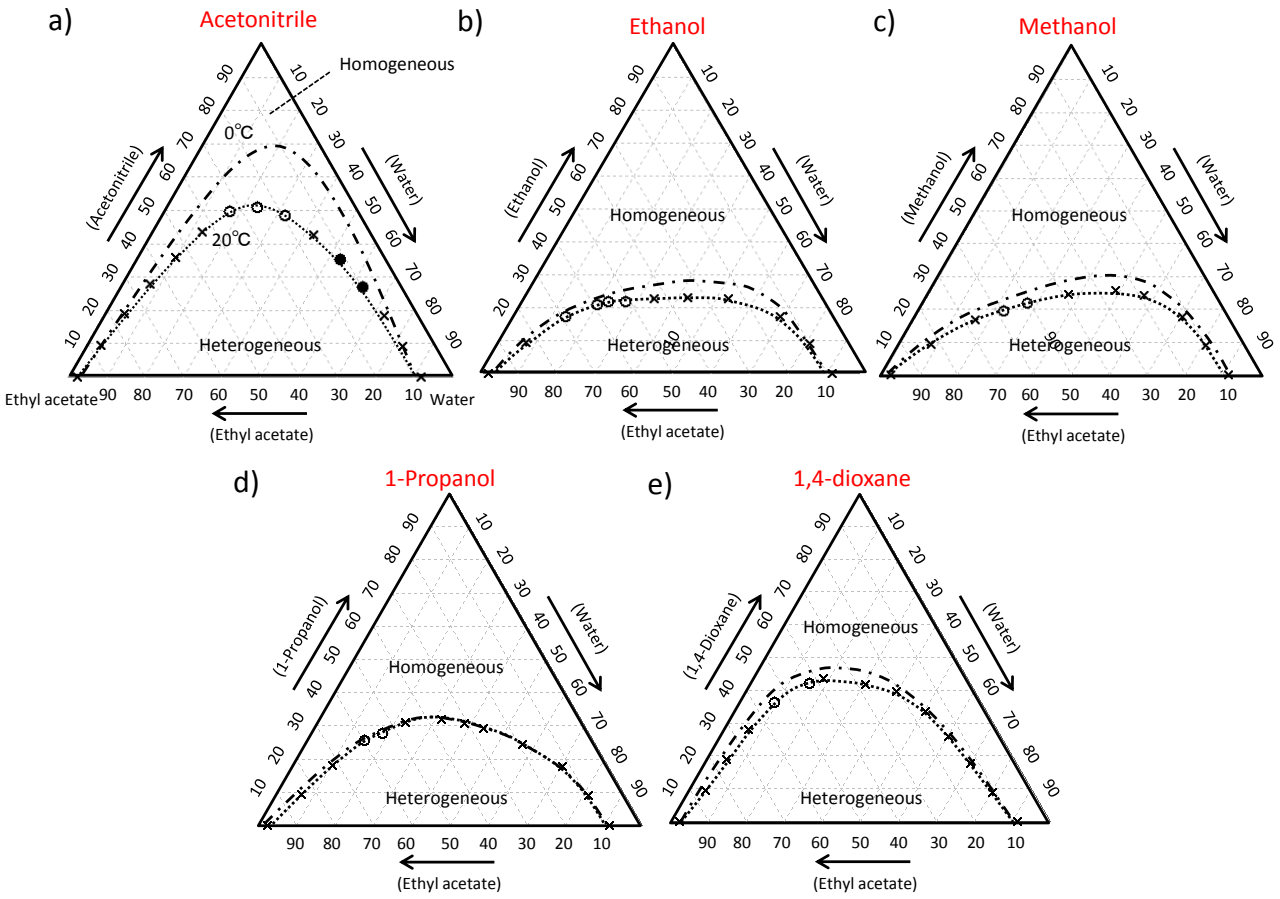

Fig. 3-2 Phase diagrams for water–hydrophilic organic solvent–ethyl acetate solvent systems, and separation performance of a 1-naphthol and 2,6-naphthalenedisulfonic acid mixture on chromatograms.

a) Acetonitrile, b) methanol, c) ethanol, d) 1-propanol, and e) 1,4-dioxane. The dotted-dashed and dotted curves show the boundaries between homogeneous and heterogeneous solutions at 0 and 20 °C. The symbols ○, ●, and × show separation with 1-naphthol eluted before 2,6-naphthalenedisulfonic acid, separation with 2,6-naphthalenedisulfonic acid eluted before 1-naphthol, and no separation, respectively. Chromatography conditions: capillary tube, 120 cm (effective length, 100 cm) of 50 μm i.d. fused-silica; carrier, water–hydrophilic organic solvent–ethyl acetate; sample injection, 20 cm height (gravity)×30 s; flow rate, 0.2 μL min^{-1}; tube temperature, 3 °C; and 1-naphthol and 2,6-naphthalenedisulfonic acid concentrations, 2 mmol L^{-1} each.

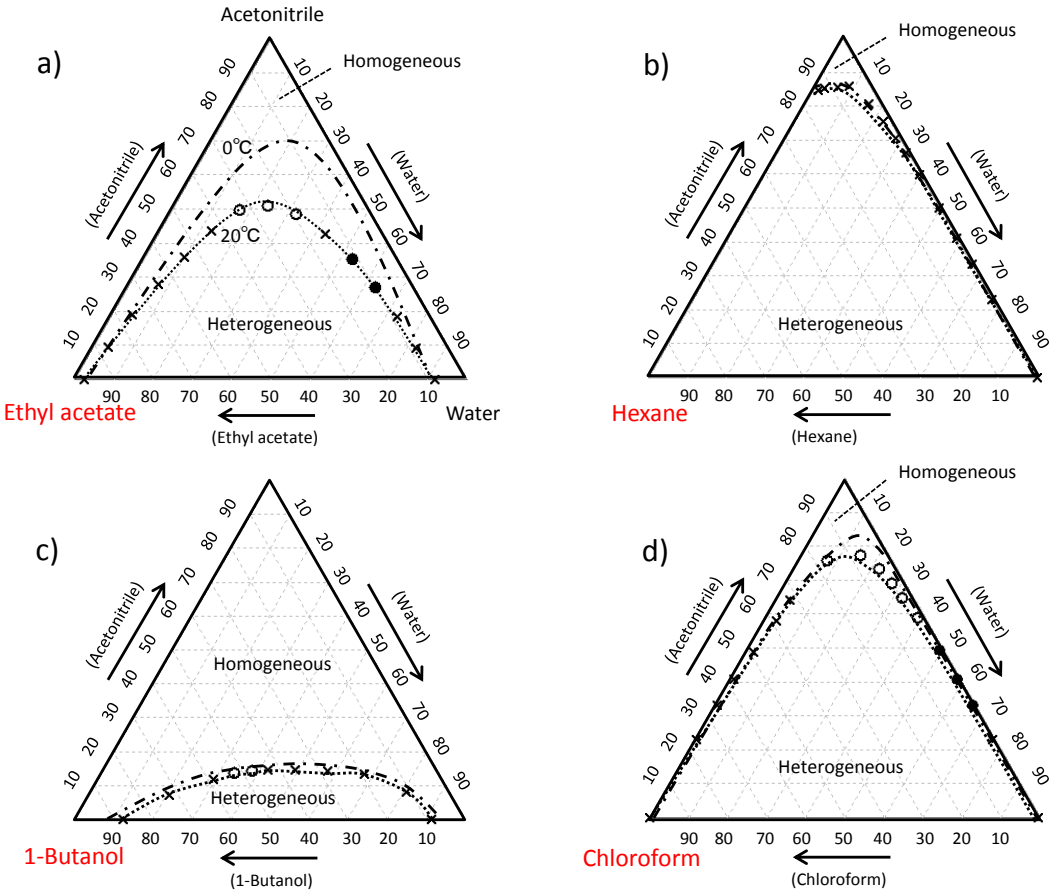

Fig. 3-3 Phase diagrams for water–acetonitrile–hydrophobic organic solvent systems, and separation performance of a 1-Naphthol and 2,6-naphthalenedisulfonic acid mixture on chromatograms.

a) Ethyl acetate, b) hexane, c) 1-butanol, and d) chloroform. The dotted-dashed and dotted curves show the boundaries between homogeneous and heterogeneous solutions at 0 and 20 °C. The symbols ○, ●, and × show separation with 1-naphthol eluted before 2,6-naphthalenedisulfonic acid, separation with 2,6-naphthalenedisulfonic acid eluted before 1-Naphthol, and no separation. The chromatography conditions are the same as those in Fig. 3-2.

of 1-naphthol and 2,6-naphthalenedisulfonic acid in TRDC was examined. The volume ratios of the components in the homogeneous ternary solvent solutions were positioned near the boundary curve at 20 °C. With an organic solvent-rich solution, 1-naphthol eluted before 2,6-naphthalenedisulfonic acid. By contrast, with a water-rich solution, 2,6-naphthalenedisulfonic acid eluted before 1-naphthol. This reversal of the elution order for the analytes was only achieved with the water–acetonitrile–ethyl acetate system. With the other ternary mixtures investigated, 1-naphthol eluted before 2,6-naphthalenedisulfonic acid with organic solvent-rich solutions and no separation occurred with water-rich solutions.

3.3.2. Preliminary experiments with water–acetonitrile–hydrophobic solvent mixtures

The hydrophobic organic solvent was ethyl acetate, chloroform, 1-butanol, or hexane. Phase diagrams of the water–acetonitrile–hydrophobic organic solvent mixtures were examined at 0 and 20 °C (Fig. 3-3). The separation performance for a model analyte mixture of 1-naphthol and 2,6-naphthalenedisulfonic acid was investigated. The volume ratios of the components in the homogeneous ternary solvent systems were positioned near the boundary curve at 20 °C. The separation order of the analytes in TRDC was reversible using different volume ratios with water–acetonitrile–chloroform and water–acetonitrile–ethyl acetate.

a) Pressure constant (1 atm)

b) Temperature constant (20 ℃)

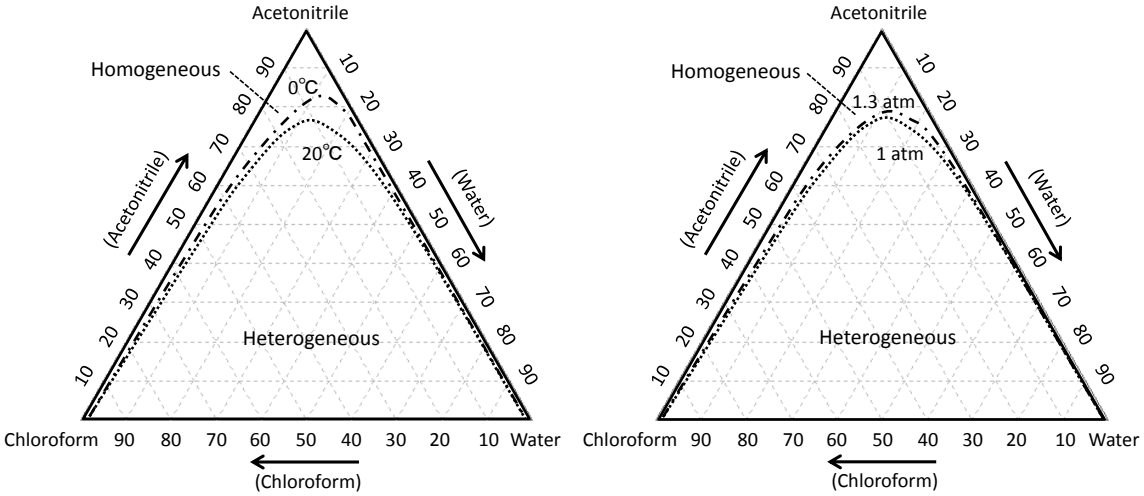

Fig. 3-4 Phase diagrams for the water–acetonitrile–chloroform solvent system. a) Constant pressure (1 atm) and b) constant temperature (20 °C).

With water–acetonitrile–1-butanol, 1-naphthol was eluted before 2,6-naphthalenedisulfonic acid when the mixture was organic solvent-rich. With the water–acetonitrile–hexane mixture, 1-naphthol and 2,6-naphthalenedisulfonic acid were not separated.

3.3.3. Phase diagrams, chromatograms, and fluorescence photographs with water–acetonitrile–chloroform

Because water–acetonitrile–chloroform performed in a similar manner to water–acetonitrile–ethyl acetate, the author examined the water–acetonitrile–chloroform system in more detail using phase diagrams, chromatograms, and fluorescence photographs. Fig. 3-4 shows the phase diagrams of the water–acetonitrile–chloroform system. At constant pressure (1 atm), as the temperature decreased from 20 to 0 °C, the boundary curve expanded (Fig. 3-4 a)). The curve also expanded as the pressure was increased from 1.0 to 1.3 atm at a constant temperature (20 °C) (Fig. 3-4 b)). These changes in the boundary curves are similar to those observed in an earlier study for water–acetonitrile–ethyl acetate.[1)]

Separation information of the 1-naphthol and 2,6-naphthalenedisulfonic acid mixture with the water–acetonitrile–chloroform system is shown in the phase diagram with the symbols (Fig. 3-5). With an organic-solvent rich carrier solution (solutions (f)–(k) in Fig. 3-5), 1-naphthol was eluted before 2,6-naphthalenedisulfonic acid. By contrast, with a water-rich carrier

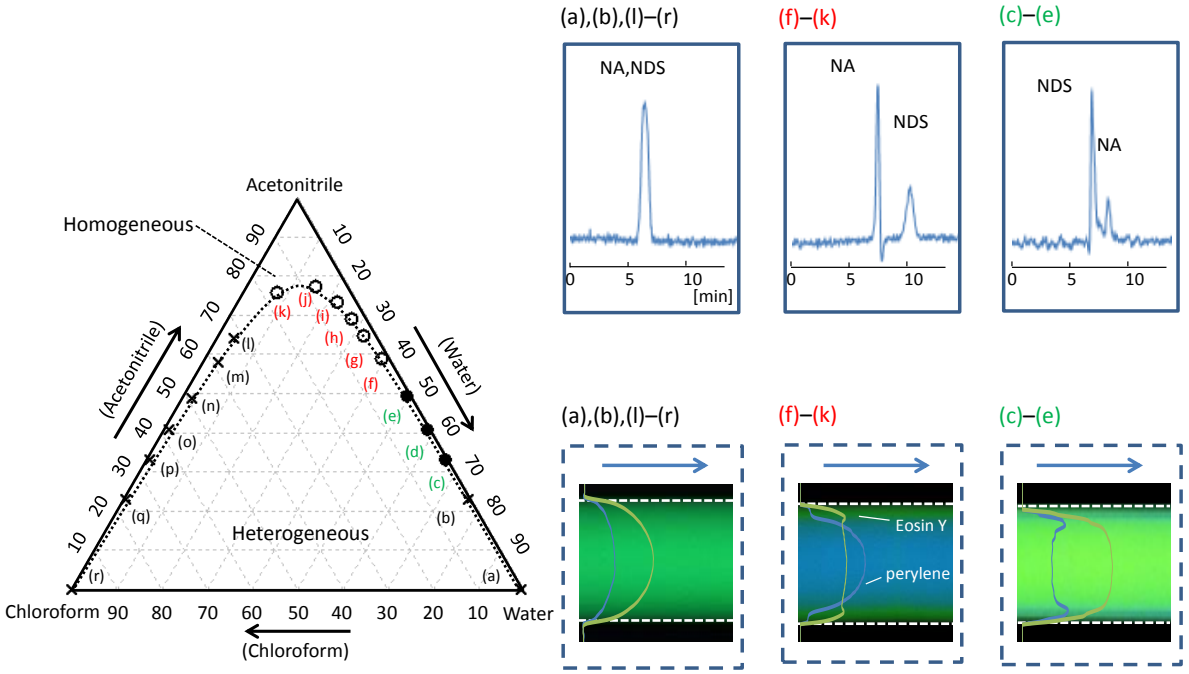

Fig. 3-5 Phase diagrams, chromatograms, and fluorescence photographs for the water–acetonitrile–chloroform solvent system.

Water–acetonitrile–chloroform volume ratios were as follows: (a) 99.5:0:0.5, (b) 76.2:23:0.8, (c) 66:33:1, (d) 58:41:1, (e) 49.5:49.5:1, (f) 39:59:2, (g) 32:65:3, (h) 27:69:4, (i) 22:73:5, (j) 15:77:8, (k) 8:76:16, (l) 4:64:32, m) 4:58:38, (n) 2:49:49, (o) 1:41:58, (p) 0.7:33:66.3, (q) 0.5:23:76.5, and (r) 0.1:0:99.9, containing perylene (~0.1 mmol L^{-1}) and Eosin Y (~1.0 mmol L). The symbols ○, ●, and × show separation with 1-naphthol (NA) eluted before 2,6-naphthalenedisulfonic acid (NDS), separation with 2,6-naphthalenedisulfonic acid eluted before 1-naphthol, and no separation. Chromatography conditions are the same as those in Fig. 3-2.

solution (solutions (c)–(e)), 2,6-naphthalenedisulfonic acid eluted before 1-naphthol. With solutions (a), (b), and (l)–(r), 2,6-naphthalenedisulfonic acid and 1-naphthol were not separated under the present conditions. Typical chromatograms are shown in Fig. 3-5.

Typical fluorescence photographs are also shown in Fig.3-5. TRDP was observed in the mixtures (f)–(k), which had an organic solvent-rich major inner phase and water-rich minor outer phase, and (c)–(e), which had a water-rich major inner phase and organic solvent-rich minor outer phase. TRDP was not observed in mixtures (a), (b), and (l)–(r). In other words, when organic solvent-rich solutions ((f)–(k)) were delivered into the capillary tube, the major phase that formed in the tube was organic solvent-rich. By contrast, when water-rich solutions ((c)–(e)) were delivered into the capillary tube, the major phase that formed in the tube was water-rich.

Separation of compounds by TRDC is based on the distribution of the hydrophilic compounds (e.g. 2,6-naphthalenedisulfonic acid) in the water-rich phase and hydrophobic compounds (e.g. 1-naphthol) in the organic solvent-rich phase. The outer phase acts as a pseudo-stationary phase under laminar flow conditions. In the present study, the elution order in the chromatograms was consistent with this separation mechanism. With an organic solvent-rich inner phase 1-naphthol eluted before 2,6-naphthalenedisulfonic acid, while with a water-rich inner phase 2,6-naphthalenedisulfonic acid eluted before 1-naphthol. The mixtures that did not show TRDP did not provide chromatographic separation in the

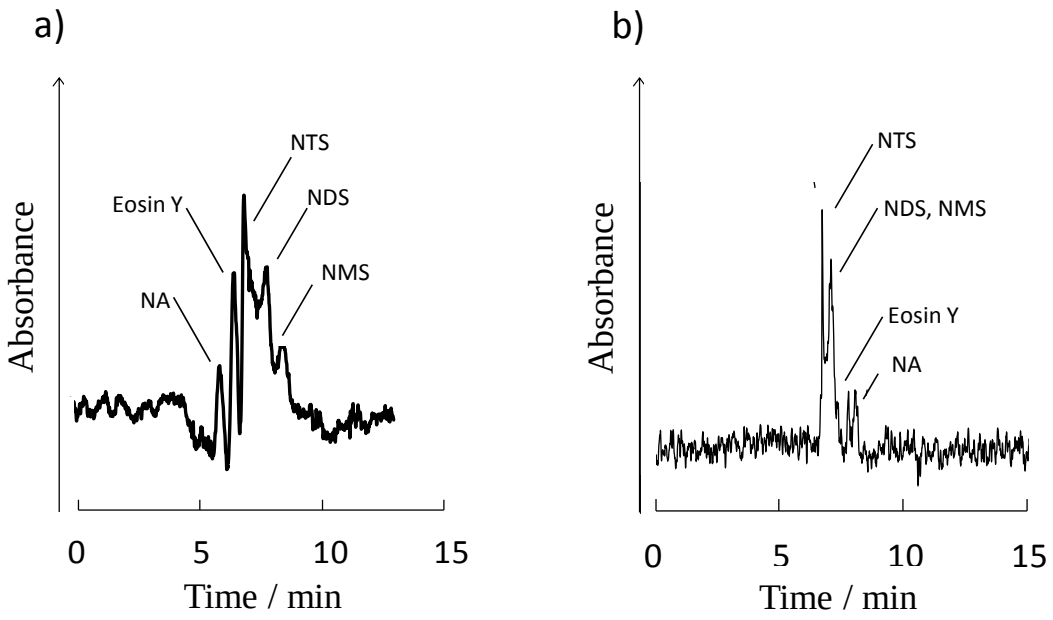

Fig. 3-6 Chromatograms of the analyte mixture of 1-naphthol (NA), Eosin Y, 1-naphthalenesulfonic acid (NS), 2,6-naphthalenedisulfonic acid (NDS), and 1,3,6-naphthalenetrisulfonic acid (NTS) obtained by TRDC with the water–acetonitrile–chloroform solvent system.

Conditions: Capillary tube, 120 cm (effective length: 100 cm) of 50 μm i.d. fused-silica; carrier, water–acetonitrile–chloroform a) organic solvent-rich (20:53:27 volume ratio) and b) water-rich (75:15:10 volume ratio); sample injection, 20 cm height (gravity)×30 s; flow rate, 0.2 μL min^{-1}; tube temperature, 3 °C; and 1-naphthol, 1-naphthalenesulfonic acid, 2,6-naphthalenedisulfonic acid and 1,3,6-naphthalenetrisulfonic acid 1 mmol L^{-1} each and Eosin Y 0.5 mmol L^{-1}.

TRDC. The TRDP and TRDC results with the water–acetonitrile–chloroform system were the same as those observed for the water–acetonitrile–ethyl acetate system. [2-5)]

3.3.4. Separation of an analyte mixture

The author examined separation of an analyte mixture (1-naphthol, Eosin Y, 1-naphthalenesulfonic acid, 2,6-naphthalenedisulfonic acid, and 1,3,6-naphthalenetrisulfonic acid) using the TRDC system with organic solvent-rich and water-rich carrier solutions prepared using the water–acetonitrile–chloroform system. The obtained chromatograms are shown in Fig. 3-6. The elution orders of the analytes were different with the organic solvent-rich and the water-rich carrier solutions, as reported for other TRDC systems.[5)] With the organic-solvent rich carrier solution, the elution order was 1-naphthol, Eosin Y, 1-naphthalenesulfonic acid, 2,6-naphthalenedisulfonic acid, and finally 1,3,6-naphthalenetrisulfonic acid (Fig. 3-6 a)). This elution order is consistent with increasingly hydrophilic character of the compounds. By contrast, with the water-rich carrier solution, the comparatively hydrophilic compound, 1,3,6-naphthalenetrisulfonic acid, was eluted first, followed by co-elution of 1-naphthalenesulfonic acid and 2,6-naphthalenedisulfonic acid, and then the hydrophobic compounds Eosin Y and 1-naphthol (Fig. 3-6 b)). This elution order was the reverse of that observed with the organic solvent-rich carrier solution.

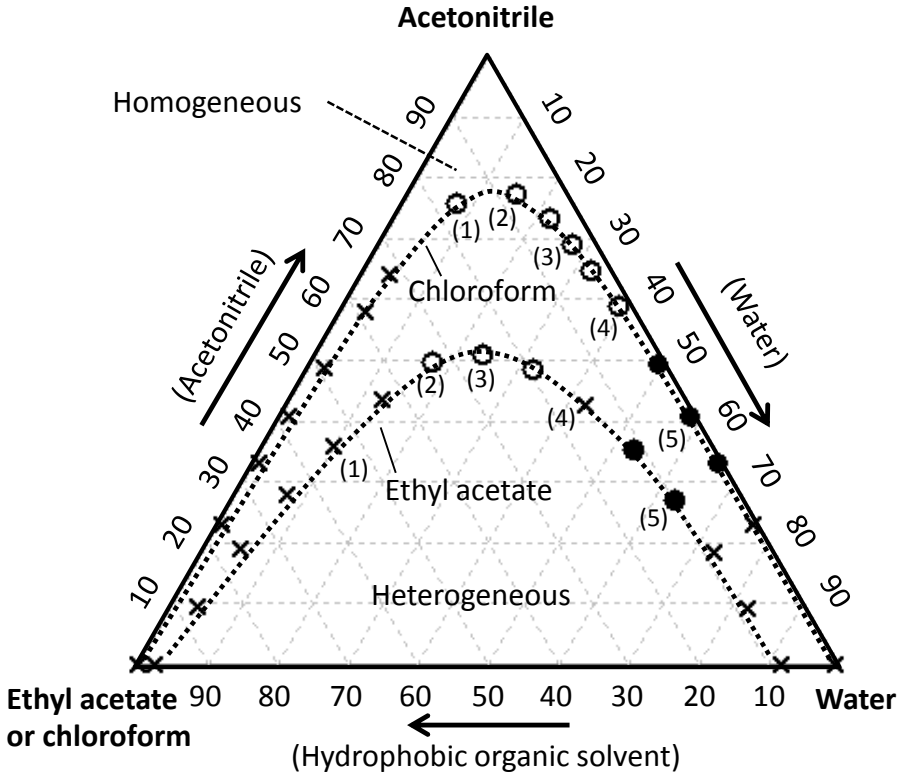

Fig. 3-7. Comparison of phase diagrams and TRDC separation performance with water–acetonitrile–ethyl acetate and water–acetonitrile–chloroform solvent systems.

The volume ratios of the upper and lower phases in a batch vessel are as follows: Water-rich:organic solvent-rich; (1) 2:98, (2) 10:90, (3) 28:72, (4) 60:40, and (5) 90:10 in the two systems. The symbols ○, ●, and × show separation with 1-naphthol eluted before 2,6-naphthalenedisulfonic acid, separation with 2,6-naphthalenedisulfonic acid eluted before 1-naphthol, and no separation.

3.3.5. Comparison of water–acetonitrile–ethyl acetate and water-acetonitrile–chloroform solvent systems

Fig. 3-7 shows the phase diagrams (20 °C) and separation performance for the water–acetonitrile–ethyl acetate and water–acetonitrile–chloroform solvent systems. The water–acetonitrile–ethyl acetate and the water–acetonitrile–chloroform solvent systems have quite different boundaries in the phase diagrams. Therefore, the author never compare their separation performance with similar ratios for the ternary components of the solvent system.

The author, tentatively, investigated the TRDC separation performance through carrier solutions with same volume ratios for the two phases, an organic solvent-rich and a water-rich, at a lower temperature in a batch vessel. The composition positions in the phase diagram, (1)–(5) in Fig 3-7, showed the same volume ratios of the two phases both for the water-acetonitrile-ethyl acetate and the water–acetonitrile–chloroform solution systems, and these ratios are also given in the figure captions. The separation performance for 1-naphthol and 2,6-naphthalenedisulfonic acid depended on the ratio of the organic solvent-rich and water-rich phases (Fig. 3-7); with the ethyl acetate system the upper and lower phases were an organic solvent-rich and water-rich solutions, respectively, while, with the chloroform system the upper and lower phases were a water-rich and organic solvent-rich solutions, respectively. TRDC separation was achieved with the chloroform system with a wider range of

Table 3-1 Comparison of separation performance with TRDC and chromatographic resolutions for water–acetonitrile-ethyl acetate and water–acetonitrile-chloroform solvent systems.
The composition number means the mixed solvent solution in Fig. 3-6. The symbols ○, ●, and × show separation with 1-naphthol eluted before 2,6-naphthalenedisulfonic acid, separation with 2,6-naphthalenedisulfonic acid eluted before NA, and no separation, respectively. The resolutions are calculated based on the chromatograms of 1-naphthol and 2,6-naphthalenedisulfonic acid separation.

Composition number	Volume ratio (water : organic solvent)	TRDC		Resolutions	
		Ethyl acetate system	Chloroform system	Ethyl acetate system	Chloroform system
(1)	2 : 98	×	○	-	0.58
(2)	10 : 90	○	○	3.8	0.77
(3)	28 : 72	○	○	5.6	0.88
(4)	60 : 40	×	○	-	2.0
(5)	90 : 10	●	●	0.75	2.0

organic solvent-rich and water-rich volume ratios than for the ethyl acetate system. The reason has not been clear yet. Chloroform is more hydrophobic (logP, 1.97) than ethyl acetate (logP, 0.73), and this might generate a more stable liquid-liquid interface between water-rich and organic solvent-rich phases through TRDP.

Table 3-1 shows the resolutions for the model analytes, 1-naphthol and 2,6-naphthalenedisulfonic acid, obtained with the ethyl acetate and the chloroform solvent systems. The ethyl acetate system provided better resolution than the chloroform system, although TRDP was observed over a wider range of volume ratios for the chloroform system than for the ethyl acetate system. The author examined the distribution ratios, *D*, in the two solvent systems with various compositions ((1)–(5) in Figs. 3-7 and 3-8) at low temperature, generating upper and lower phases, in a batch vessel. *D* is given by the ratio of analyte concentration in the organic-solvent rich phase to analyte concentration in the water-rich phase. If $D>1$, most of the analyte is dissolved in the organic solvent-rich phase, and if $D<1$, most of the analyte is dissolved in the water-rich phase. The concentrations of the analytes in the two phases were determined using capillary electrophoresis with a calibration curve.

For 1-naphthol, all the *D* values (solutions (1)–(5)) were greater than one, which indicates it was easier for 1-naphthol to dissolve in an organic solvent-rich solution than a water-rich solution. The D values of the ethyl acetate system (4.2–14.5) were larger than those of the chloroform system (1.5–3.0). For 2,6-naphthalenedisulfonic acid, all the *D* values (solutions

a) Water-acetonitrile-ethyl acetate

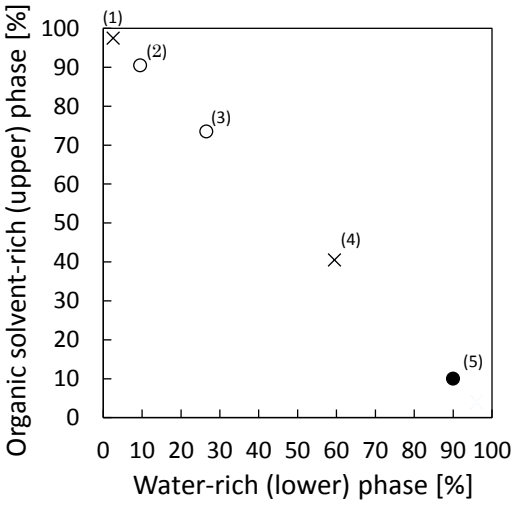

b) Water-acetonitrile-chloroform

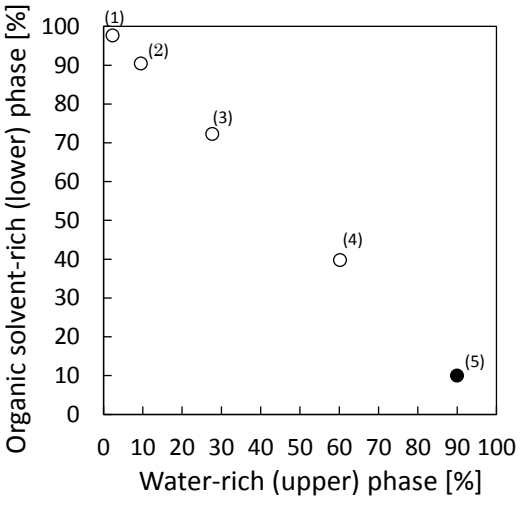

Fig. 3-8 The separation performance with various volume ratios of upper and lower phases in a) water–acetonitrile–ethyl acetate and b) water–acetonitrile–chloroform solvent systems.

The volume ratios of the upper and lower phases in a batch vessel are as follows: Water-rich:organic solvent-rich; (1) 2:98, (2) 10:90, (3) 28:72, (4) 60:40, and (5) 90:10 in the two systems. The symbols of ○, ●, and × mean show separation with 1-naphthol eluted before 2,6-naphthalenedisulfonic acid, separation with 2,6-naphthalenedisulfonic acid eluted before 1-naphthol, and no separation.

(1)–(5)) were less than one, which indicates it was easier for 2,6-naphthalenedisulfonic acid to dissolve in a water-rich solution than an organic solvent-rich solution. The *D* values of the ethyl acetate system (0.5–0.25) were smaller than those of the chloroform system (0.30–0.65). Consequently, 1-naphthol dissolves in the organic solvent-rich phase and 2,6-naphthalenedisulfonic acid in the water-rich phase with the ethyl acetate system more effectively than the chloroform system. That is, the trends observed with the *D* values are consistent with the better resolution for 1-naphthol and 2,6-naphthalenedisulfonic acid observed with the ethyl acetate system compared with the chloroform system.

3.4. Conclusion

The author examined various water–hydrophilic organic solvent–hydrophobic organic solvent systems for TDRP and TRDC. Phase diagrams, fluorescence photographs, and chromatograms for a water–acetonitrile–chloroform solvent system showed particular TRDP and TRDC. The performance of this solvent system in TRDC was comparable to that of a water–acetonitrile–ethyl acetate system. The change of separation performance due to the difference of the carrier solution was discussed from the distribution ratio of the sample. The results of this study provide basic data on the microfluidic behavior, TRDP, and the separation technology, TRDC, with the studied solvent systems.

References

1) S. Fujinaga, K. Unesaki, S. Negi, M. Hashimoto, K. Tsukagoshi, *Anal. Methods*, **4**, 3884 (2012).

2) M. Murakami, N. Jinno, M. Hashimoto, and K. Tsukagoshi, *Anal. Sci.*, **27**, 793 (2011).

3) N. Jinno, M. Murakami, K. Mizohata, M. Hashimoto, and K. Tsukagoshi, *Analyst*, **136**, 927 (2011).

4) K. Tsukagoshi, *Anal. Sci.*, **30**, 65 (2014).

5) N. Jinno, M. Murakami, M. Hashimoto, K. Tsukagoshi, *Anal. Sci.*, **26**, 737 (2010).

Chapter 4

Introduction of Absorption Reagent to Tube Radial Distribution Chromatography for Separation and Online Detection of Metal Ion

4.1. Introduction

The TRDC system worked without applying high voltages or using specific columns, monolithic or packed, in contrast to other capillary separation techniques, such as capillary electrophoresis and capillary electrochromatography. Various types of analyte, such as organic compounds,[1] amino acids,[2] proteins,[2-4] nucleosides,[5] metal ions,[3,5] metal complexes,[3,5] fluorescent compounds,[4] and optical isomers,[6] were analyzed using the TRDC system. However, metal ions and metal complexes were separated and detected by the TRDC system equipped with chemiluminescence detection. The metal ions and metal complexes show catalytic activity for luminol-hydrogen peroxide chemiluminescence reaction. Although chemiluminescence detection has several advantages, such as no requirement for a light source and high sensitivity, it requires a hydrogen peroxide delivery line and pump, mixing device, and flow detection cell to perform chemiluminescence analysis in the system. In this study, Chrome Azurol S as an absorption reagent was introduced into the TRDC system for metal ion separation and online detection. Metal ions, i.e. Co(II), Cu(II), Ni(II), Al(III), and Fe(III), as models were examined by the TRDC system. Characteristic individual absorption characteristics and elution times were obtained as the result of complex formation between the metal ions and Chrome Azurol S even in the water–acetonitrile–ethyl acetate mixture solution. The successful use of the absorption reagent in the TRDC system with the water-hydrophilic/ hydrophobic organic solvent

mixture for online metal ion analysis indicated that the TRDC system and TRDP are attractive and applicable in separation science.

4.2. Experimental

4.2.1. Reagents and capillary tubes

Water was purified with an Elix UV 3 system (Millipore, Billerica, MA, USA). All reagents used were obtained commercially and were of analytical grade. Chrome Azurol S, 1-naphthol, 2,6-naphthalenedisulfonic acid, Co(II), Cu(II), Ni(II), Al(III), and Fe(III) (chloride salts), as well as Ni(II) (nitrate salt), acetonitrile, and ethyl acetate were purchased from Wako Pure Chemical Industries (Osaka, Japan). Fused-silica capillary tubes (inner diameter: 75 μm) were purchased from GL Science (Tokyo, Japan).

4.2.2. Apparatus and procedures

A fused-silica capillary tube (75 μm id, 110 cm length; 90 cm effective length), a microsyringe pump (MF-9090; Bioanalytical Systems, West Lafayette, IN, USA), and an absorption detector (modified SPD-6AV spectrophotometric detector; Shimadzu, Kyoto, Japan) comprised the TRDC system with absorption detection. The tube temperature was controlled by immersing the capillary tube (40 cm) in water maintained at 20 °C in a beaker with constant stirring. A water–acetonitrile–ethyl acetate

mixture in the volume ratio of 3:8:4 including 20mM Chrome Azurol S was used as a carrier solution. Analyte solutions, including 1-naphthol, 2,6-naphthalenedisulfonic acid, and the metal ions, were prepared with the carrier solution. The analyte solution was introduced directly into the capillary inlet side via the gravity method (30 cm height for 20 s). After analyte injection, the capillary inlet was connected through a joint to a microsyringe. The syringe was set on the microsyringe pump. The carrier solution was fed into the capillary tube at a definite flow rate (ca. 0.8 μL min^{-1}) under laminar flow conditions. On-capillary absorption detection was performed with the detector, 254 nm for 1-naphthol and 2,6-naphthalenedisulfonic acid or 600 nm for metal ions.

4.3. Results and Discussion

4.3.1. Absorption spectra for metal ion-Chrome Azurol S complexes

The molecular structure of Chrome Azurol S is shown in Fig. 4-1. Chrome Azurol S is used as an absorption reagent for metal ion detection through the complex formation reaction with metal ions in aqueous solution.[7-9] First, whether Chrome Azurol S reacts with metal ions to produce a complex in the ternary mixed solvents of water–acetonitrile–ethyl acetate (3:8:4 volume ratio) as well as whether the complex shows characteristic absorption in the ternary mixed solvent solution was examined. Absorption spectra based on metal ion-Chrome Azurol S

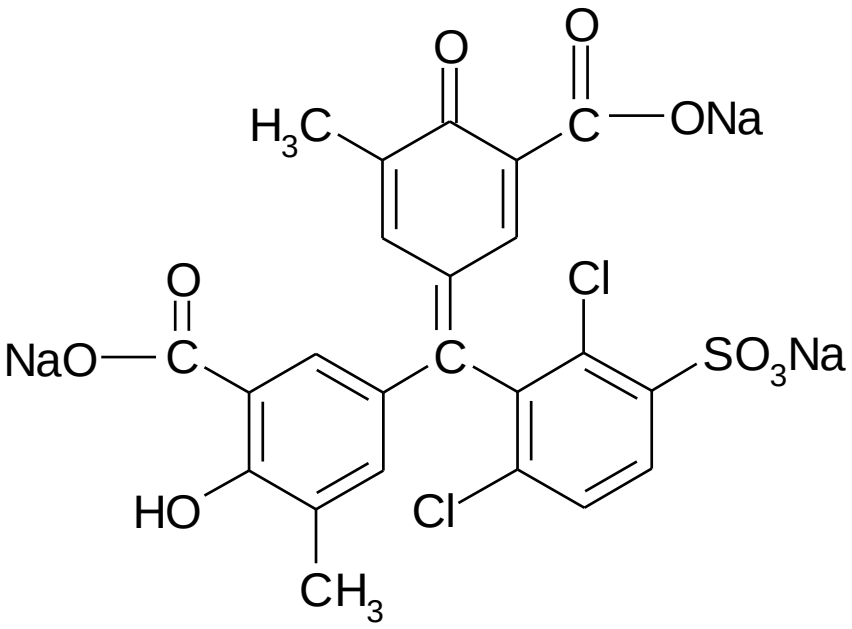

Fig. 4-1 The molecular structure of Chrome Azurol S as an absorption reagent.

complex formation in the ternary mixed solvents of water–acetonitrile–ethyl acetate (3:8:4 volume ratio) are shown in Fig. 4-2 together with the analytical conditions. It was clearly shown that the metal ions, Co(II), Cu(II), Ni(II), Al(III), and Fe(III), had specific absorption spectra through complex formation with Chrome Azurol S in the ternary mixed solvent solution, compared with the absorption spectrum of Chrome Azurol S itself in the absence of any metal ions. The wavelength of 600 nm was used for online metal detection in the TRDC system equipped with absorption detection in the following experiments.

4.3.2. Phase diagram of the ternary mixed solvents including Chrome Azurol S

A phase diagram for the ternary mixture solvents of water–acetonitrile (hydrophilic organic solvent)–ethyl acetate (hydrophobic organic solvent) including 20mM Chrome Azurol S was examined in a vessel at a temperature of 22 °C. The obtained phase diagram is shown in Fig. 4-3. As shown in the figure, 20mM Chrome Azurol S was not dissolved in the ternary mixed solvent solutions with a water component ratio of less than ca. 12 volume %. The phase diagram showed that each component ratio of the solvents made a homogeneous (one homogeneous phase) or heterogeneous (two homogeneous phases) solution. The curve in the figure indicates the boundary between homogeneous and heterogeneous phases. In Chapter 2 or Chapter 3, the TRDC system

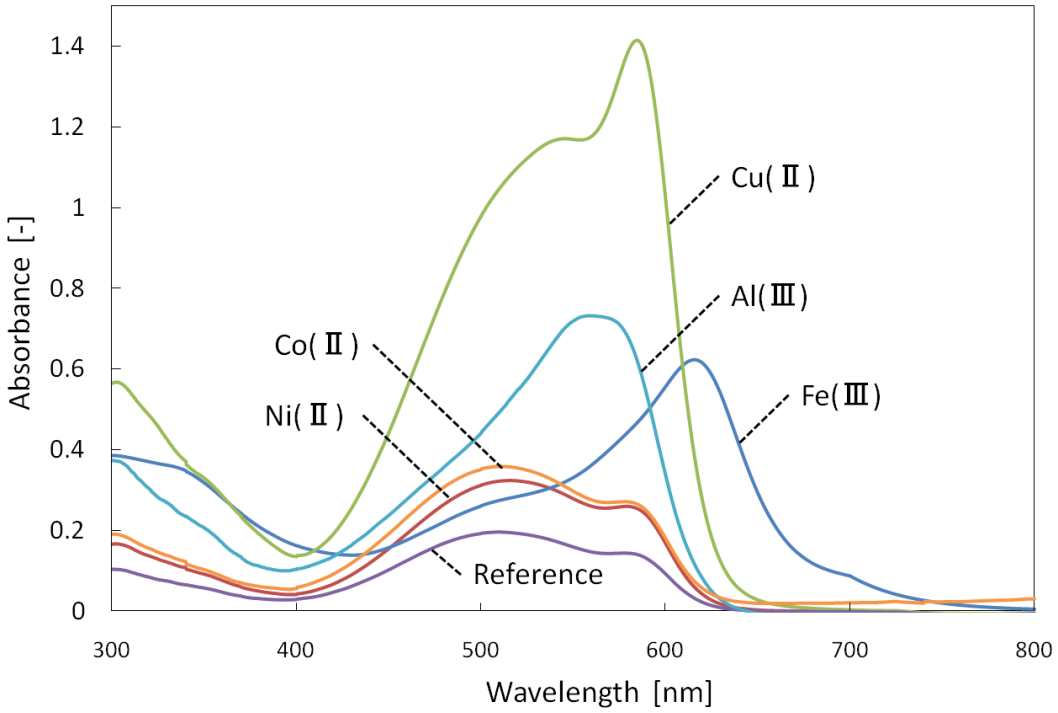

Fig. 4-2 Absorption spectra of the metal ion–Chrome Azurol S complex in the ternary mixed solvents of water–acetonitrile–ethyl acetate (3:8:4 volume ratio).

Conditions: 0.1 mM Chrome Azurol S and 0.1 mM metal ion (Co(II), Cu(II), Ni(II), Al(III), and Fe(III); chloride salts).

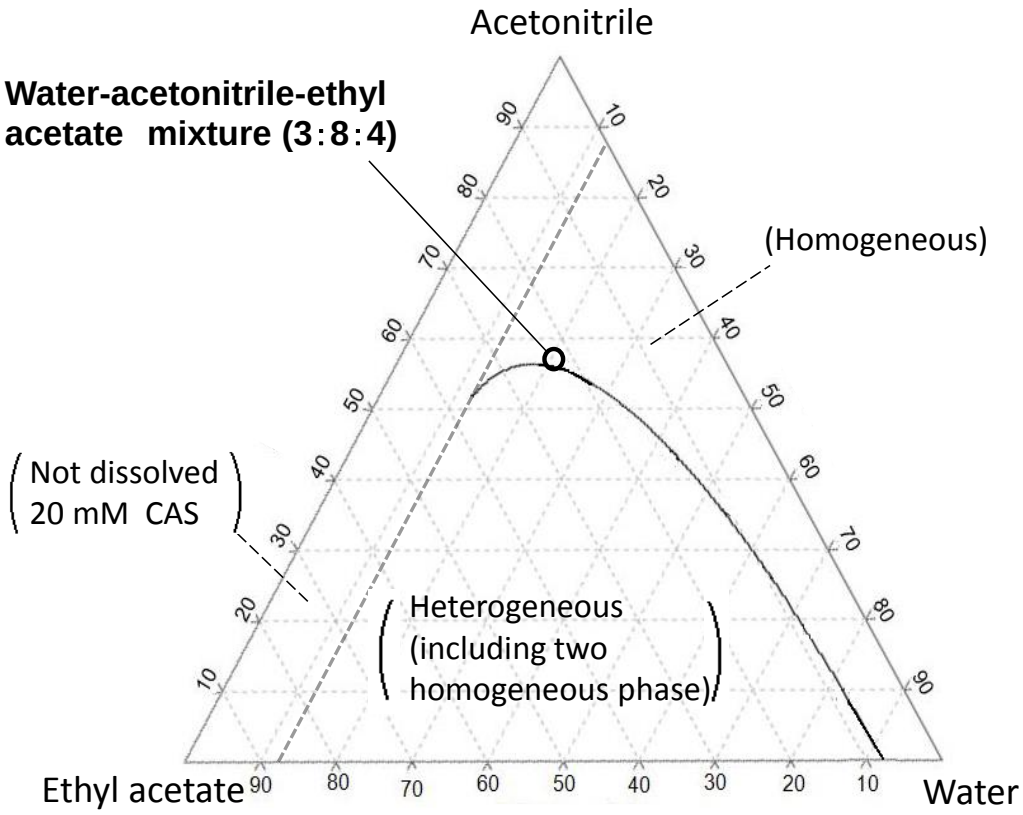

Fig. 4-3 A phase diagram for the ternary mixture solvents of water–acetonitrile–ethyl acetate mixture including 20 mM Chrome Azurol S.

Chrome Azurol S (20 mM) is not dissolved in the ternary mixed solutions that possess the component ratio of water less than ca.12 volume %. The curve in the diagram indicates the boundary between homogeneous and heterogeneous phases.

was used with specific homogeneous carrier solutions with component ratios of solvents that were positioned near the homogeneous–heterogeneous solution boundary curve in the phase diagram. Such specific carrier solutions caused a tube radial distribution of the carrier solvents in the capillary tube under laminar flow conditions, i.e. the TRDP. In addition, in the TRDC system using the fused-silica capillary tube, the organic solvent-rich carrier solution had better resolution than the water-rich carrier solution.[1)] In this study, the homogeneous solution of water–acetonitrile–ethyl acetate mixture (3:8:4 volume ratio) including 20mM Chrome Azurol S, the component ratio of which was near the boundary curve in the phase diagram (Fig. 4-3), was used as a carrier solution in the present TRDC system using the fused-silicacapillary tube.

4.3.3. Separation and detection of 1-naphthol and 2,6-naphthalenedisulfonic acid

The TRDP leads to the formation of inner and outer phases, i.e. a kinetic liquid-liquid interface, in a capillary tube under laminar flow conditions. In this case using the water–acetonitrile–ethyl acetate mixture (3:8:4 volume ratio) including 20mM Chrome Azurol S carrier solution (organic solvent-rich carrier solution), the organic solvent-rich major inner phase was generated around the middle of the tube, whereas the water-rich minor outer phase was formed near the inner wall. In the TRDC system, the outer phase that moved relatively little under laminar flow conditions acted

as a pseudo-stationary phase. Analytes were distributed between the inner and outer phases due to their nature, undergoing chromatographic separation. To confirm that the TRDP occurred in the capillary tube under the present analytical conditions, a mixture of 1-naphthol and 2,6-naphthalenedisulfonic acid was injected into the present TRDC system that was designed for the separation and detection of metal ions through complex formation between a metal ion and Chrome Azurol S. The mixture of them has been used as a model analyte for the TRDC system. The obtained chromatogram is shown in Fig. 4-4. 1-Naphthol (hydrophobic) and 2,6-naphthalenedisulfonic acid (hydrophilic) were separated and detected (254 nm) in this order. The first peak of 1-naphthol was eluted near the average linear velocity under laminar flow conditions. The reasonable elution behavior observed on the chromatogram supported the occurrence of TRDP in the present TRDC system.

4.3.4. Chromatograms of metal ions

The metal ions Co(II), Cu(II), Ni(II), Al(III), and Fe(III) were examined in the present TRDC system. The obtained individual chromatograms are shown in Fig. 4-5 together with the analytical conditions. The elution times and peak areas of the metal ions are summarized in Table 4-1 with those of 1-naphthol and 2,6-naphthalenedisulfonic acid shown in Fig. 4-4. As shown in the table, the elution times of Co(II), Ni(II), Al(III), Fe(III), and Cu(II) metal

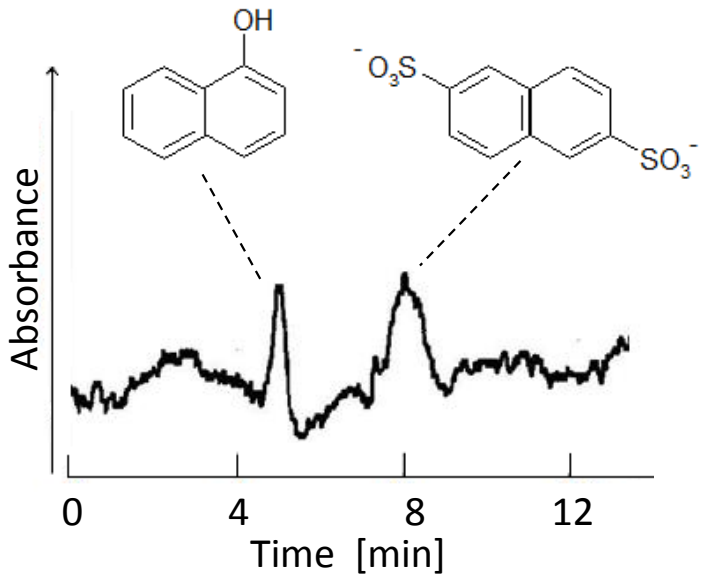

Fig. 4-4 Chromatograms of the mixture analyte solution of 1-naphthol and 2,6-naphthalenedisulfonic acid obtained by the TRDC system.

Conditions: Capillary tube, 110 cm (effective length: 90 cm) of 75 μm i.d. fused-silica; carrier, water-acetonitrile-ethyl acetate (3:8:4 volume ratio) including 20 mM Chrome Azurol S; sample injection, 30 cm height (gravity) × 20 s; flow rate, 0.5 μL min^{-1}; and 1-naphthol and 2,6-naphthalenedisulfonic acid, 1 mM each.

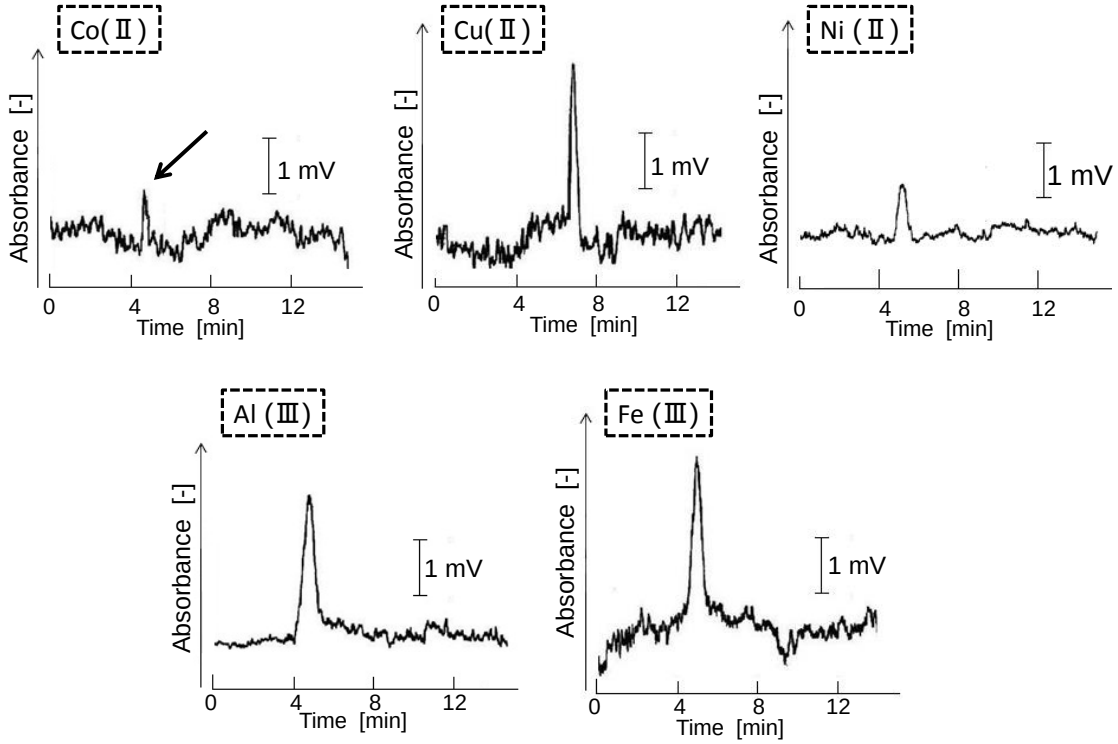

Fig. 4-5 Chromatograms of the metal ions obtained by the TRDC system.

Conditions: Capillary tube, 110 cm (effective length: 90 cm) of 75 μm i.d. fused-silica; carrier, water-acetonitrile-ethyl acetate (3:8:4 volume ratio) including 20 mM Chrome Azurol S; sample injection, 30 cm height (gravity) × 20 s; flow rate, 0.5 μL min^{-1}; and metal ions, 1 mM each.

Table 4-1 Elution times and peak areas of analytes

Analyte	Elution time [min]	Peak area [mV·s]
1-Naphtol	5.0	11.6
2,6-NDS	8.1	20.9
Cu(Ⅱ)	6.8	25.5
Co(Ⅱ)	4.7	8.3
Ni(Ⅱ)	5.2	13.1
Al(Ⅲ)	5.4	50.9
Fe(Ⅲ)	6.3	46.5

Analyte concentration, 1.0 mM

ions increased in this order. The elution order will be discussed later. Tentatively, the Al(III) and Cu(II) mixture as well as Co(II) and Cu(II) mixture were analyzed in the present TRDC system. The obtained chromatograms are shown in Fig. 4-6. As shown in the figures, they were completely separated and detected on the chromatograms. To obtain quantitative information, the calibration curves of Al(III) and Cu(II) were examined by the TRDC system. Al(III) and Cu(II) were linearly determined over the range of 0.2–5mM (coefficient of correlation 0.997) and 0.2–4mM (coefficient of correlation 0.994), respectively.

4.3.5. Molar ratios of metal ion to Chrome Azurol S on complex formation

The molar ratios of the metal ions to Chrome Azurol S at complex formation in the ternary mixed solvents of water–acetonitrile–ethyl acetate mixture were examined with the standard molar ratio method. To each 1.0mM metal ion solution (0.5 mL) were added various concentrations of Chrome Azurol S solution (4.5 mL) to give the metal ion- Chrome Azurol S mixture solution including 0.1mM metal ion and 0.025–0.400mM Chrome Azurol S, where all the solutions were prepared with the ternary mixed solvents of water–acetonitrile–ethyl acetate mixture (3:8:4 volume ratio). Fig. 4-7 shows the relationship between the molar ratio of Chrome Azurol S to Fe(III) and the absorption due to complex formation. From the figure, it was clearly shown that the molar ratio of Fe(III) to Chrome Azurol S was 1:2. In a similar way, the molar ratios of the other metal ions, Co(II), Ni(II),

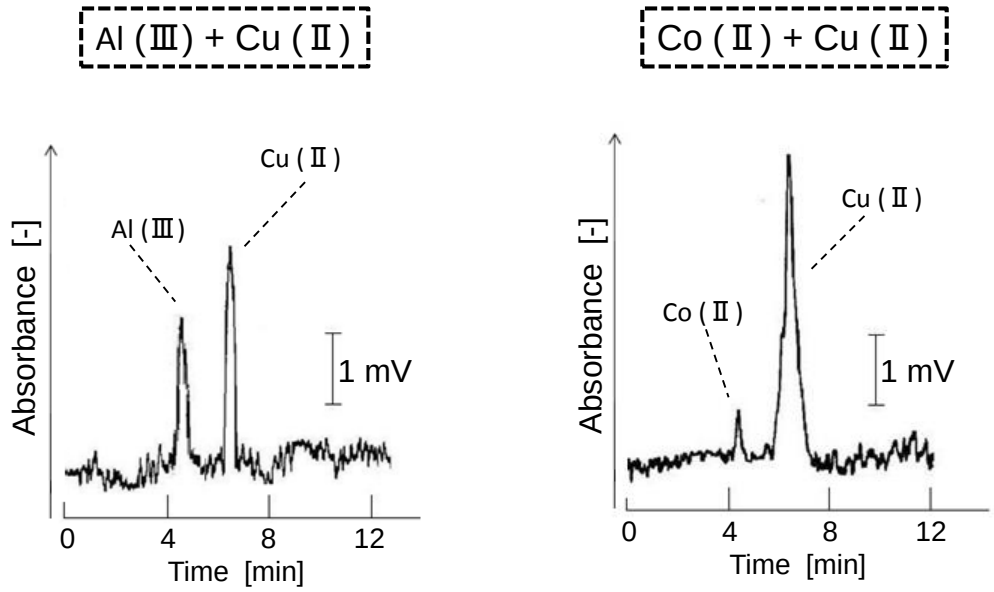

Fig. 4-6 Chromatograms of the mixtures of metal ions, Al(III) and Cu(II) mixture as well as Co(II) and Cu(II) mixture, obtained by the TRDC system.

Conditions: Capillary tube, 110 cm (effective length: 90 cm) of 75 μm i.d. fused-silica; carrier, water–acetonitrile–ethyl acetate (3:8:4 volume ratio) including 20 mM Chrome Azurol S; sample injection, 30 cm height (gravity) × 20 s; flow rate, 0.5 μL min^{-1}; and Co(II), Cu(II), and Al(III), 1 mM each.

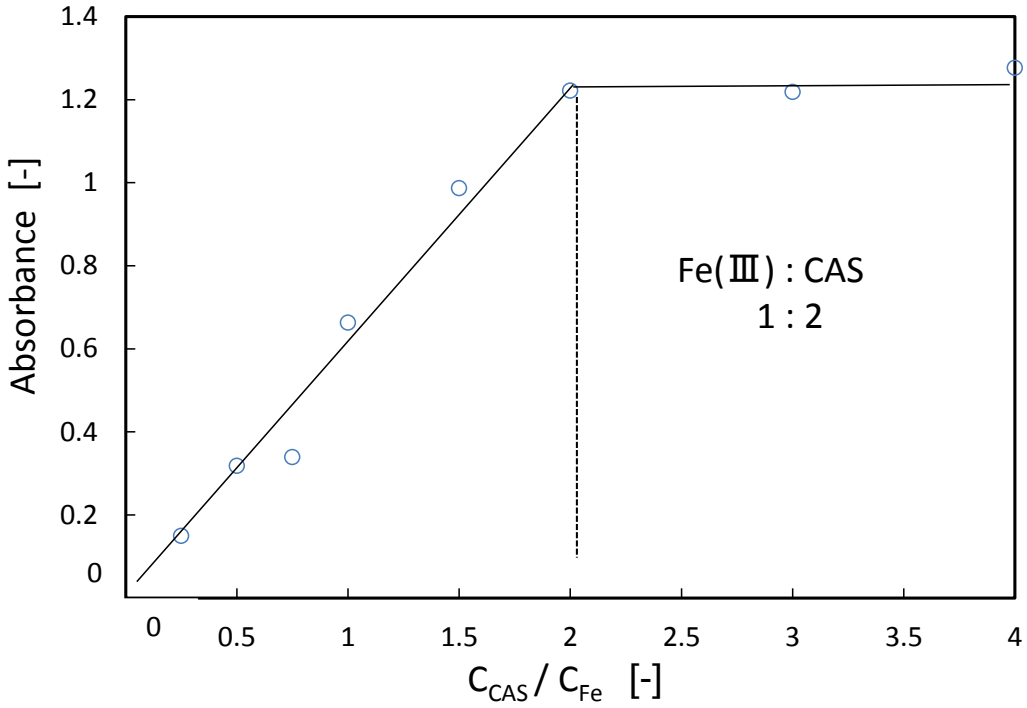

Fig. 4-7 The relationship between the molar ratio of Chrome Azurol S to Fe(III) and the absorption due to the complex formation.

To each 1.0 mM metal ion solution (0.5 mL) was added various concentrations of Chrome Azurol S solution (4.5 mL) to give the metal ion-Chrome Azurol S mixture solution including 0.1 mM metal ion and 0.025-0.400 mM Chrome Azurol S, where all the solutions were prepared with the ternary mixed solvents of water–acetinotrile–ethyl acetate mixture (3:8:4 volume ratio).

Cu(II), and Al(III), to Chrome Azurol S were examined, and respective values were 1:1, 1:1, 1:2, and 1:1.

4.3.6. Elution order and separation mechanism

The TRDP in the present TRDC system created an organic solvent-rich major inner phase and the water-rich minor outer phase in the capillary tube. Hydrophilic Chrome Azurol S was distributed in the water-rich minor outer phase that acted as a pseudo-stationary phase on chromatography. Complex formation between the metal ion and Chrome Azurol S must make the complex more hydrophobic through charge counteraction concerning the positive charge of the metal ion, negative charge of Chrome Azurol S, or the counteranion (chloride ion). That is, the complexes would be effectively distributed in the organic solvent-rich major inner phase that acts as a mobile phase, leading to earlier elution time in the TRDC system. However, due to the natural hydrophilic nature of Chrome Azurol S, the complexes with lower stabilities showed earlier elution times. Furthermore, the molar ratio of metal ion to Chrome Azurol S of 1:1 would elute earlier than that of 1:2. With regard to bivalent metal ions, the elution order of Co(II), Ni(II), and Cu(II) was consistent with the Irving– Williams series (Co(II)<Ni(II)<Cu(II)) and the molar ratios calculated above (the ratio of metal ion to Chrome Azurol S; 1:1 for Co(II) and Ni(II) as well as 1:2 for Cu(II)). For trivalent metal ions, the elution order of Al(III) and Fe(III) was also consistent with the molar ratios

calculated above (1:1 for Al(III) and 1:2 for Fe(III)).

4.3.7. Different elution behavior between nickel(II) chloride and nickel(II) nitrate

In the experiments performed in the present study, the nickel(II) nitrate solution as an analyte showed a later elution time (7.5 min) than nickel(II) chloride (5.2 min). The difference in elution time between nickel(II) chloride and nickel(II) nitrate showed excellent reproducibility. Although the reason is not yet clear, the electron density and the ion diameter of the counteranion, chloride or nitrate anion, may influence the hydrophobicity of the complexes. By taking advantage of the elution behavior of nickel(II) nitrate, the author attempted to separate a metal ion mixture solution including Co(II), Cu(II), and Al(III) (chloride salts) as well as Ni(II) (nitrate salt) by the present TRDC system. The obtained chromatogram is shown in Fig. 4-8. Co(II), Al(III), Cu(II), and Ni(II) were completely separated and detected with good reproducibility by the present TRDC system.

4.4. Conclusion

Metal ions and metal complexes were separated and detected by the TRDC system equipped with chemiluminescence detection. Although chemiluminescence detection has several advantages, such as lack of light

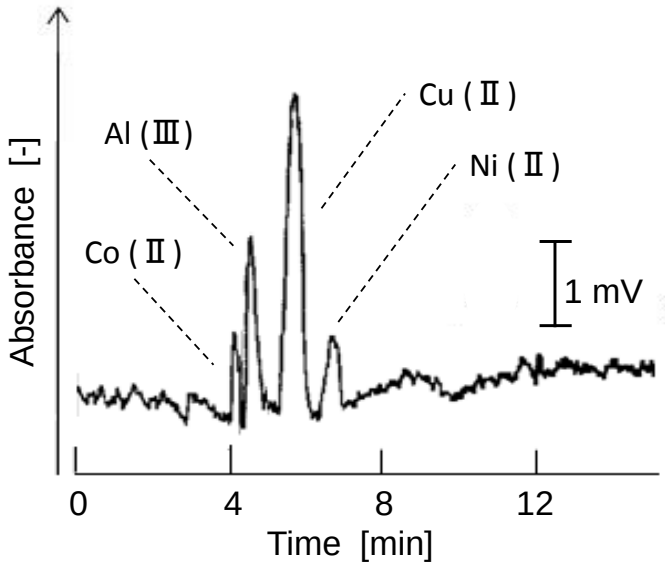

Fig. 4-8 Chromatograms of the mixtures of metal ions, Co(II), Cu(II), Al(III), and Fe(III) (chloride salts) as well as Ni(II) (nitrade salt).

Conditions: Capillary tube, 110 cm (effective length: 90 cm) of 75 μm i.d. fused-silica; carrier, water-acetonitrile-ethyl acetate (3:8:4 volume ratio) including 20 mM Chrome Azurol S; sample injection, 30 cm height (gravity) × 20 s; flow rate, 0.5 μL min^{-1}; and metal ions, 1 mM each.

source requirements and high sensitivity, it requires an oxidant delivery line and pump, solution mixing device, and flow detection cell for performing chemiluminescence flow analysis. In this study, Chrome Azurol S as an absorption reagent was introduced into the TRDC system for metal ion separation and online absorption detection. Characteristic individual absorption characteristics and elution times were obtained as the result of complex formation between the metal ions and Chrome Azurol S in the water–acetonitrile–ethyl acetate mixture solution. Co(II), Al(III), Cu(II), and Ni(II) were completely separated and detected in this order online by the TRDC system with absorption detection. The system worked without applying a high voltage and without using any specific columns. Metal separation was performed using an untreated open tubular fused-silica capillary. The successful use of the absorption reagent in the TRDC system with the water-hydrophilic/hydrophobic organic solvent mixture for online metal ion analysis will expand the use of TRDP in further research.

References

1) N. Jinno, M. Itano, M. Hashimoto, and K. Tsukagoshi, *Talanta*, **79**, 1348 (2009).
2) N. Jinno, M. Murakami, M. Hashimoto, and K. Tsukagoshi, *Anal. Sci.*, **26**, 737 (2010).
3) N. Jinno, M. Hashimotok, and K. Tsukagoshi, *Anal. Sci.*, **27**, 259 (2011).
4) Y. Masuhara, N. Jinno, M. Hashimoto, and K. Tsukagoshi, *Chem. Lett.*,

39, 688 (2010).

5) K. Yoshida, N. Jinno, M. Hashimoto, and K. Tsukagoshi, *Sci. Eng. Rev. Doshisha Univ.*, **51**, 198 (2011).

6) S. Ishimoto, Y. Kudo, N. Jinno, M. Hashimoto, and K. Tsukagoshi, *Anal. Methods*., **2**, 1377 (2010).

7) N. Jinno, K. Tsuji, K. Shikatani, M. Hashimoto, and K. Tsukagoshi, *J. Sep. Sci*., **32**, 4099 (2009).

8) S. Ishimoto, N. Jinno, M. Hashimoto, and K. Tsukagoshi, *Anal. Sci.*, **26**, 641 (2010).

9) W. J. Bernhard, F. P. C. Blamey, J. V. Hanna, P. M. Kopittke, G. L. Kerven, and N. W. Menzies, *J. Agric. Food. Chem.*, **58**, 5553 (2010).

10) Z. Marczenko, and H. Kalowska, *Anal. Chimica. Acta.*, **123**, 279 (1981).

11) P. Pakalns, *Anal. Chimica. Acta*., **32**, 57 (1965).

Chapter 5

Consideration of Tube Radial Distribution Phenomenon under Laminar Flow Conditions Based on the Weber Number

5.1. Introduction

Liquid–liquid flows have a wide range of applications in lab-on-a-chip devices and microreactors. Liquid–liquid flows using immiscible mixed solvents, oil and water, in conventional tubes and mixing procedures have been studied.[1-4] When the mixed solvents flows are successfully controlled, various types of flow patterns, such as droplet, slug, and annular flows, are observed in the tube. Flow patterns generated from immiscible mixed solvents were discussed in terms of dimensionless numbers, especially, the Weber number.[3,4] In this study, dimensionless number, Weber number, was calculated for the first time for microfluidic flows in TRDP using a ternary mixed solvent solution of water-hydrophilic/hydrophobic organic solvent, and the relationship between the Weber number and TRDP formation was investigated.

5.2. Experimental

5.2.1. Reagents and capillary tubes

Water was purified with an Elix 3 UV system (Millipore Co., Billerica, MA, USA). Analytical grade reagents perylene, Eosin Y, acetonitrile, ethyl acetate, and chloroform were purchased from Wako Pure Chemical Industries, Ltd. (Osaka, Japan). Fused-silica capillary tubes (inner diameter: 50 μm) were purchased from GL Science (Tokyo, Japan).

5.2.2. Phase diagrams

Phase diagrams were constructed for the ternary mixed solvents of water–hydrophilic/hydrophobic organic solvents (water–acetonitrile–ethyl acetate and water–acetonitrile–chloroform systems) at 20 °C in a batch vessel. The phase diagram included the solubility curve that separates the component ratios of the solvents into homogeneous (single-phase) and heterogeneous (two-phase) areas.

5.2.3. Interfacial tension calculation

The surface tensions of the upper (organic solvent-rich) and lower (water-rich) solutions (upon conversion of the homogeneous solution into the heterogeneous solution) were measured with a surface tension balance. The interfacial tension (Σ) was calculated using the following equation:[5)]

$$\sigma = \frac{\sigma_o + \sigma_w - 2\sqrt{\sigma_o \sigma_w}}{1 - 0.015\sqrt{\sigma_o \sigma_w}} \qquad (1)$$

where σ_o is the surface tension of the organic solvent-rich phase (O) and σ_w is the surface tension of the water-rich phase (W).

5.2.4. Fluorescence microscope-charge-coupled device (CCD) camera system

To monitor the TRDP, the capillary tube was set up accordingly and observed under a fluorescence microscope-CCD camera system. Ternary

water–hydrophilic/hydrophobic organic solvent systems with various component ratios and comprising perylene (0.05–0.1 mM) and Eosin Y (0.1–1.0 mM) were used. The fluorescence in the capillary tube (total length: 120 cm) was monitored at 20 cm from the tube outlet using a fluorescence microscope (BX51; Olympus, Tokyo, Japan) equipped with an Hg lamp, a filter (U-MWU2; excitation wavelength: 330–385 nm, emission wavelength: 420 nm), and a CCD camera (JK-TU53H). The temperature of the capillary tube was maintained at 3 °C using a thermo-heater (Thermo Plate MATS-555RO; Tokai Hit Co., Shizuoka, Japan). Perylene and Eosin Y emit light at 470 and 550 nm, respectively. Accordingly, the resulting fluorescence observed was mainly blue and green.

5.3. Results and Discussion

5.3.1. Superficial velocity in TRDP

Various types of oil–water (immiscible solvents) flows in a tube were examined and discussed in terms of dimensionless numbers such as the Capillary, Reynolds, and Weber numbers.[1-4] More specifically, the Weber number has been used to examine the flow patterns of droplet, slug, and annular flows in a tube.[3,4] The Weber number, We_i, is expressed according to the following equation:

$$We_i = \frac{\rho_i V_i^2 D}{\Sigma} \quad (2)$$

where ρ_i is the density, V_i is the superficial velocity, D is the inner diameter,

and Σ is the interfacial tension. Subscript i refers to the organic solvent-rich solution (O) or water-rich solution (W). The value of $\rho_i V_i^2 D$ corresponds to the inertial force. Hence, the Weber number is defined as the ratio of inertial force to the interfacial tension (interfacial force). The inertial force tends to extend the interface in the direction of the flow and maintain a continuous fluid. In contrast, the interfacial force tends to minimize the interfacial energy by reducing the oil–water interfacial area, leading to the formation of droplets and plugs.

Fig. 5-1 shows illustrations of the flow systems, immiscible mixed solvent and water–hydrophilic/hydrophobic organic solvent, and their typical flow patterns in a tube. For typical immiscible mixed solvent solutions, the superficial velocities are obtained by dividing the flow rates in the individual delivery tubes, oil and water lines, by the cross–section of the tube, mixing single line (Fig. 5-1(a)).[3)] In contrast, in ternary mixed solvents, the apparent flow rates of the organic solvent-rich and water-rich phases in the capillary single tube are first obtained by multiplying the flow rate in the capillary tube by the volume percentages of the upper (organic-solvent-rich) and lower (water-rich) phases in a batch vessel. The superficial velocities are then calculated by dividing the apparent flow rates by the cross-section of the capillary tube with the equation below, that was expressed in Fig. 5-1(b).

$$V_i = Q_i / A \quad (Q_i = Q \times X_i) \tag{3}$$

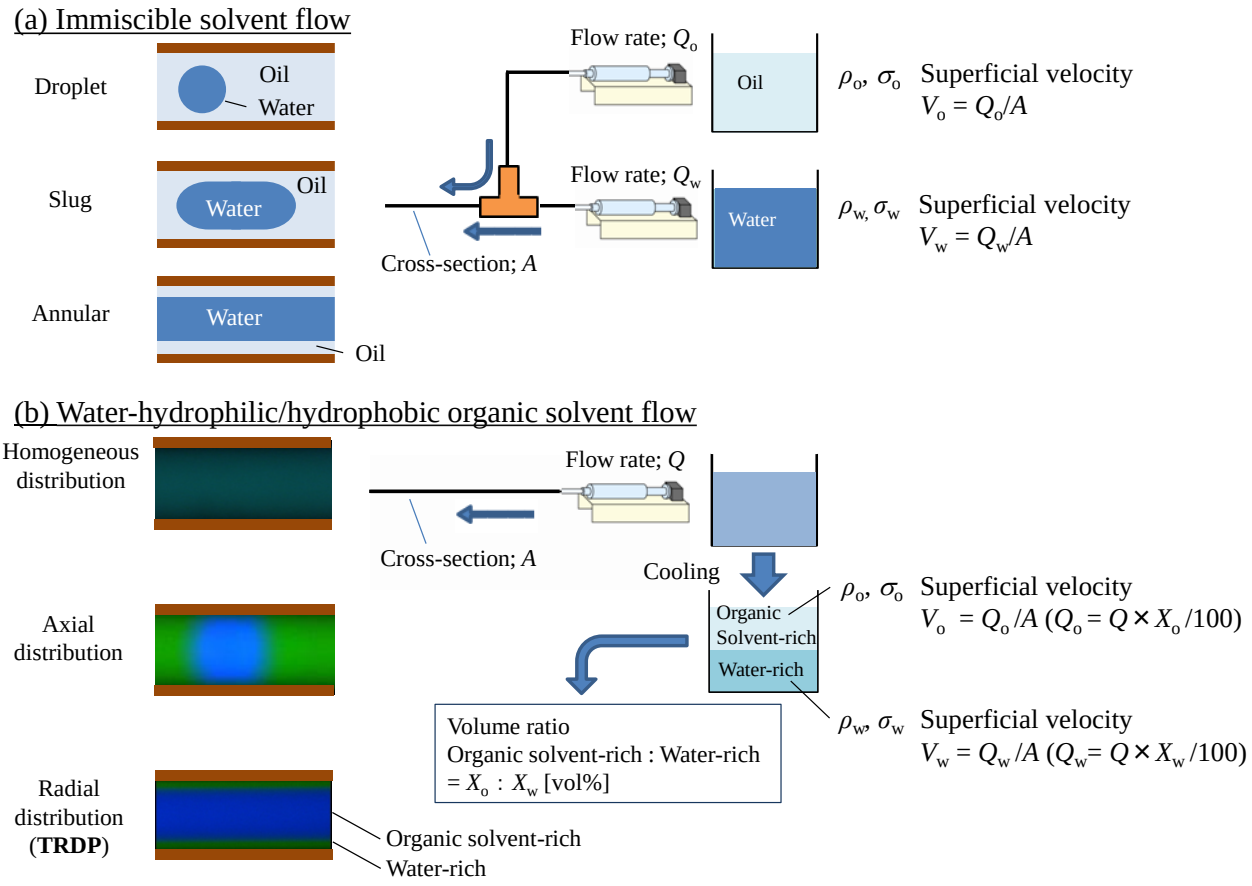

Fig. 5-1 Illustration of the flow systems and typical flow patterns. (a) Immiscible mixed solvents flow and (b) water–hydrophilic/hydrophobic organic solvent flow systems.

5.3.2. Flow patterns of ternary mixed solvents of water–hydrophilic/hydrophobic organic solvents

Foroughi et al. reported the relationship between the flow patterns and associated Weber numbers for immiscible mixed solvents solutions.[3)] Generally, when immiscible solutions (i.e., O and W) were fed into the mixing single tube with the two individual flow lines, as shown in Fig. 5-1(a), and the flow rate of solution O was constant and that of solution W gradually increased, specific flow patterns in the single tube were generated. A droplet flow was observed when the flow rate and the Weber number of solution W were relatively small and the interfacial tension in the droplet of W was dominant relative to the inertial force. A slug flow was observed when the flow rate and the Weber number of solution W were at intermediate values and the inertial force and interfacial tension in the slug of W were comparable. An annular flow was observed when the flow rate and the Weber number of solution W were relatively large and the inertial force in the inner phase of W was dominant relative to the interfacial tension.

When the ternary mixed solution of water–hydrophilic/hydrophobic organic solvent was delivered to a capillary tube, the solvents molecules were radially distributed in the tube under certain flow conditions, that is, TRDP. In a similar way to the immiscible mixed solvent system, the author examined flow patterns using varying component ratios of the ternary solvents in the flow system as shown in Fig. 5-1(b). Specific flow patterns

in the capillary tube were observed, as depicted in the phase diagrams in Fig. 5-2: TRDP (organic solvent-rich inner phase and water-rich outer phase (○), and water-rich inner phase and organic solvent-rich outer phase (●)) and non-TRDP (axial distribution (△) and heterogeneous distribution (×)) for the water–acetonitrile–ethyl acetate and water–acetonitrile–chloroform systems. The relationship between the flow patterns and Weber numbers is discussed in the following section. The Reynolds number was roughly estimated to be less than 0.1 under all the conditions.

5.3.3. Relationship between the volume ratios, Weber numbers, and flow patterns in the ternary mixed solvents flow system

The volume ratios of the generated upper (organic solvent-rich) and lower (water-rich) phases at varying component ratios of the ternary mixed solvents in a batch vessel at low temperature (3 °C) were examined. Additionally, the Weber numbers of the inner (organic solvent-rich or water-rich) and outer (water-rich or organic solvent-rich) phases in the ternary mixed solvent flow system were calculated with the equation of (2) as well as those of (1) and (3) under the conditions of the flow rate, 0.2 μl min^{-1}, and the capillary inner diameter, 50 μm, by using the data mentioned below (the average densities, the average surface tensions and superficial velocities). The densities and surface tensions were little changed among the separated phases as follows. The densities for No.

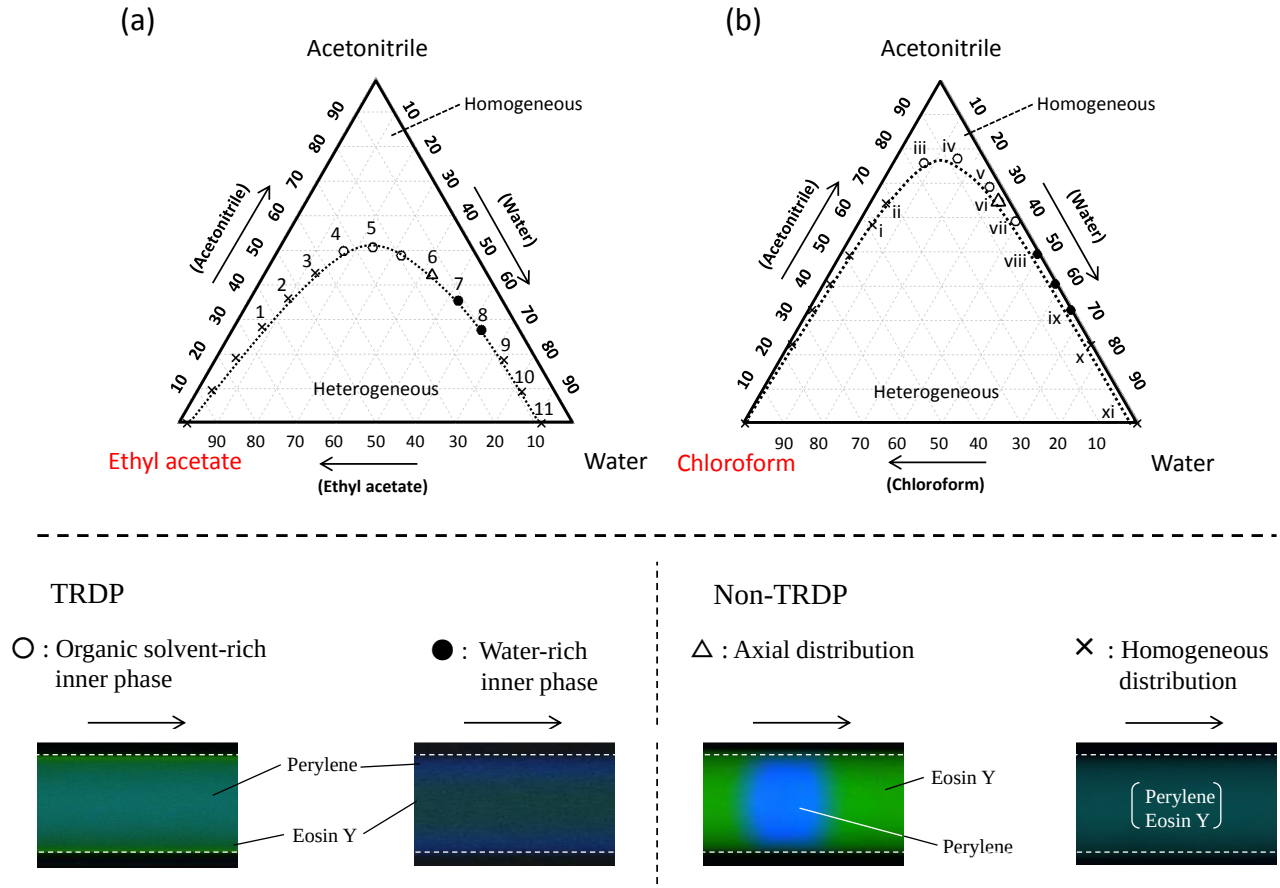

Fig. 5-2 Phase diagram of (a) water–acetonitrile–ethyl acetate and (b) water–acetonitrile–chloroform systems determined at 20 °C.

TRDP conditions: Capillary tube, 120 cm (effective length: 100 cm) of 50 μm i.d. fused-silica; flow rate, 0.20 μL min^{-1}; temperature 3 °C. The flow patterns are denoted as follows: TRDP, organic solvent-rich inner phase and water-rich outer phase (○), and water-rich inner phase and organic solvent-rich outer phase (●); non-TRDP, axial distribution (△) and homogeneous distribution (×). The solutions of No. 1–11 in (a) and those of No. i–xi in (b) were examined in order to discuss Weber number in the later sections.

1–11 in water–acetonitrile–ethyl acetate system were ρ_o; 849–853 kg m^{-3} (the average, 851 kg m^{-3}) and ρ_w; 947–956 kg m^{-3} (the average, 953 kg m^{-3}) as well as those for No. i-xi in water–acetonitrile–chloroform system were ρ_o; 878–892 kg m^{-3} (the average, 885 kg m^{-3}) and ρ_w; 935–947 kg m^{-3} (the average, 941 kg m^{-3}). The surface tension for No. 1–11 in water–acetonitrile–ethyl acetate system were σ_o; 26–28 mN m^{-1} (the average, 27.2 mN m^{-1}) and σ_w; 46–51 mN m^{-1} (the average, 47.9 mN m^{-1}) as well as those for No. i–xi in water–acetonitrile–chloroform system were σ_o; 31–32 mN m^{-1} (the average, 31.4 mN m^{-1}) and σ_w; 37–41 mN m^{-1} (the average, 39.7 mN m^{-1}). On the other hand, superficial velocities were drastically changed with the solutions of No. 1–11 and No. i–xi as shown in Table 5-1. The flow patterns, TRDP and non-TRDP, in the capillary tube were determined on a fluorescence microscope-CDD system. The two following systems were studied: water–acetonitrile–ethyl acetate and water–acetonitrile–chloroform. The results are summarized in Fig. 5-3. Notation of the flow patterns, expressed with symbols, ○, ●, △, and ×, is similar to that employed in Fig. 5-2.

As observed in Fig. 5-3, similar relationships between the volume ratios, Weber numbers, and flow patterns for both ternary mixed solvent systems studied (water–acetonitrile–ethyl acetate and water–acetonitrile–chloroform) were determined. At the water-rich (organic solvent-rich) phase volume ratio of ~50 vol% where the Weber numbers of the two phases were comparable ($|We_w - We_o| < 5.6\times10^{-6}$), TRDP was not observed; an axial distribution flow (△) was observed. In this case, the

Table 5-1 The data of volume ratios of organic solvent-rich (X_o) to water-rich (X_w) phase and superficial velocities (V_i) for the separated phases, upper and lower, of the solutions No. 1–11 in Fig. 5-2(a) (a : water (H_2O)–acetonitrile (CH_3CN)–ethyl acetate (AcOEt) system) and the solution No. i–xi in Fig. 5-2(b) (b : H_2O–CH_3CN–chloroform ($CHCl_3$) system).

(a)

Solution numbers [-]	Volume ratios for ternary mixed solvents (H_2O : CH_3CN : AcOEt)	Volume ratios in a batch vessel		Superficial velocities V_i [$\times 10^{-3}$ m s^{-1}]	
		Upper phase (X_o)	Lower phase (X_w)	Upper phase (V_o)	Lower phase (V_w)
1	7.4 : 27.8 : 64.8	98	2	1.66	0.0340
2	9.9 : 36.0 : 54.1	96	4	1.63	0.0679
3	13.0 : 43.5 : 43.5	93	7	1.58	0.119
4	17.0 : 49.8 : 33.2	90	10	1.53	0.170
5	23.7 : 50.8 : 25.4	73	27	1.24	0.458
6	42.6 : 42.6 : 14.9	40	60	0.679	1.02
7	53.1 : 35.4 : 11.5	24	76	0.407	1.29
8	63.1 : 27.0 : 9.9	10	90	0.170	1.53
9	73.1 : 18.3 : 8.7	7	93	0.119	1.58
10	82.2 : 9.1 : 8.6	4	96	0.0679	1.63
11	91.7 : 0.0 : 8.3	2	98	0.0340	1.66

(b)

Solution numbers [-]	Volume ratios for ternary mixed solvents (H_2O : CH_3CN : $CHCl_3$)	Volume ratios in a batch vessel		Superficial velocities V_i [$\times 10^{-3}$ m s^{-1}]	
		Upper phase (X_o)	Lower phase (X_w)	Upper phase (V_o)	Lower phase (V_w)
i	3.5 : 57.9 : 38.6	98	2	1.66	0.0340
ii	3.8 : 64.1 : 32.1	97	3	1.65	0.0509
iii	7.6 : 75.9 : 16.5	93	7	1.58	0.119
iv	15.4 : 77.2 : 7.4	90	10	1.53	0.170
v	27.6 : 68.9 : 3.5	72	28	1.22	0.475
vi	32.3 : 64.6 : 3.1	53	47	0.900	0.798
vii	39.3 : 58.9 : 1.8	40	60	0.679	1.02
viii	49.5 : 49.5 : 1.1	7	93	0.119	1.58
ix	66.1 : 33.0 : 0.9	4	96	0.0679	1.63
x	76.3 : 22.9 : 0.8	3	97	0.0509	1.65
xi	99.5 : 0.0 : 0.5	2	98	0.0340	1.66

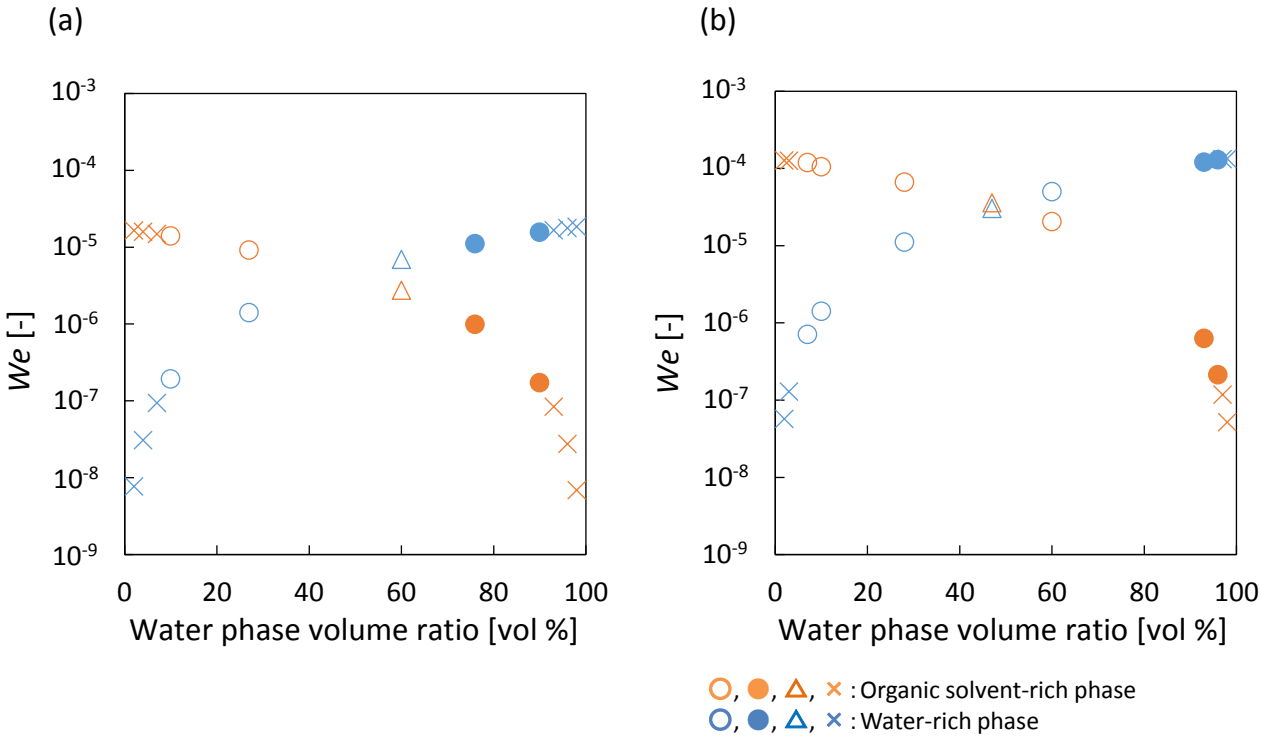

Fig. 5-3 Relationship between the water phase volume ratio and Weber number for the following systems: (a) water–acetonitrile–ethyl acetate (the solutions of No. 1–11 in Fig. 5-2(a) and (b) water–acetonitrile–chloroform (the solutions of No. i–xi in Fig. 5-2(b).

TRDP conditions: Capillary tube, 120 cm (effective length: 100 cm) of 50 μm i.d. fused-silica; flow rate, 0.20 μL min^{-1}. The flow patterns are denoted as follows: TRDP, organic solvent-rich inner phase and water-rich outer phase (○), and water-rich inner phase and organic solvent-rich outer phase (●); non-TRDP, axial distribution (△) and homogeneous distribution (×).

inertial force and interfacial tension in the phases were comparable. When the water-rich (organic solvent-rich) phase volume ratios were considerably small (< 5 vol%) or large (> 95 vol%), TRDP was not observed; a homogeneous flow (×) was observed. The significantly small Weber number (We_w or We_o < 1.3×10^{-7}) or inertial force could not maintain a continuous flow. In contrast, when the water-rich (organic solvent-rich) phase volume ratios were 5–30 vol% and 60–95 vol%, TRDP was clearly observed; an organic solvent-rich inner phase and water-rich outer phase (○) or a water-rich inner phase and organic solvent-rich outer phase (●) were formed. In this case, the inner phase that had a larger volume ratio possessed a relatively larger Weber number than that of the outer phase, leading to a dominant inertial force relative to the interfacial tension. Similar relationships between the Weber numbers (the ratio of the inertial force to the interfacial tension) in the larger volume phase and flow patterns (annular flow or TRDP flow) in immiscible mixed solvent solutions[3] and ternary mixed solvent solution of water–hydrophilic/hydrophobic organic solvent were observed.

5.4. Conclusion

The dimensionless number, Weber number, was used to examine TRDP formation, including the inner and outer phases, in the water–acetonitrile–ethyl acetate and water–acetonitrile–chloroform systems. An interesting relationship between the Weber number and inner

and outer phase formation in TRDP was determined at least for the two model systems in this experiment. TRDP was clearly observed in the capillary tube when the Weber numbers of the organic solvent-rich and water-rich phases differed. The current findings are an extension of the application of the TRDP concept to investigate microfluidic behaviors, and thus present potential in developing new systems based on microfluidic technology relying on liquid–liquid interfacial processes such as chromatography and extraction.

References

1) M. N. Kashid, and D. W. Agar, *Chem. Eng. J.*, **131**, 1 (2007).
2) A. L. Dessimoz, L. Cavin, A. Renken, and L. K. Minker, *Chem. Eng. Sci.*, **63**, 4035 (2008).
3) H. Foroughi, and M. Kawaji, *Int. J. Multiphase Flow*, **37**, 1147 (2011).
4) M. N. Kashid, and L. K. Minsker, *Chem. Eng. Process*, **50**, 972 (2012).
5) T. Ami, K. Awata, H. Umekawa, and M. Ozawa, *Jpn. J. Multiphase Flow*, **26**, 302 (2012).

Chapter 6

Investigation of Inner and Outer Phase Formation in Tube Radial Distribution Phenomenon Using Various Types of Mixed Solvent Solutions

6.1. Introduction

The phase separation of aqueous systems containing polymers, micelles, and ionic liquids is well known, and has been used in the fields of analytical chemistry and separation science since the last century.[1–5] For example, aqueous micellar solutions of specific non-ionic surfactants separate into two distinct phases when heated above a certain temperature (cloud point), i.e., a temperature-induced phase separation occurs.[6–10] One phase behaves as an almost surfactant-free aqueous solution (aqueous phase), whereas the other phase is a concentrated surfactant solution (surfactant-rich phase). Hydrophobic compounds dissolved in the aqueous micellar solution are extracted into the surfactant-rich phase, whereas hydrophilic compounds remain in the aqueous phase.

Fluorous or fluorocarbon chemistry, which involves phase separation processes, has been also investigated since the study reported by Horváth and Rábai in 1994.[11] The phase separation of fluorous (fluorocarbon)–organic (hydrocarbon) solvent mixed solutions has been applied in separation science.[12,13] Mixed solutions of fluorous–organic solvents separate into two distinct phases in a batch vessel when cooled below a certain temperature,[14] with the lower phase comprising an almost pure fluorous solvent and the upper phase consisting of an organic solvent. Based on this phase separation system, liquid–liquid and liquid–solid extractions have been reported using a variety of fluorous solvents.[15–17]

Against the above phase separation solution systems, a ternary mixed solvent system to produce TRDP is a relatively new phase separation system. The author have discussed the phase formation of TRDP generated with a ternary mixed solvent solution of water–hydrophilic/hydrophobic solvents from the viewpoints of the volume ratios of the phases in Chapter 2～5. [18,19] However, comprehensive information about the factors influencing the formation of the inner and outer phases in the TRDP is still lacking for various types of mixed solutions. To this effect, the phase diagrams, viscosities of the two phases (upper and lower phases) in a batch vessel, volume ratios of the phases, and bright-light or fluorescence photograph of the TRDP were examined by using various kinds of phase separation solutions. General discussion on the formation of TRDP has been based on the experimental data, and the TRDP with water–surfactant mixed solution was applied as an attempt to a capillary TRDC, leading to a clue of expanding various TRDP to their applications with distinguished features.

6.2. Experimental

6.2.1. Reagents and capillary tubes

Water was purified with an Elix 3 UV system (Millipore Co., Billerica, MA). All reagents used were obtained commercially and were of analytical grade. Perylene, Eosin Y, Rhodamine B, Orange G, acetonitrile, ethyl

acetate, tetradecafluorohexane, 1-naphthol, and 2,6-naphthalenedisulfonic acid were purchased from Wako Pure Chemical Industries, Ltd. (Osaka, Japan). Triton X-100, Triton X-114, hexane, potassium hydroxide (KOH), potassium chloride (KCl), and dipotassium hydrogenphosphate (K_2HPO_4) were purchased from Nacalai Tesque, Inc. (Kyoto, Japan). Supplies of 1-butyl-3-methylimidazolium chloride ([C_4mim]Cl) 1-ethyl-3-methylimidazolium methylphosphonate ([C_2mim]MP) were purchased from Tokyo Chemical Industry Co., Ltd. (Tokyo, Japan). Fused-silica capillary tubes (50 or 75 μm i.d.) were purchased from GL Science (Tokyo, Japan).

6.2.2. Phase diagrams

Phase diagrams were constructed for the six types of the mixed solvent solutions: ternary water–hydrophilic/hydrophobic organic solvents (water–acetonitrile–ethyl acetate), water–surfactant (water–Triton X-100–KCl), water–ionic liquid (water–[C_4mim]Cl–KOH, water–[C_4mim]Cl–K_2HPO_4, and water–[C_2mim]MP–K_2HPO_4), and fluorous–organic solvents (tetradecafluorohexane–hexane). All phase diagrams, regardless of the composition system, included solubility curves that separated the component ratio areas into homogeneous (single-phase) and heterogeneous (two-phase) areas in a batch vessel.

6.2.3. Viscosity measurement

The homogeneous solutions of all the mixed solvent systems were converted to heterogeneous solution systems that comprised two phases, the upper and lower phases, by changing the temperature. The viscosities of the upper and lower solutions were measured with a viscometer (HAAKE RheoScope 1; Thermo Scientific, Sydney, NSW, Australia).

6.2.4. Bright-field or fluorescence microscope-CCD camera system

The bright-field or fluorescence microscope-CCD camera system was equipped with the fused-silica capillary tube. The fluorescent dye-containing mixed solvent solution that was introduced in the capillary tube was observed using a microscope (BX51; Olympus, Tokyo, Japan) and a CCD camera (JK-TU53H; Toshiba, Tokyo, Japan) for bright-field and fluorescence imaging. For the latter imaging, the microscope was equipped with an Hg lamp and a filter (U-MWU2; excitation wavelength: 330 – 385 nm, emission wavelength: > 420 nm). The temperature of the capillary tube was maintained using a thermo-heater (Thermo Plate MATS-555RO; Tokai Hit Co., Shizuoka, Japan).

6.2.5. Capillary TRDC

The open-tubular capillary chromatography, TRDC, mainly comprised a microsyringe pump (MF-9090, Bioanalytical Systems, Inc.,

West Lafayette, IN), a fused-silica capillary tube (total length: 150 cm and effective length: 100 cm), a thermo-heater, and a fluorescence detector (excitation wavelength: 290 nm and emission wavelength: 355 nm, modified FR-535 fluorescence detector, Shimadzu Co., Kyoto, Japan). An aqueous solution containing 2 wt% Triton X-100 and 2.4 M KCl or 2 wt% Triton X-114 was used as carrier solution. A model analyte solution comprising 1-naphthol (1 mM) and 2,6-naphthalenedisulfonic acid (1 mM) dissolved in the carrier solution was prepared. The analyte solution was injected into the capillary inlet using the gravity method (from 30 cm height and for 30 s), and then fed into the capillary tube at a flow rate of 1.0 μL min^{-1}.

6.3. Results and Discussion

6.3.1. Phase diagrams including solubility curves

Phase diagrams were constructed for the six types of mixed solvent systems studied, namely, water–acetonitrile–ethyl acetate, water–Triton X-100–KCl, tetradecafluorohexane–hexane, water–[C_4mim]Cl–KOH, water–[C_4mim]Cl–K_2HPO_4, and water–[C_2mim]MP–K_2HPO_4 (Fig. 6-1). The compositions shown on the axes of the phase diagrams are different depending on the system studied. The phase diagram of water–acetonitrile–ethyl acetate was based on the solvent volume percentage of each component. The phase diagrams of water–Triton X-100–KCl and tetradecafluorohexane–hexane were constructed according

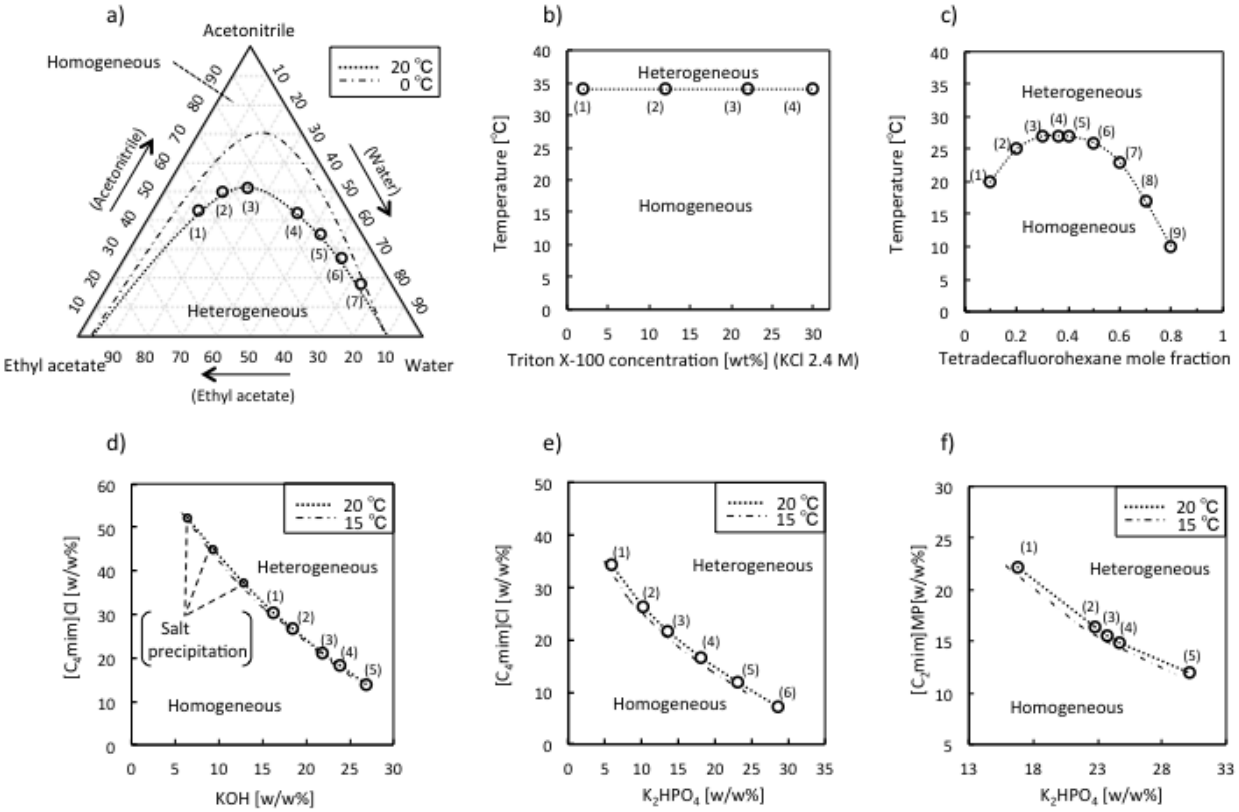

Fig. 6-1 Phase diagrams incorporating solubility curves of a) water–acetonitrile–ethyl acetate, b) water–Triton X-100–KCl (2.4 M), c) tetradecafluorohexane–hexane, d) water–$[C_4mim]Cl$–KOH, e) water–$[C_4mim]Cl$–K_2HPO_4, and f) water–$[C_2mim]MP$–K_2HPO_4. The homogeneous solution mixtures, at the associated components composition, as denoted by the numbers in square brackets in the phase diagrams were used for subsequent experiments.

to the relationship between the temperature and concentration of Triton X-100 (wt%) or mole fraction of tetradecafluorohexane. The phase diagram of water–ionic liquid–salt was constructed based on the relationship between the concentrations of the salt and ionic liquid. Regardless, all phase diagrams included solubility curves that separate the component ratio areas of the solvents into the two phases, i.e., homogeneous (single-phase) and heterogeneous (two-phases). In other words, the homogeneous solution changed to a heterogeneous solution or the heterogeneous solution changed to a homogeneous solution upon alteration of the temperature in the batch vessel. The solubility curves in the phase diagrams were constructed by examining the cloud points where the solvent solutions changed from homogeneous (single phase) to heterogeneous (two phases) solutions by adding the solvent (or solute) at a definite temperature or by altering temperature at a definite composition.

The homogeneous mixtures, at the associated component ratios that were positioned near the solubility curves in the phase diagrams and designated by the numbers in square brackets in the individual phase diagrams (Fig. 6-1), separated into two phases (upper and lower) in the batch vessel upon change in the temperature. The viscosities and volume ratios of the upper and lower phases were examined; furthermore, the homogeneous solutions were delivered into the capillary tube to observe the TRDP using bright-field or fluorescence microscopy, as discussed in the following sections.

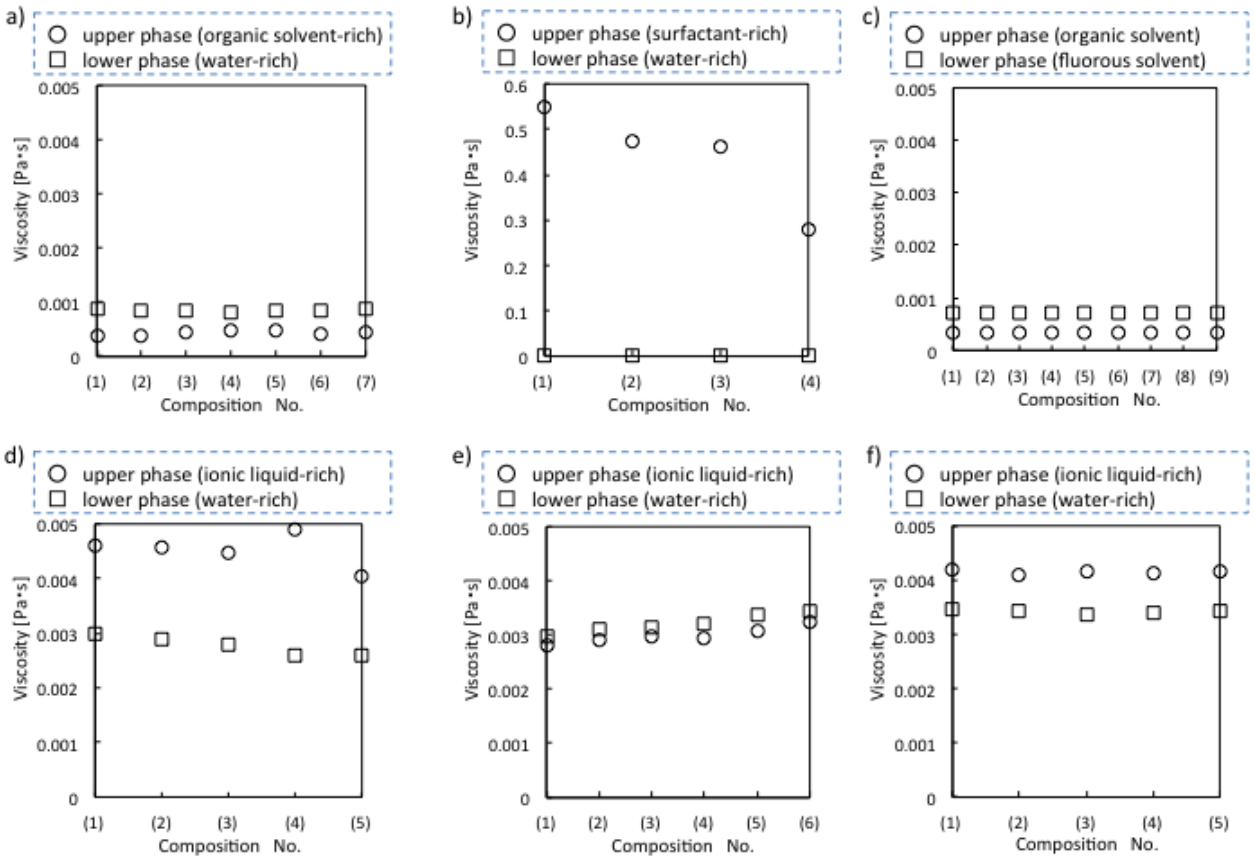

Fig. 6-2 Viscosities of the (○) upper and (□) lower phases of the solvent mixtures, with different solvent compositions, denoted by the numbers in square brackets in Fig. 6-1: a) water–acetonitrile–ethyl acetate, b) water–Triton X-100–KCl (2.4 M), c) tetradecafluorohexane–hexane, d) water–[C_4mim]Cl–KOH, e) water–[C_4mim]Cl–K_2HPO_4, and f) water–[C_2mim]MP–K_2HPO_4.

6.3.2. Viscosities of the upper and lower phases

The viscosities of the upper and lower solutions of the different mixed solvent systems following phase separation were examined. The relationship between the designated solution mixture of a specific component's composition and the associated viscosity for each system is shown in Fig. 6-2. The differences in viscosities between the upper and lower solutions of the water–acetonitrile–ethyl acetate, water–Triton X-100–KCl, tetradecafluorohexane–hexane, water–[C_4mim]Cl–KOH, water–[C_4mim]Cl–K_2HPO_4, and water–[C_2mim]MP–K_2HPO_4 systems were estimated to be respectively 0.42, 440, 0.36, 1.7, 0.22, and 0.73 mPa•s. The system may be tentatively classified according to the degree of difference in viscosities of the upper and lower phases for the following discussion: large (> around 0.73 mPa•s) and small (< around 0.42 mPa•s). A large viscosity difference between the upper and lower phases was observed for the water–Triton X-100–KCl, water–[C_4mim]Cl–KOH, andwater–[C_2mim]MP–K_2HPO_4 systems, whereas a small viscosity difference was observed for the water–acetonitrile–ethyl acetate, tetradecafluorohexane–hexane, and water–[C_4min]Cl–K_2HPO_4 systems.

6.3.3. Volume ratios of the upper and lower phases

The volume ratios of the upper and lower phases of the solvent mixtures designated by the numbers in square brackets in the phase

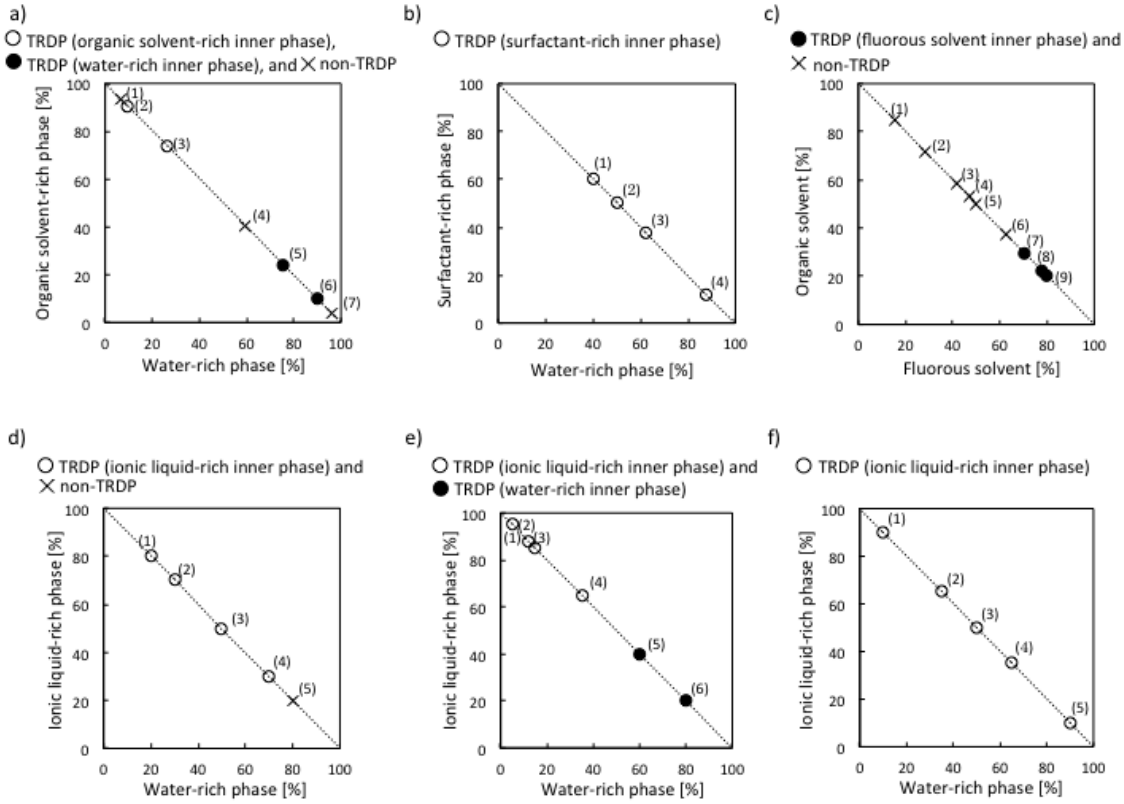

Fig. 6-3 Relationship between the development of the TRDP and the volume contents of the lower and upper phases. Symbols ○ and ● denote the observation of the TRDP, whereas symbol × implies that the TRDP was not observed. Plots containing symbols ○ and ● show the reversible distribution patterns of the inner and outer phases.

Conditions: a) Water–acetonitrile–ethyl acetate (flow rate: 0.2 μL min^{-1}; temperature: 0 °C); b) water–Triton X-100–KCl (2.4 M) (flow rate: 5.0 μL min^{-1}; temperature: 34 °C); c) tetradecafluorohexane–hexane (flow rate: 5.0 μL min^{-1}; temperature: 10 °C); d) water–[C_4mim]Cl–KOH (flow rate: 1.0 μL min^{-1}; temperature: 15 °C); e) water–[C_4mim]Cl–K_2HPO_4 (flow rate: 1.0 μL min^{-1}; temperature: 15 °C); and f) water–[C_2mim]MP–K_2HPO_4 (flow rate: 1.0 μL min^{-1}; temperature: 15 °C). Capillary tube inner diameter: a) 50 μm and b)–f) 75 μm.

diagrams were evaluated. The upper/lower phase ratios for the mixed solvent systems: water–acetonitrile–ethyl acetate (20 → 0 °C), water–Triton X-100–KCl (20 → 34 °C), tetradecafluorohexane–hexane (20 → 10 °C), water–[C_4mim]Cl–KOH (20 → 15 °C), water–[C_4mim]Cl–K_2HPO_4 (20 → 15 °C), and water–[C_2mim]MP–K_2HPO_4 (20 → 15 °C) varied as a function of the composition ratios which were from 90:10 to 4:96 (organic solvent-rich/water-rich), from 60:40 to 12:88 (surfactant-rich/water-rich), from 85:15 to 20:80 (organic solvent /fluorous solvent), from 80:20 to 20:80 (ionic liquid-rich/water-rich), from 95:5 to 20:80 (ionic liquid-rich/water-rich), and from 90:10 to 10:90 (ionic liquid-rich/water-rich). The volume ratios of the upper and lower phases are shown in Fig. 6-3.

6.3.4. Evaluation of the TRDP

The homogeneous solutions were delivered to the capillary tube under laminar flow conditions. The solvent behaviors, TRDP and non-TRDP were assessed using bright-field or fluorescence microscopy. Typical photographs showing the development of TRDP are shown in Fig. 6-4. Interestingly, the solution mixtures of water–Triton X-100–KCl, water–[C_4mim]Cl–KOH, and water–[C_2mim]MP–K_2HPO_4 generated the TRDP in the surfactant-rich inner phase and the ionic liquid-rich inner phase, regardless of the volume ratios of the two phases or component ratios of the solvents. In contrast, the solution mixtures of

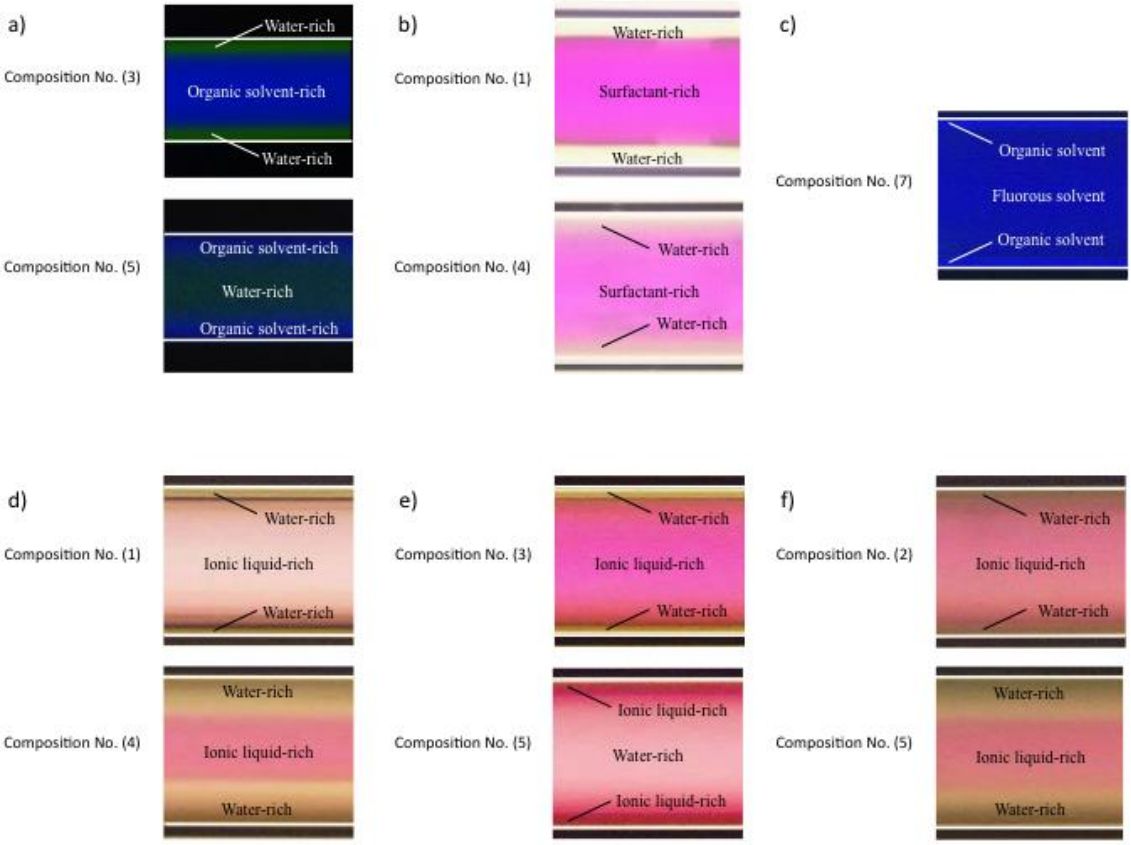

Fig. 6-4 Bright-field and fluorescence photographs showing the development of the TRDP in the different systems.
Conditions: a) water–acetonitrile–ethyl acetate (flow rate: 0.2 μL min^{-1}; temperature: 0 °C; and 1 mM Eosin Y and 0.1 mM perylene); b) water–Triton X-100–KCl (2.4 M) (flow rate: 5.0 μL min^{-1}; temperature: 34 °C; and 5 mM Rhodamine B); c) tetradecafluorohexane–hexane (flow rate: 5.0 μL min^{-1}; temperature: 10 °C; and 0.1 mM perylene); d) water–$[C_4mim]Cl$–KOH (flow rate: 1.0 μL min^{-1}; temperature: 15 °C; and 5 mM Rhodamine B); e) water–$[C_4mim]Cl$–K_2HPO_4 (flow rate: 1.0 μL min^{-1}; temperature: 15 °C; and 2 mM Rhodamine B); and f) water–$[C_2mim]MP$–K_2HPO_4 (flow rate: 1.0 μL min^{-1}; temperature: 15 °C; and 5 mM Rhodamine B). Capillary tube inner diameter: a) 50 μm and b)–f) 75 μm.

water–acetonitrile–ethyl acetate, tetradecafluorohexane–hexane, and water–[C_4min]Cl–K_2HPO_4 generated the TRDP in the major volume inner phase and minor volume outer phase. That is, an inverse (reversible) distribution pattern was observed with a change in the volume ratios of the solvents. For example, when considering the water–acetonitrile–ethyl acetate system, introduction of the organic solvent-rich mixed solution to the capillary tube generated an organic solvent-rich major inner phase and a water-rich minor outer phase; in contrast, introduction of the water-rich mixed solution to the capillary tube produced a water-rich major inner phase and an organic solvent-rich minor outer phase.

The TRDP processes in the different mixed solvent systems are denoted by the symbols ○, ●, and ×, and vary according to the lower and upper phases volume content (Fig. 6-3). The symbols ○ and ● denote the development of TRDP, whereas symbol × implies that TRDP was not observed in a given system at a particular upper/lower volume composition. The mixed solvent systems that include both symbols ○ and ● in the figures demonstrate the occurrence of a reversible distribution pattern of the inner and outer phases in accordance with the phase composition.

6.3.5. Investigation of the inner and outer phase formation

The factors influencing the formation of the inner and outer phases, i.e., non-reversible TRDP or reversible TRDP, were evaluated based on the viscosities and volume ratios of the upper and lower phases, and TRDP

observations. When the difference in the viscosities between the two phases was large (> approximately 0.73 mPa•s), the phase with the larger viscosity developed as the inner phase regardless of the volume ratios. Conversely, when the difference in the viscosities between the two phases was small (< approximately 0.42 mPa•s), the phase with the larger volume content formed as the inner phase. The relationship between viscosity differences and two type phase formation is discussed in the next chapter.

6.3.6. Capillary TRDC

A capillary TRDC system was tentatively developed using a fused-silica capillary tube as the separation column and an aqueous micellar solution (2 wt% Triton X-100 and 2.4 M KCl or 2 wt% Triton X-114 solution) as a carrier solution. The Triton X-114 solution is a well-known typical micelle aqueous two-phase separation system. Hydrophobic 1-naphthol and hydrophilic 2,6-naphthalenedisulfonic acid (2,6-NDS) as a model mixture was examined in the current TRDC system. The obtained chromatograms are shown in Fig. 6-5 as an initial result. In this study, 1-Naphthol and 2,6-NDS were separated and detected in this order; the Triton X-114 system without salt gave better resolutions. The effects of salts on separation performance in TRDC might be examined and considered in the future with the mixed solvent solutions of water-surfactant and water-ionic liquid systems including salts. The elution order was expected based on the distribution of the aqueous micellar

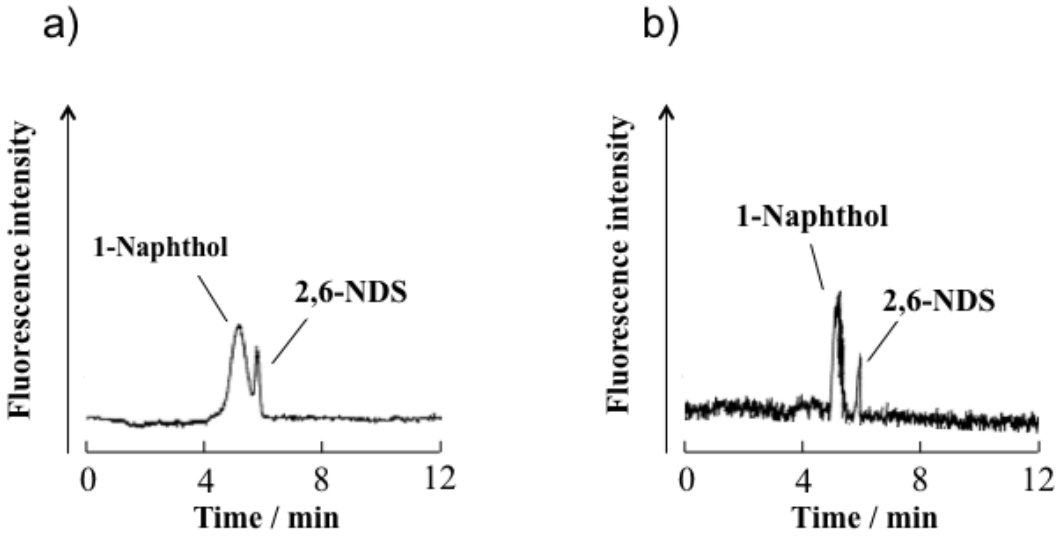

Fig. 6-5 Chromatograms of the present capillary TRDC system: a) 2 wt.% Triton X-100 and 2.4 M KCl at 34 °C and b) 2 wt.% Triton X-114 at 23 °C.

Conditons: Capillary tube, 150 cm (effective length: 100 cm) of 75 µm i.d. fused-silica; flow rate: 1.0 µL min^{-1}; and analyte concentration: 1 mM.

solution that generated a surfactant-rich inner phase (hydrophobic) and a surfactant-poor outer phase (hydrophilic). The hydrophilic outer phase acted as a pseudo-stationary phase under laminar flow conditions. The two peaks were identified according to individual analyte analyses.

6.4 Conclusion

The TRDP generates a kinetic liquid–liquid interface in a microspace upon introduction of a homogeneous mixed solvent solution in a microspace under laminar flow conditions. The factors determining the formation of the inner and outer phases in the microspace were assessed by examining the phase diagrams incorporating solubility curves, viscosities of the upper and lower phases in a batch vessel, volume ratios of the phases, and development of the TRDP using microscopy imaging. When the difference in the viscosities between the two phases was large (> around 0.73 mPa•s), the phase with the higher viscosity formed as the inner phase regardless of the volume ratios, whereas when the difference in viscosities was small (< around 0.42 mPa•s), the phase with the larger volume ratio formed as the inner phase. This finding is a gateway to future work in the TRDP research area.

References

1) K. E. Gutowski, G. A. Broker, H. D. Willauer, J. G. Huddleston, R. P.

Swatloski, J. D. Holbrey, and R. D. Rogers, *J. Am. Chem. Soc.*, **125**, 6632 (2003).

2) Z. Li, Y. Pei, H. Wang, J. Fan, and J. Wang, *TrAC, Trends Anal. Chem.*, **29**, 1336 (2010).

3) Y. Lu, W. Lu, W. Wang, Q. Guo, and Y. Yang, *Talanta*, **85**, 1621 (2011).

4) C. Wua, J. Wanga, H. Wanga, Y. Pei, and Z. Li, *J. Chromatogr. A*, **1218**, 8587 (2011).

5) J. Han, Y. Wang, Y. Li, C. Yu, and Y. Yan, *J. Chem. Eng. Data*, **56**, 3679 (2011).

6) H. Watanabe and H. Tanaka, *Talanta*, **25**, 585 (1978).

7) K. Fujinaga, *Anal. Sci.*, **9**, 479 (1993).

8) T. Saitoh, H. Tani, T. Kamidate, and H. Watanabe, *TrAC, Trends Anal. Chem.*, **14**, 213 (1995).

9) T. M. Z. Moattar and R. Sadeghi, *Fluid Phase Equilib.*, **203**, 177 (2002).

10) P. L. Trindade, M. M. Diogo, D. M. F. Prazeres, and C. J. Marcos, *J. Chromatogr. A*, **1082**, 176 (2005).

11) T. I. Horváth and J. Rábai, *Science*, **266**, 72 (1994).

12) K. Nakashima, F. Kubota, M. Goto, and T. Maruyama, *Anal. Sci.*, **25**, 77 (2009).

13) J. Lim and T. M. Swager, *Angew. Chem., Int. Ed.*, **49**, 7486 (2010).

14) H. Matsuda, A. Kitabatake, M. Kosuge, K. Tochigi, and K. Ochi, *Fluid Phase Equilib.*, **297**,187 (2010).

15) C. Dennis and Z. R. Lee, *Green Chem.*, G3, (2001).

16) M. Masato, M. Hasegawa, D. Sadachika, S. Okamoto, M. Tomioka, Y.

Ikeya, A. Masuhara, and Y. Mori, *Tetrahedron Lett.*, **48**, 4147 (2007).

17) T. Maruyama, K. Nakashima, F. Kubota, and M. Goto, *Anal. Sci.*, **23**, 763 (2007).

18) M. Murakami, N. Jinno, M. Hashimoto, and K. Tsukagoshi, *Anal. Sci.*, **27**, 793 (2011).

19) K. Tsukagoshi, *Anal. Sci.*, **30**, 65 (2014).

Chapter 7

Consideration of Tube Radial Distribution Phenomenon under Laminar Flow Conditions Based on the Viscous Dissipation

7.1. Introduction

In Chapter 6, the phase diagrams, viscosities of the two phases (upper and lower phases) in a batch vessel, volume ratios of the phases, and bright-field or fluorescence photographs of the TRDP were examined by using two-phase separation mixed solvent solutions[1-5] such as ternary water–hydrophilic/hydrophobic organic solvent mixed solution, water–micelle mixed solution, water–ionic liquid mixed solution, and fluorocarbon/hydrocarbon organic solvent mixed solution. However, comprehensive information about the factors influencing the configuration of the inner and outer phases in the TRDP is still lacking for various types of mixed solutions. In this Chapter, the inner and outer phase configuration in TRDP was, for the first time, considered based on the viscous dissipation principle in a fluidic flow using various types of mixed solvent solutions.

7.2. Experimental

7.2.1. Reagents and materials

Acetonitrile, ethyl acetate, chloroform, and tetradecafluorohexane were purchased from Wako Pure Chemical Industries, Ltd. (Osaka, Japan). Triton X-100, hexane, potassium hydroxide (KOH), potassium chloride (KCl), and dipotassium hydrogenphosphate (K_2HPO_4) were purchased from

Nacalai Tesque, Inc. (Kyoto, Japan). 1-Butyl-3-methylimidazolium chloride ([C_4mim]Cl) and 1-ethyl-3-methylimidazolium methylphosphonate ([C_2mim]MP) were purchased from Tokyo Chemical Industry Co., Ltd. (Tokyo, Japan). Fused silica capillary tubes (inner diameter: 50 or 75 μm) were purchased from GL Science (Tokyo, Japan).

7.2.2. Viscosity measurement

The homogeneous solutions of all the mixed solvent systems were converted in batch vessels into heterogeneous solution systems that comprised two phases—upper and lower—by changing the temperature. The viscosities of the upper and lower solutions were measured with a viscometer (HAAKE RheoScope 1; Thermo Scientific, Sydney, Australia).

7.2.3. Bright-field or fluorescence microscope-charged-couple device (CCD) camera system

The bright-field or fluorescence microscope-CCD camera system was equipped with a fused silica capillary tube (inner diameter: 50 or 75 μm). The fluorescent dye-containing mixed solvent solution that was introduced into the capillary tube was observed using a microscope (BX51; Olympus, Tokyo, Japan) and a CCD camera (JK-TU53H; Toshiba, Tokyo, Japan) for bright-field and fluorescence imaging. For the latter imaging, the microscope was equipped with an Hg lamp and a filter (U-MWU2; excitation

wavelength: 330–385 nm, emission wavelength: >420 nm). The temperature of the capillary tube was controlled using a thermo-heater (Thermo Plate MATS-555RO; Tokai Hit Co., Shizuoka, Japan).

7.3. Results and Discussion

7.3.1. Inner and outer phase configuration in TRDP using various types of two-phase separation mixed solvent solutions

In Chapter 6, the phase diagrams, viscosities of the two phases (upper and lower) in a batch vessel, volume ratios of the phases, and bright-field or fluorescence photographs of the TRDP were examined using different two-phase separation mixed solvent solutions such as ternary water–hydrophilic/hydrophobic organic solvent mixed solution (water–acetonitrile–ethyl acetate), water–micelle mixed solution (water–Triton X-100–KCl), water–ionic liquid mixed solution (water–[C_4mim]Cl–KOH, water–[C_4mim]Cl–K_2HPO_4, and water–[C_2mim]MP–K_2HPO_4), and fluorocarbon/hydrocarbon organic solvent mixed solution (tetradecafluorohexane–hexane). In this Chapter, in addition to the above two-phase separation mixed solvent solutions, a ternary water–acetonitrile–chloroform mixed solution was examined. The phase diagrams, viscosities of the two phases (upper and lower) in a batch vessel, volume ratios of the phases, and fluorescence photographs of the TRDP for the water–acetonitrile–chloroform system are shown in Fig. 7-1.

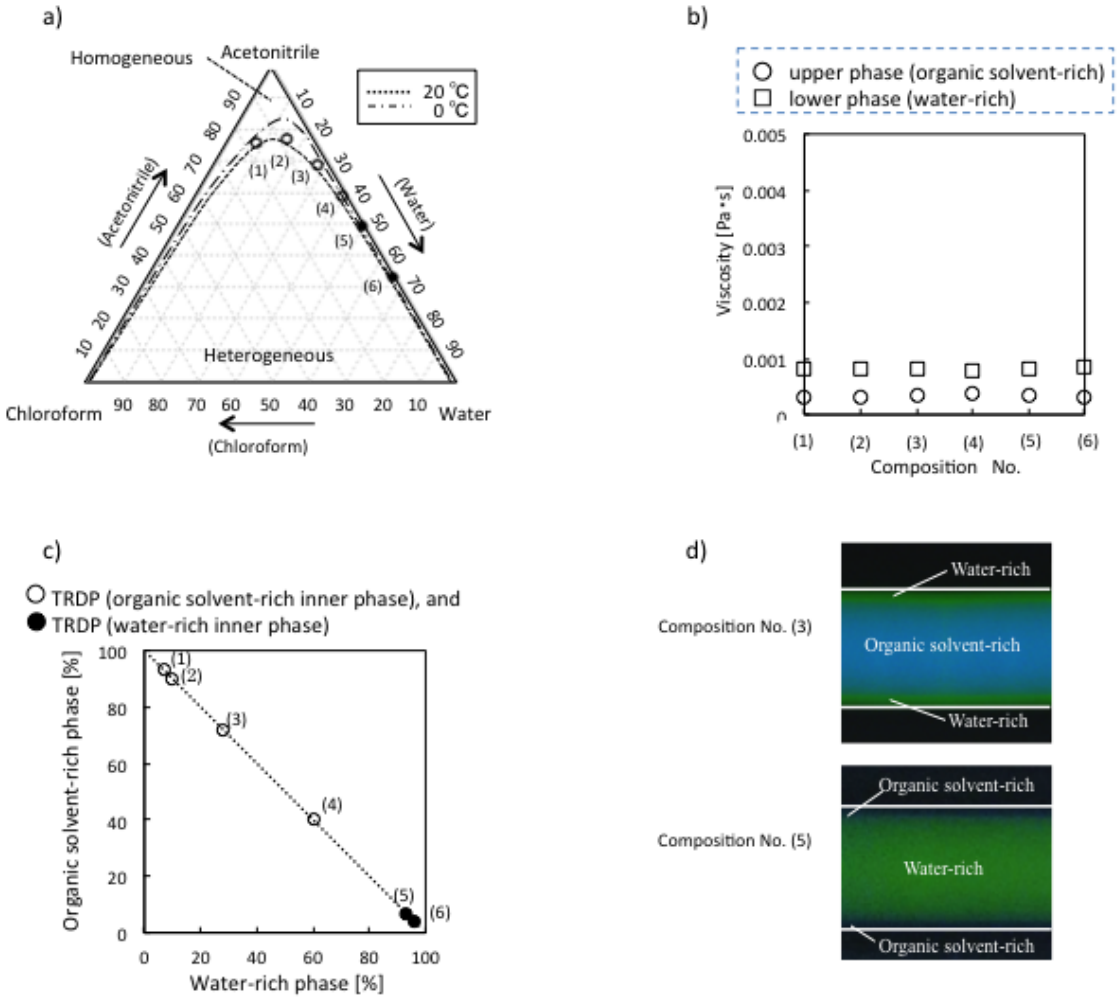

Fig. 7-1 Results pertaining to the water–acetonitrile–chloroform mixed solvent solution.

a) Phase diagrams featuring solubility curves. b) Viscosities of the (○) upper and (□) lower phases in a batch vessel with different solvent compositions denoted by the numbers in brackets in a). c) Relationship between the development of the TRDP and volume contents of the lower and upper phases. Symbols ○ and ● denote the observation of the TRDP (○, organic solvent-rich inner phase and ●, water-rich inner phase). Flow rate, 0.2 μL min^{-1}; temperature, 0 °C; and capillary tube inner diameter, 50 μm. d) Fluorescence photographs showing the development of the TRDP. Fluorescence dye: 1 mM eosin Y and 0.1 mM perylene. The other conditions are the same as those stated for c).

The differences in the viscosity of the upper and lower solutions of the water–acetonitrile–ethyl acetate, water–acetonitrile–chloroform, water–Triton X-100–KCl, water–[C_4mim]Cl–KOH, water–[C_4mim]Cl–K_2HPO_4, and water–[C_2mim]MP–K_2HPO_4 systems were estimated to be approximately 0.42, 0.49, 440, 1.7, 0.22, and 0.73 mPa s,[5] respectively. The systems could be tentatively classified according to the degree of difference in the viscosity of the upper and lower phases: that is, as large (approximately >0.73 mPa s) and small (approximately <0.49 mPa s). A large viscosity difference between the upper and lower phases was observed for the water–Triton X-100–KCl, water–[C_4mim]Cl–KOH, and water–[C_2mim]MP–K_2HPO_4 systems, whereas a small viscosity difference was observed for the water–acetonitrile–ethyl acetate, water–acetonitrile–chloroform, and water–[C_4min]Cl–K_2HPO_4 systems.

The following finding has become a gateway to the present work in TRDP research. When the difference in viscosity between the two phases was large (approximately >0.73 mPa s), the phase with the higher viscosity formed as the inner phase regardless of the volume ratio, whereas when the difference was small (approximately <0.49 mPa s), the phase with the larger volume formed as the inner phase. Fig. 7-2 shows the relationship between the difference in the viscosity between the two phases and the TRDP configuration.

7.3.2. Principle of viscous dissipation[6–9]

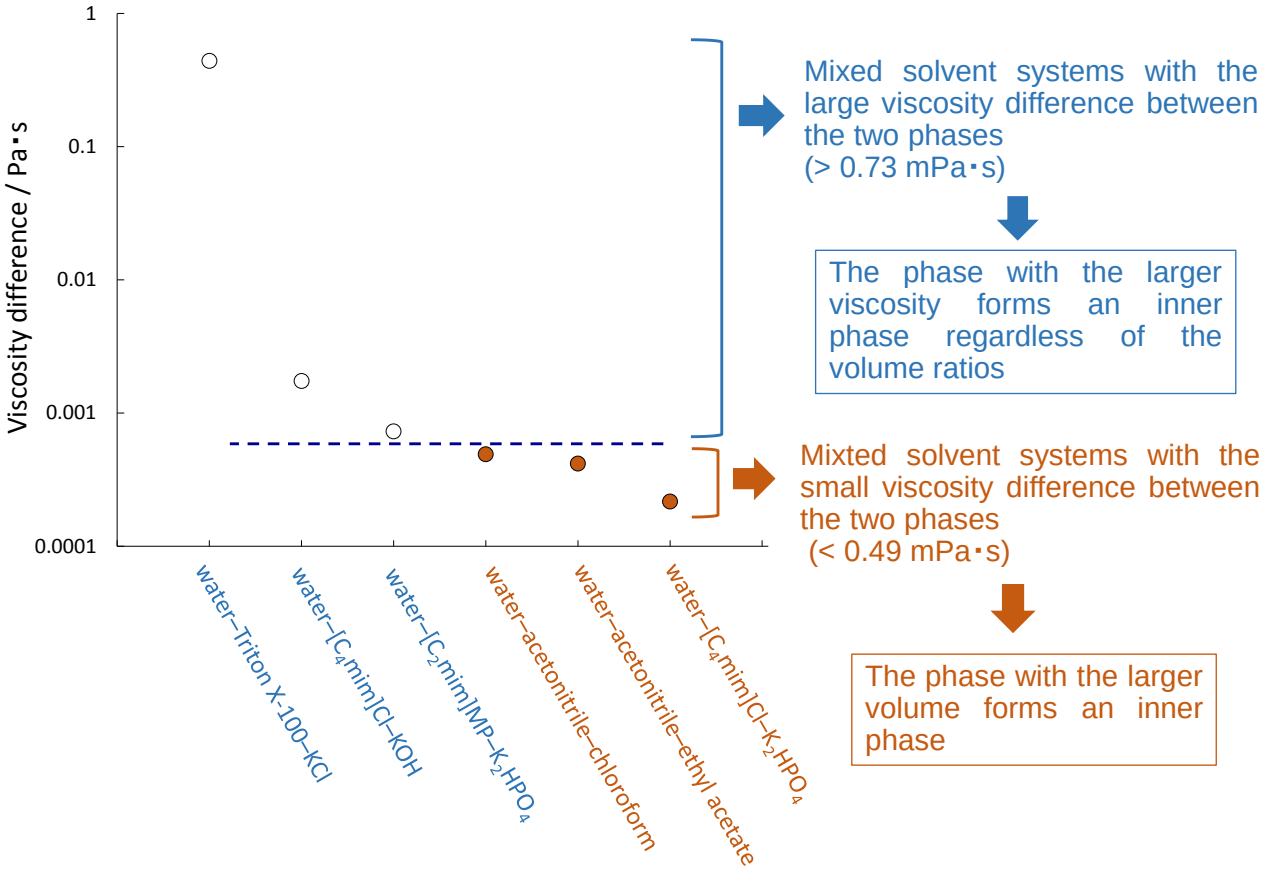

Fig. 7-2 Viscosity difference between the upper and lower phases for various types of two-phase separation mixed solvent solutions from the viewpoint of inner and outer phases in TRDP.
Symbol ○: The phase with the higher viscosity formed as the inner phase regardless of the volume ratio in TRDP. Symbol ●: The phase with the larger volume formed as the inner phase.

In fluid mechanics, viscous dissipation is manifested by the transformation of kinetic energy into thermal energy through fluidic viscosity. The viscous dissipation (E) per unit length in a two-phase flow of solvents a and b is expressed as follows.

$$E = \sum_{j=a,b} \int_{\Omega_j} \left\{ \frac{1}{2} \mu_j (\nabla u_j)^2 \right\} dV \quad (1)$$

Parameter Ω_j refers to the volume occupied by the solvents, and μ_j and u_j represent the viscosity and velocity of the solvents (j = a (for solvent a) or b (for solvent b)), respectively. According to the principle of viscous dissipation, the fluidic flow flows to maintain the solvent distribution that is determined by the minimum value extracted from the equation.

The principle of viscous dissipation is explained for an annular flow formed by immiscible mixed solvents in Fig. 7-3. The two types of solvents are immiscible and have different viscosities. As depicted in Fig. 7-3, the annular flow features an inner phase and an outer phase,and there are two distribution patterns X and Y. The viscous dissipation energies are estimated with Eq. (1) for the patterns X and Y. For example, an annular flow may form as pattern X when the viscous dissipation energy for pattern X is smaller than that of pattern Y, according to the principle of viscous dissipation.

7.3.3. Equations of viscous dissipation (Eqs. (2)–(25))[9)]

To derive concrete equations of viscous dissipation, typical annular flows in an immiscible multi-phase flow, as shown in Fig. 7-4, were

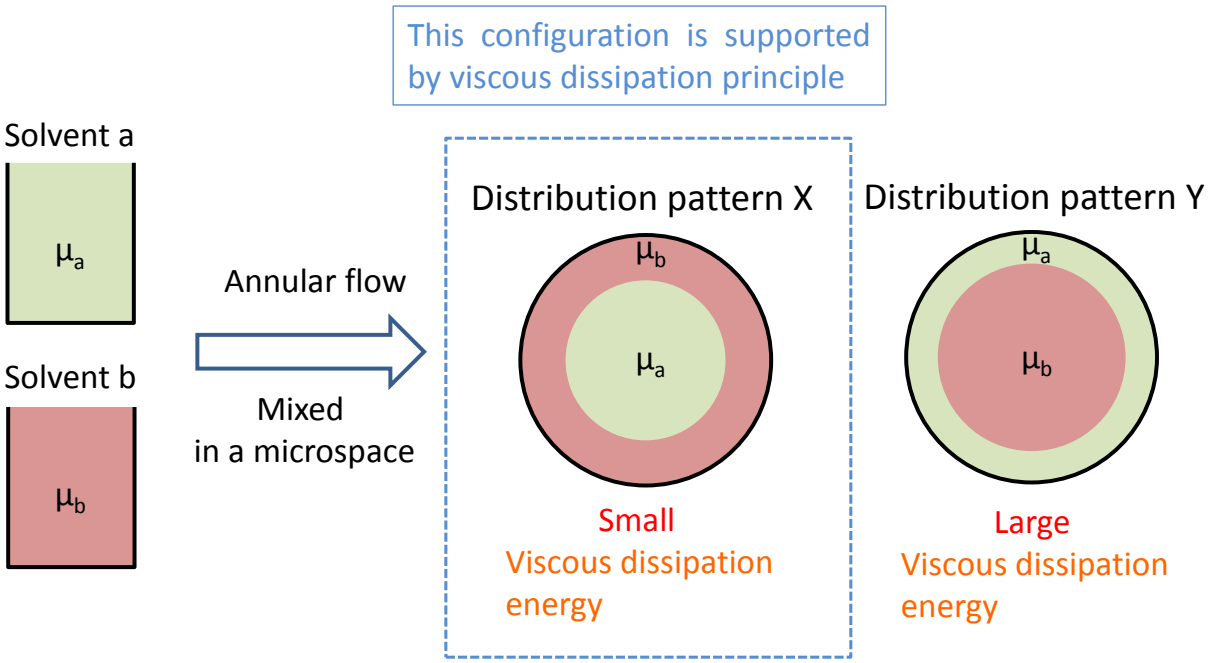

Fig. 7-3 Schematic illustrating the principle of viscous dissipation for annular flows with immiscible mixed solvents.

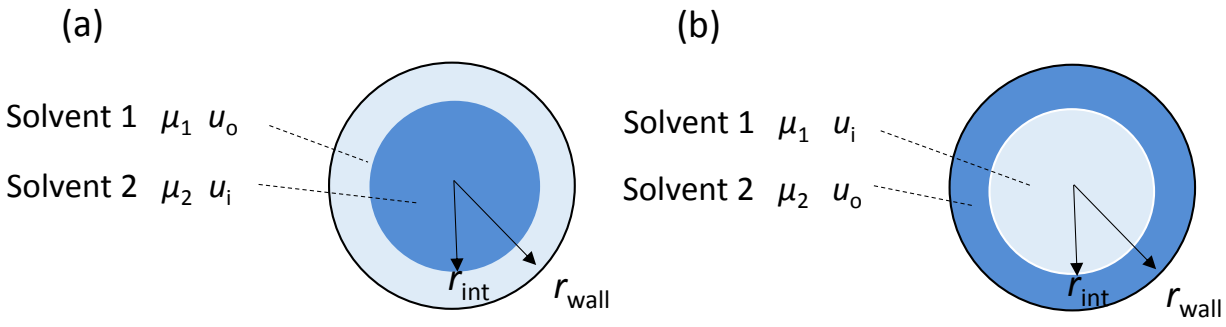

Fig. 7-4 Typical annular flows generated with solvent 1 (with μ_1 and u_o or u_i) and solvent 2 (μ_2 and u_i or u_o), where ($\mu_1 < \mu_2$), respectively forming as the (a) outer and inner phases or (b) inner and outer phases.

examined. Solvent 1 (with μ_1 and u_o or u_i) and solvent 2 (μ_2 and u_i or u_o) with $\mu_1 < \mu_2$ were introduced as the outer and inner phases, or vice versa. Fig. 7-4 (a) shows the solvent distribution featuring the higher viscosity solvent as the inner phase and Fig. 7-4 (b) shows the solvent distribution featuring the lower viscosity solvent as the inner phase. The viscous dissipation for the inner (E_i) and outer phases (E_o) is described as follows.

$$E_i = \int_{\Omega_i} \left\{\frac{1}{2}\mu_i(\nabla u_i)^2\right\} dV_i = \int_0^{r_{int}} \left\{\frac{1}{2}\mu_i(\nabla u_i)^2\right\} \times 2\pi r dr \quad (2)$$

$$E_o = \int_{\Omega_o} \left\{\frac{1}{2}\mu_o(\nabla u_o)^2\right\} dV_o = \int_{r_{int}}^{r_{wall}} \left\{\frac{1}{2}\mu_o(\nabla u_o)^2\right\} \times 2\pi r dr \quad (3)$$

Parameter r is the radius of the flow in the tube (precisely, r_{int} and r_{wall} are the distances from the center of the tube to the liquid–liquid interface and to the inner wall, respectively, as shown in Fig. 7-4) and superscripts i and o refer to the inner and outer phases, respectively. The total energy (E_t) can be calculated by combining Eqs. (2) and (3) such that $E_t = E_i + E_o$.

In the case presented in Fig. 7-4 (a), that is, the inner phase is formed by solvent 2 (μ_2 and u_i), and the outer phase is formed by solvent 1 (μ_1 and u_o), first, the velocities of the inner phase (u_i) and outer phase (u_o) are calculated. The viscosities of the inner phase and outer phase are denoted as μ_2 and μ_1 respectively. The equation for describing the velocity of the inner or outer phase is derived from the Navier–Stokes equation of cylindrical coordinate systems as follows.

$$u = -\frac{\Delta P}{4\mu L} r^2 + C \quad (4)$$

Parameter ΔP is the pressure loss in the capillary, L is the effective length of the capillary, and C is the constant of integration.

Considering the boundary conditions as follows: at the wall surface, $r = r_{wall}$, $u_o = 0$ and at the liquid–liquid interface, $r = r_{int}$, $u_i = u_o$, and viscosity ratio, $H = \mu_1/\mu_2$ ($0 < H < 1$ for $\mu_1 < \mu_2$) and G value for convenience, G = ΔP/L, the following equations are obtained.

$$u_i = \frac{G}{4\mu_1}\left\{r_{\text{wall}}^2 - Hr^2 - r_{\text{int}}^2(1-H)\right\} \quad (5)$$

$$u_o = \frac{G}{4\mu_1}\left(r_{\text{wall}}^2 - r^2\right) \quad (6)$$

When the velocity values are used in the viscous dissipation equation, the following equations are obtained.

$$E_i = \frac{\pi H G^2}{16\mu_1} r_{\text{int}}^4 \quad (7)$$

$$E_o = \frac{\pi G^2}{16\mu_1}(r_{\text{wall}}^4 - r_{\text{int}}^4) \quad (8)$$

The total viscous equation energy can then be described as follows.

$$E_t = E_i + E_o = \frac{\pi G^2}{16\mu_1}\{(r_{\text{wall}}^4 - r_{\text{int}}^4) + Hr_{\text{int}}^4\} \quad (9)$$

The flow rate, Q, is expressed as follows.

$$Q_j = \int_{\Omega_j} u_j \, dV_j \quad (10)$$

The flow rates of the inner phase (Q_i) and outer phase (Q_o) are expressed as follows.

$$Q_i = \frac{\pi G}{8\mu_1}\left(r_{\text{wall}}^4 - 2r_{\text{wall}}^2 r_{\text{int}}^2 + r_{\text{int}}^4\right) \quad (11)$$

$$Q_o = \frac{\pi G}{8\mu_1}\left[-r_{\text{int}}^4(2-H) + 2r_{\text{wall}}^2 r_{\text{int}}^2\right] \quad (12)$$

The total flow rate, Q_t, whereby $Q_t = Q_i + Q_o$ can be expressed as follows.

$$Q_t = \frac{\pi G}{8\mu_1}\left(r_{\text{wall}}^4 - 2r_{\text{wall}}^2 r_{\text{int}}^2 + r_{\text{int}}^4\right) + \frac{\pi G}{8\mu_1}\left[-r_{\text{int}}^4(2-H) + 2r_{\text{wall}}^2 r_{\text{int}}^2\right] \quad (13)$$

Accordingly, G is expressed as follows.

$$G = \frac{8Q\mu_1}{\pi[r_{\text{wall}}^4+(H-1)r_{\text{int}}^4]} \quad (14)$$

Finally, E_t for the case of Fig. 4 (a) is expressed as follows.

$$E_t = E_i + E_o = \frac{4Q^2\mu_1}{\pi[r_{\text{wall}}^4+(H-1)r_i^4]} \quad (15)$$

In the case presented in Fig. 7-4 (b), that is, the inner phase is formed by solvent 1 (μ_1 and u_i), and the outer phase is formed by solvent 2 (μ_2 and u_o), first, the velocities of the inner (u_i) and outer (u_o) phases are calculated in a similar manner to that for the case shown in Fig. 7-4 (a) as follows.

$$u_i = \frac{G}{4\mu_1}\left\{-r^2 + H\left(r_{\text{wall}}^2 - r_{\text{int}}^2\right) + r_{\text{int}}^2\right\} \quad (16)$$

$$u_o = \frac{GH}{4\mu_1}\left(r_{\text{wall}}^2 - r^2\right) \quad (17)$$

In the above equations, the viscosities of the inner and outer phases are represented as μ_1 and μ_2, respectively, and the viscosity ratio, H, is expressed as $H = \mu_1/\mu_2$ ($0 < H < 1$ for $\mu_1 < \mu_2$). When the velocity values are substituted in the viscous dissipation equation, the following equations are obtained.

$$E_i = \frac{\pi G^2}{16\mu_1} r_{\text{int}}^4 \quad (18)$$

$$E_o = \frac{\pi H G^2}{16\mu_1}(r_{\text{wall}}^4 - r_{\text{int}}^4) \quad (19)$$

Accordingly, E_t is expressed as follows.

$$E_t = E_i + E_o = \frac{\pi G^2}{16\mu_1}\{r_{\text{int}}^4 + H(r_{\text{wall}}^4 - r_{\text{int}}^4)\} \quad (20)$$

The flow rates of the inner and outer phases are expressed as follows.

$$Q_i = \frac{\pi G}{8\mu_1}\left(r_{int}^4 + 2Hr_{wall}^2 r_{int}^2 - 2Hr_{int}^4\right) \quad (21)$$

$$Q_o = \frac{\pi G}{8\mu_1}\left[Hr_{wall}^4 - 2Hr_{wall}^2 r_{int}^2 + Hr_{int}^4\right] \quad (22)$$

The total flow rate, Q_t, can be calculated as follows.

$$Q_t = \frac{\pi G}{8\mu_1}\left(r_{int}^4 + 2Hr_{wall}^2 r_{int}^2 - 2Hr_{int}^4\right) + \frac{\pi G}{8\mu_1}\left[Hr_{wall}^4 - 2Hr_{wall}^2 r_{int}^2 + Hr_{int}^4\right] \quad (23)$$

Parameter G is expressed as follows.

$$G = \frac{8Q\mu_{1,}}{\pi\left[(1-H)r_{int}^4 + Hr_{wall}^4\right]} \quad (24)$$

Finally, E_t for the case of Fig. 4 (b) is expressed as follows.

$$E_t = E_i + E_o = \frac{4Q^2\mu_1}{\pi\left[r_{int}^4 + H\left(r_{wall}^4 - r_{int}^4\right)\right]} \quad (25)$$

7.3.4. Calculation of viscous dissipation

As mentioned above, the author examined the TRDP in various types of two-phase separation mixed solvent solutions (Fig. 7-1, 6-3, and 6-4) using microscope-CCD camera systems. The viscous dissipation energy for the solution compositions that generated TRDP was calculated for the six types of mixed solvent solutions studied. Specifically, the viscous dissipation energy values for the two distribution patterns shown in Fig. 7-4 (a) and (b) were calculated using Eqs. (15) and (25), respectively.

Tables 7-1 and 7-2 summarize the values of the viscous dissipation

Table 1 Viscous dissipation energy data of annular flows for the two distribution patterns shown in Fig. 7-4 (a) and (b) when the difference in viscosity between the two phases was large (approximately >0.73 mPa s) and associated water-rich phase volume ratios.

Under these conditions of (a)–(c), the phase with the higher viscosity formed as the inner phase regardless of the volume ratio. The values of the viscous dissipation energy shown in red indicate that TRDP was actually observed in the two distribution patterns.

(a) Water–Triton X-100–KCl

Water rich-phase volume ratio [%]	Viscous dissipation energy [$\times 10^{-7}$ J·m^{-1}·s^{-1}]	
	Distribution pattern (a)	Distribution pattern (b)
40	63.4	15700
50	49.4	11400
62	45.4	8770
88	41.2	2160

The viscosities of water-rich phase (μ_1), 1.00 [mPa·s], and surfactant-rich phase (μ_2), 442 [mPa·s].

(b) Water-[C_4mim]Cl-KOH

Water rich-phase volume ratio [%]	Viscous dissipation energy [$\times 10^{-7}$ J·m^{-1}·s^{-1}]	
	Distribution pattern (a)	Distribution pattern (b)
20	6.02	8.19
30	5.62	8.03
50	5.18	7.64
70	4.72	7.10

The viscosities of water-rich phase (μ_1), 2.78 [mPa·s], and ionic liquid-rich phase (μ_2), 4.52 [mPa·s].

(c) Water-[C_2mim]mp-K_2HPO_4

Water rich-phase volume ratio [%]	Viscous dissipation energy [$\times 10^{-7}$ J·m^{-1}·s^{-1}]	
	Distribution pattern (a)	Distribution pattern (b)
10	6.75	7.49
35	6.29	7.26
50	6.13	7.28
65	6.12	7.12
90	6.11	6.84

The viscosities of water-rich phase (μ_1), 3.42 [mPa·s], and ionic liquid-rich phase (μ_2), 4.14 [mPa·s].

Table 2 Viscous dissipation energy data of annular flows for the two distribution patterns shown in Fig. 7-4 (a) and (b) when the difference in viscosity between the two phases was small (approximately <0.49 mPa s) and associated water-rich phase volume ratios. Under these conditions of (a)–(c), the phase with the larger volume formed as the inner phase. The values of the viscous dissipation energy shown in red indicate that TRDP was actually observed in the two distribution patterns.

(a) Water-acetonitrile-ethyl acetate

Water rich-phase volume ratio [%]	Viscous dissipation energy [$\times 10^{-7}$ J·m^{-1}·s^{-1}]	
	Distribution pattern (a)	Distribution pattern (b)
10	0.138	0.209
27	0.167	0.262
76	0.198	0.298
90	0.213	0.311

The viscosities of organic solvent-rich phase (μ_1), 0.431 [mPa·s], and water-rich phase (μ_2), 0.848 [mPa·s].

(b) Water-acetonitrile-chloroform

Water rich-phase volume ratio [%]	Viscous dissipation energy [$\times 10^{-7}$ J·m^{-1}·s^{-1}]	
	Distribution pattern (a)	Distribution pattern (b)
7	0.111	0.176
28	0.121	0.241
60	0.144	0.264
93	0.197	0.298
96	0.203	0.303

The viscosities of organic solvent-rich phase (μ_1), 0.335 [mPa·s], and water-rich phase (μ_2), 0.825 [mPa·s].

(c) Water-[C_4mim]Cl-K_2HPO_4

Water rich-phase volume ratio [%]	Viscous dissipation energy [$\times 10^{-7}$ J·m^{-1}·s^{-1}]	
	Distribution pattern (a)	Distribution pattern (b)
5	5.20	5.30
12	5.21	5.40
15	5.30	5.52
35	5.30	5.68
60	5.56	5.98
80	5.75	6.11

The viscosities of ionic liquid-rich phase (μ_1), 3.00 [mPa·s], and water-rich phase (μ_2), 3.22 [mPa·s].

energy obtained for the two distribution patterns together with the component ratios of the solvents and the viscosities of the two phases; the values for the distribution pattern that was actually observed as TRDP are written in red. When the difference in the viscosity between the two phases was large (approximately >0.73 mPa s) (Table 7-1), a large difference in the viscous dissipation energy between the solvent distribution patterns was observed. Furthermore, the distribution pattern that was theoretically determined by the viscous dissipation principle corresponded to that actually observed in the photograph in the experiment. Thus, the phase with the higher viscosity formed as the inner phase.

In contrast, when the viscosity difference between the phases was small (approximately <0.49 mPa s), a small difference in the viscous dissipation energy between the solvent distribution patterns was observed. Furthermore, the distribution pattern of the solvents did not always correspond to the viscous dissipation principle. In other words, the phase with the larger volume formed as the inner phase.

Joseph et al.[10] reported the instability of the flow formed by two immiscible liquids with different viscosities in a tube. The experiments showed a tendency for the thinner fluid to encapsulate the thicker fluid. The authors described the distribution pattern by the viscous dissipation principle, which postulated that the extent of viscous dissipation was minimized at a given flow rate. Considering a circular tube, the principle predicted a concentric configuration with the more viscous fluid located at the core. However, a linear stability analysis, as performed by the authors,

revealed that though this configuration was stable when the more viscous fluid occupied most of the tube, it was not stable when the tube mostly contained a thinner fluid. Therefore, the authors concluded that the viscous dissipation principle did not always hold, and that the volume ratio of the two fluids was a crucial factor for the configuration in the small viscosity difference between the thicker and thinner ones.

The consideration and conclusion of an annular flow formed by an immiscible multi-phase flow by Joseph et al. were in accordance with the author's experimental data and viscous dissipation calculation data of TRDP.

7.4 Conclusion

The current findings are expected to be useful in analytical science including microflow analysis research. TRDP was observed using a microscope-CCD camera system; six types of two-phase separation mixed solvent solutions were examined. The viscous dissipation energy was also calculated for the solution component ratios that generated the TRDP. When the difference in viscosity between the two phases was large, the phase with the higher viscosity formed as the inner phase in the TRDP regardless of the volume ratio. The distribution pattern of the solvents was supported by the viscous dissipation principle. In contrast, when the viscosity difference was small, the phase with the larger volume formed as the inner phase in the TRDP. The distribution pattern of the solvents did not

always correspond to the viscous dissipation principle. It is interesting and useful to note that the distribution pattern of TRDP or TRDF in PS-MPF could be considered on the basis of the viscous dissipation principle and the report of the linear stability analysis, similarly to that of annular flows in conventional immiscible multi-phase flows.

References

1) N. Jinno, M. Murakami, K. Mizohata, M. Hashimoto, and K. Tsukagoshi, *Analyst*, **135** 927 (2011).
2) M. Murakami, N. Jinno, M. Hashimoto, and K. Tsukagoshi, *Anal. Sci.*, **27**, 793 (2011).
3) S. Fujinaga, K. Unesaki, S. Negi, M. Hashimoto, and K. Tsukagoshi, *Anal. Methods*, **4**, 3884 (2012).
4) K. Tsukagoshi, *Anal. Sci.*, **30**, 65 (2014).
5) S. Fujinaga, K. Unesaki, Y. Kawai, K. Kitaguchi, K. Nagatani, M. Hashimoto, K. Tsukagoshi, and J. Mizushima, *Anal. Sci.*, **30**, 1005 (2014).
6) A. E. Everagae, *Trans. Soc. Rheol.*, **17**, 629 (1973).
7) J. H. Southern, and R. L. Ballman, *Appl. Polymer Symp.*, **20**, 175 (1973).
8) D. L. Maclean, *Trans. Aoc. Rheol.*, **17**, 385 (1973).
9) M. C. Williams, *AlChE J.*, **21**, 1204 (1975).
10) D. D. Joseph, Y. Renardy, and M. Renardy, *J. Fluid Mech.*, **141**, 309

(1984).

Chapter 8

Conclusion

The author constructed the capillary chromatography based on specific fluidic behavior of mixed solvent in microspace and considered the fluidic behavior. When the homogeneous solutions of two-phase separation systems are delivered to a microspace, the homogeneous solutions change to the heterogeneous solutions, generating a hydrodynamic liquid-liquid interface with inner and outer phases. This fluidic behavior, TRDP, is applied to the capillary chromatography(TRDC), and its separation mechanism is investigated by analytical conditions. In addition, the TRDP is novel fluidic behavior, and its generation mechanism is considered from the experimental data and calculation.

Chapter 2 investigates generation condition of TRDP in terms of inner diameters of capillary, tube temperature, tube effective lengths, and flow rates. Furthermore, the pressure and linear velocity are calculated from these conditions and used to TRDP generation. In addition, mixture analyte solution of 1-naphthol, 1-naphthalenesulfonic acid, 2,6-naphthalenedisulfonic acid, and 1,3,6-naphthalenetrisulfonic acid were separated in these conditions, and the author considered TRDC separation mechanism.

In Chapter 3, the author examined various water–hydrophilic organic solvent–hydrophobic organic solvent systems for TDRP and TRDC. Phase diagrams, fluorescence photographs, and chromatograms for a water–acetonitrile–chloroform solvent system showed particular TRDP and TRDC. The performance of this solvent system in TRDC was comparable to that of a water–acetonitrile–ethyl acetate system.

In Chapter 4, Chrome Azurol S as an absorption reagent was introduced into the TRDC system for metal ion separation and online absorption detection. Characteristic individual absorption characteristics and elution times were obtained as the result of complex formation between the metal ions and Chrome Azurol S in the water–acetonitrile–ethyl acetate mixture solution. Co(II), Al(III), Cu(II), and Ni(II) were completely separated and detected in this order online by the TRDC system with absorption detection. The system worked without applying a high voltage and without using any specific columns.

In Chapter 5, the dimensionless number, Weber number, was used to examine TRDP formation, including the inner and outer phases, in the water–acetonitrile–ethyl acetate and water–acetonitrile–chloroform systems. An interesting relationship between the Weber number and inner and outer phase formation in TRDP was determined at least for the two model systems in this experiment. TRDP was clearly observed in the capillary tube when the Weber numbers of the organic solvent-rich and water-rich phases differed.

In Chapter 6, the factors determining the formation of the inner and outer phases in the microspace were assessed by examining the phase diagrams incorporating solubility curves, viscosities of the upper and lower phases in a batch vessel, volume ratios of the phases, and development of the TRDP using microscopy imaging. When the difference in the viscosities between the two phases was large (> around 0.73 mPa•s), the phase with the higher viscosity formed as the inner phase regardless of the volume

ratios, whereas when the difference in viscosities was small (< around 0.42 mPa•s), the phase with the larger volume ratio formed as the inner phase.

In Chapter 7, the viscous dissipation energy was also calculated for the solution component ratios that generated the TRDP. When the difference in viscosity between the two phases was large, the phase with the higher viscosity formed as the inner phase in the TRDP regardless of the volume ratio. The distribution pattern of the solvents was supported by the viscous dissipation principle. In contrast, when the viscosity difference was small, the phase with the larger volume formed as the inner phase in the TRDP. The distribution pattern of the solvents did not always correspond to the viscous dissipation principle.

In summary, the effect of flow conditions and mixed solvent systems to TRDP and TRDC is investigated, and the TRDC became able to separate analytes more sensitively and separate novel kind of analyte, metal ions. Furthermore, the TRDP generation is considered by calculation of Weber number, and the phase formation of is considered by calculation of the viscous dissipation. From these results, the theory of TRDP in generation and phase formation is elucidated, and the author has contributed to the elucidation of the TRDP, novel fluidic behavior,

Acknowledgements

The author wishes to express his sincere gratitude to Professor Kazuhiko Tsukagoshi for his continuous guidance, many discussions, and suggestions throughout the performance of this work and to Professor Jiro Mizushima for discussions in some part of this work.